The hydrologically active rootzone in climate models

Fransje van Oorschot

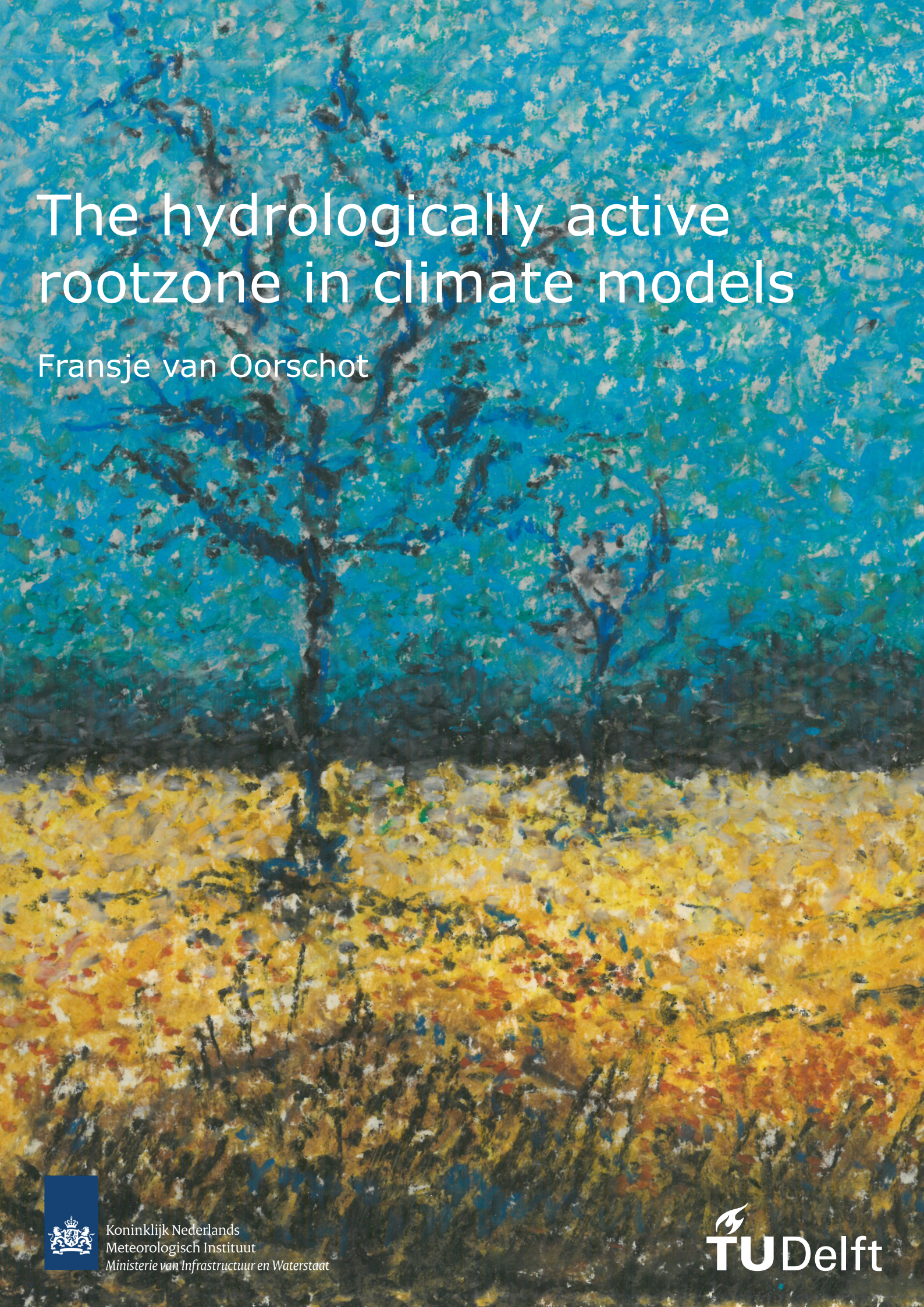

Koninklijk Nederlands
Meteorologisch Instituut
Ministerie van Infrastructuur en Waterstaat

TU Delft

MSc thesis Watermanagement

The hydrologically active rootzone in climate models

by
Fransje van Oorschot

to obtain the degree of Master of Science

at the faculty of Civil Engineering and Geosciences at Delft University of Technology,

to be defended publicly on Thursday February 20, 2020 at 16.00.

Student number: 4363701

Thesis committee:	Dr. M. Hrachowitz,	TU Delft, Chairman
	Dr. ir. R.J. van der Ent,	TU Delft
	Dr. A. Alessandri,	KNMI
	Prof. dr. ir. B.J.H. van de Wiel,	TU Delft

An electronic version of this thesis is available at http://repository.tudelft.nl/.

Frontpage: Personal collection

Koninklijk Nederlands
Meteorologisch Instituut
Ministerie van Infrastructuur en Milieu

TU Delft

Preface

This thesis explores the representation of the hydrologically active rootzone in climate models and contributes to the development of climate models which is of utmost importance for future studies on climate change. My work was very challenging and I am very proud of the end results that I am presenting in this report. I have learnt a lot during this research and I am very thankful to all who made it possible for me to do this extremely interesting and challenging research project. I am very grateful to Markus, Ruud and Andrea who really motivated and supported me during the thesis. Your enthusiasm about this research was very inspiring to me. I would also like to thank Bas for joining my thesis committee to provide an independent opinion on the research.

Lastly, special thanks to my friends and family who always supported and motivated me during my studies at TU Delft.

Fransje van Oorschot

Delft, February 2020

Summary

Climate models have difficulties in predicting the frequency and intensity of future droughts on regional scales, possibly caused by inadequate representation of land surface hydrological processes. Vegetation is controlling the Earth's water and energy balance by transporting water from the subsurface to the atmosphere, through its roots. The water storage capacity in the vegetation's rootzone is a key parameter in predicting evaporation fluxes in land surface models because its size determines how long into the dry season vegetation is able to evaporate. Ecosystems design the size of their rootzone water storage reservoir to optimally function and to overcome dry periods, based on climatic conditions.

Whereas climate is the major driver of root development, the rootzone storage capacity in the HTESSEL land surface scheme is only dependent on soil type and modelled soil depth. Moreover, the model describes root parameters by tables based on scarce observations of individual plants that do not represent ecosystem scales. This research aims to analyse the effect of the climate-based mass balance method for estimating the maximum water storage capacity in the vegetation's rootzone on the representation of water and energy fluxes in the HTESSEL land surface model. Maximum rootzone water storage capacities are estimated for 15 river catchments in Australia based on catchment-scale water balances. These estimates are implemented in the current surface parameterisation of the HTESSEL land surface model and offline simulations are performed. The current model performance and the model performance with adapted rootzone water storage capacities are evaluated regarding simulation of water and energy fluxes.

According to this study, the storage capacity in the vegetation's rootzone represented in HTESSEL is larger than the mass-balance derived estimates. The model strongly overestimates evaporation fluxes and thereby underestimates river discharge, with larger relative simulation errors in the dry season than in the wet season. The climate-based mass balance total rootzone water storage capacities have small effects on the representation of water and energy fluxes by the model, but contribute to a consistent improvement in predicting these fluxes. Nash Sutcliffe Efficiencies of the modelled river flows improve on average from 0.44 in the base model to 0.51 in the model with mass balance rootzone water storage capacities. The results indicate that the inadequate rootzone representation is a source of modelling error. However, it is expected that other hydrological process are also inadequately represented by the model, as the modelling simulation errors remain large when implementing mass balance rootzone water storage capacities. Moreover, it was found that internal vegetation dependent model parameters strongly influence the simulated fluxes and could therefore be another source of model bias. This study shows that investigating uncertainties in the representation of the rootzone in the HTESSEL land surface model is paramount. More research on the representation of hydrological processes in land surface models could lead to significant improvements in climate model predictions.

Table of Contents

List of Symbols

E	Total actual evaporation	$[LT^{-1}]$
E_a	Actual evaporation	$[LT^{-1}]$
E_i	Interception evaporation	$[LT^{-1}]$
E_p	Potential evaporation	$[LT^{-1}]$
E_t	Soil evaporation	$[LT^{-1}]$
E_t	Transpiration	$[LT^{-1}]$
f	Annual evaporation variation factor	[-]
P	Total precipitation	$[LT^{-1}]$
P_e	Effective precipitation	$[LT^{-1}]$
Q	Total river discharge	$[LT^{-1}]$
Q_{sb}	Subsurface runoff	$[LT^{-1}]$
Q_s	Surface runoff	$[LT^{-1}]$
S_D	Storage deficit	[L]
S_i	Interception water storage	[L]
S_R	Rootzone water storage	[L]
T	Return period	[years]
γ	Hydraulic conductivity	$[ms^{-1}]$
λ	Hydraulic diffusivity	$[m^2s^{-1}]$
λ_E	Latent heat of vaporisation	$[Jkg^{-1}]$
ρ_a	Air density	$[kgm^{-3}]$
ρ_w	Water density	$[kgm^{-3}]$
θ	Moisture content	[-]
C_H	High vegetation coverage	[-]
C_H	Low vegetation coverage	[-]
D	Layer thickness	[L]
D_a	Atmospheric water vapor deficit	[kPa]
i	Tile	[-]
k	Soil layer	[-]
R	Root distribution	[-]
r_c	Canopy resistance	$[sm^{-1}]$

R_{S}	Downward shortwave radiation	$[\mathrm{Wm}^{-2}]$
$r_{\mathrm{S,min}}$	Minimum canopy resistance	$[\mathrm{sm}^{-1}]$
S_θ	Root extraction rate	$[\mathrm{m}^3\mathrm{m}^{-3}\mathrm{s}^{-1}]$
z	Layer depth	[L]
EF	Evaporation Factor	[-]
LAI	Leaf Area Index	[-]
MAF	Moisture Availability Factor	[-]
ZF	Fraction of frozen soil	[-]
ZLIQ	Liquid water fraction	[-]
A	Abercrombie River	
Av	Avoca River	
D	Dogwood Creek	
EA	East Alligator River	
EB	East Baines River	
G	Gregory River	
He	Herbert River	
K	Kent River	
Mi	Mitchell River	
Mu	Murrumbidgee River	
Na	Namoi River	
No	Normanby River	
P	Paroo River	
R	Reedy Creek	
W	Wenlock River	

List of Figures

List of Tables

1 Introduction

1.1 Research context

Climate models describe the interactions between the atmosphere, the land surface, oceans and sea ice and are used for predictions of future climate patterns. The models are able to reproduce temperature and rainfall patterns on global scales, but on regional scales the confidence of the predictions is lower (Pachauri et al., 2014). On the land surface, vegetation is controlling the water cycle by partitioning precipitation into evaporation and runoff by transporting water through their roots to the atmosphere and is thereby a key in the prediction of land surface-atmosphere feedbacks (Milly, 1994; Seneviratne et al., 2010). One of these feedback mechanisms occurs during droughts, that are expected to occur more frequent in the future (Pachauri et al., 2014). Dry periods are characterised by high temperatures and low precipitation rates, which leads to a decrease in soil water, causing vegetation water stress. As a result of this, the moisture flow from the land-surface to the atmosphere decreases, leading to dryer air, less precipitation and in turn enhanced vegetation water stress. Inadequate representation of hydrological processes in land surface models could be a cause for model difficulties in regional drought predictions (Pitman, 2003).

The water storage capacity in the rootzone (S_{R}) is the key parameter for describing vegetation's root extraction and thereby the ability of vegetation to maintain transpiration into the dry season (Milly, 1994). The development of the rootzone water storage capacity on ecosystem scales can be explained by evolution theory. Ecosystems develop their above- and below-ground biomass to reach an optimum of their functioning which includes infiltration, moisture retention, nutrient uptake and drainage (Savenije & Hrachowitz, 2017). Over time, vegetation develops a rooting system in order to avoid water shortages and thereby to overcome dry periods. Ecosystems optimise their hydrologically active rootzone according to climatic conditions in order to maintain transpiration and thereby productivity (Guswa, 2008; Kleidon, 2004). Although vegetation's roots drive the Earth's water cycle and contribute for 20%-40% to the total biomass of trees, research mainly focuses on the above-ground part of ecosystems because root observations are difficult, time consuming and imprecise, which leads to poorly understood global distributions of S_{R} (Brunner, Herzog, Dawes, Arend, and Sperisen, 2015; Yang, Donohue, and McVicar, 2016). Therefore, different methods for estimating rootzone storage capacities in hydrological and land surface models have been developed.

In situ observations of rooting depths of individual plants provide direct information on vegetation's subsurface structures. These observations are extrapolated to global rooting depth estimates for different terrestrial biomes (Canadell et al., 1996; Jackson et al., 1996; Schenk and Jackson, 2002a, 2002b). Observational data is combined with vegetation and soil types in look-up tables, that describe global estimates of rooting depths and distributions. The literature based look-up table approach is applied in global land surface and hydrological models for estimating rootzone storage capacities (L. Wang-Erlandsson, Van Der Ent, Gordon, and Savenije, 2014; Schmied et al., 2014).

Inverse modelling provides indirect estimates of rootzone water storage capacities by simulating rooting depths based on satellite observations (Kleidon, 2004). Calibration of the rootzone water storage capacity is commonly applied in hydrological studies (Lan Wang-Erlandsson et al., 2016). In this approach modelling parameters are indirectly fitted towards hydrological parameters on catchment scales (Winsemius, Schaefli, Montanari, & Savenije, 2009). In optimisation models, rooting depths are estimated based on minimising vegetation's water stress and maximising vegetation's productivity for given soil and climate characteristics (Kleidon & Heimann, 1998).

The mass balance approach describes total rootzone storage capacities based on long-term water

balances on catchment scale and has shown plausible estimates of S_R (Gao et al., 2014). In this method S_R is considered to be fully climate driven and independent of soil and vegetation type. Total rootzone storage capacities are estimated as the maximum storage deficit, corresponding to the cumulative difference between effective precipitation and transpiration within a certain time period, assuming that the vegetation has continuous access to water. Although hydrological data is needed for this method, it does not require observational data of soil and rooting depths. Moreover, the method allows for time-varying rootzone storage capacities which are relevant in climate change and land use change studies (Capell et al., 2016). Furthermore, De Boer-Euser, McMillan, Hrachowitz, Winsemius, and Savenije (2016) showed improved modelling performance applying mass balance derived S_R rather than soil derived estimates and Lan Wang-Erlandsson et al. (2016) proved hydrological model improvements by implementing global S_R estimates based on satellite-products rather than S_R from look-up tables.

1.2 Problem statement

Inadequate representation of the hydrologically active rootzone in land surface models could lead to errors in the prediction of water and energy fluxes by these models. The vegetation's rootzone is an essential part in land surface models, because roots drive water fluxes from the subsurface to the atmosphere. Whereas climate is the main driver for root development (Guswa, 2008; Kleidon, 2004), land surface models follow a look-up table approach which does not account for climate variability in describing the vegetation's rootzone. The main issues in the rootzone parameterisation in the currently used land surface models are as follows:

- Vegetation types and corresponding root systems are described as fixed model input maps whereas vegetation species and their rooting systems are dynamic and dependent on climatic parameters (Sivandran and Bras, 2013; Gentine, D'Odorico, Lintner, Sivandran, and Salvucci, 2012).
- Rootzone parameterisation is based on scarce in situ observations of individual plants that do not represent spatial variability on ecosystem scales (Lan Wang-Erlandsson et al., 2016).
- Rooting depths and root available water are limited by a fixed model soil depth which does not allow for root extraction from deep reservoirs (Canadell et al., 1996).

1.3 Research objective

Considering the problems mentioned in Section 1.2, a different approach for rootzone parameterisation in land surface models is proposed. This approach is based on a holistic strategy describing rootzone storage capacities based on ecosystem-scale optimisation instead of point scale observations. This research aims to investigate the potential of a holistic approach for estimating S_R in a land surface model. The main research question is:

What is the effect of the climate-based mass balance method for estimating the maximum water storage capacity in the vegetation's rootzone on the representation of water and energy fluxes in the HTESSEL land surface model?

Firstly, rootzone storage capacities are estimated with the mass balance approach in Australian river catchments. The mass balance method is used in this research because it is a time-efficient tool for estimating catchment-scale S_R directly based on hydrological data. Moreover, it has the ability to respresent the time-dynamic behaviour of vegetation which would allow for an adaptive modelling approach. Secondly, strategies for implementing the rootzone storage capacities in the HTESSEL surface parameterisation are developed. Lastly, the performance of the HTESSEL base model and the HTESSEL model with an adapted rootzone parameterisation are evaluated regarding water and energy fluxes.

1.4 Relevance

This exploratory study is important for the development of land surface models as the mentioned issues could lead to biases in water and energy flux predictions. If successful results are found, the mass balance method could be implemented in an adaptive module representing vegetation and rootzone storage capacity dynamics in a land surface model. Improving the subsurface hydrology in land surface models contributes to more representative climate models, leading to more adequate future climate simulations which is of utmost importance as global and regional climates are changing.

2 Theoretical framework

This chapter presents theoretical knowledge that is required in this research. Section 2.1 describes the relevant land surface-atmosphere interactions and Section 2.2 presents theory on soil moisture. Section 2.3 and Section 2.4 present climate classification theories and information on climate modelling respectively.

2.1 Land surface-atmosphere interactions

The global climate system is a result of interactions between the five natural components of the Earth: the atmosphere, the hydrosphere, the cryosphere, the land surface and the biosphere.

The land surface interacts with the atmosphere through energy and water fluxes. Figure 2.1 presents the main fluxes of the energy and water interactions between the land surface and the atmosphere.

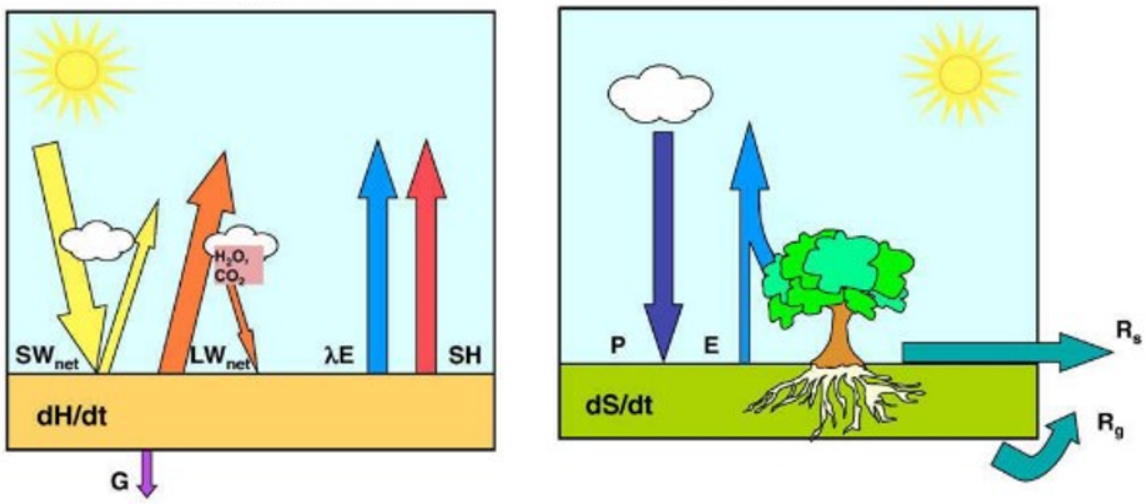

(a) Land energy balance *(b)* Land water balance

Figure 2.1: Land surface-atmosphere interactions (Equations 2.1 and 2.2) (Seneviratne et al., 2010)

The energy balance of a surface soil layer is described by Equation 2.1.

$$\frac{dH}{dt} = R_{\mathrm{n}} - SH - \lambda E - G \tag{2.1}$$

dH/dt is the change of energy over time, R_{n} is the net radiative flux, which is the difference between incoming shortwave radiation and outgoing longwave radiation. SH the sensible heat flux, λE the latent heat flux and G the ground heat flux. The latent heat flux is a function of evaporation and condensation of water vapor at the land surface. λ is the specific latent heat of evaporation and E is the evaporation rate. An increase in outgoing evaporation fluxes leads to an increase in outgoing long-wave radiation and a decrease of land surface temperatures.

The water balance of a surface soil layer is described by Equation 2.2.

$$\frac{dS}{dt} = P - E - R_{\mathrm{s}} - R_{\mathrm{g}} \tag{2.2}$$

The change in storage over time (dS/dt) is equal to incoming precipitation (P) minus outgoing evaporation (E), surface runoff (R_{s}) and groundwater discharge (R_{g}). The two runoff terms can

be combined in discharge term Q. Over the long term, the change in storage is negligible and the water balance is described by Equation 2.3.

$$0 = P - E - Q \tag{2.3}$$

The evaporation flux (E) controls both the energy and the water balance and is therefore an important link in the Earth's global climate system. Evaporation described in Equations 2.1 to 2.3 is actual evaporation which is limited by energy and water availability. Potential evaporation is the maximum evaporation that could occur with the available energy when there is no water shortage. The total actual evaporation flux can be divided into four components: open water evaporation, transpiration, interception evaporation and soil evaporation. At the land surface, the three latter fluxes are of importance. Precipitation intercepted by vegetation can evaporate directly from the plants surface, known as interception evaporation. Soil evaporation is direct evaporation from the moisture present in the top of the soil. These two fluxes occur at short timescales, directly after a rainfall event. Transpiration is the process of water transport via the roots, through the plants, to the atmosphere. The transpiration flux contributes to the total evaporation for longer timescales than interception and soil evaporation because water is stored in the subsurface. Transpiration is a more complex process than the other evaporation fluxes because the plants physiology plays a role. It is essential for plants because water transport allows evaporative cooling of the plants and uptake of CO_2, that is needed for photosynthesis, through gas exchange. Moreover, it enhances nutrient uptake from the soil and provides the plant water needed for its structure and functioning (Brunner et al., 2015).

Studies have found that transpiration is the major land surface evaporation flux. Global transpiration accounts for 70% of the total land surface evaporation whereas soil evaporation and interception evaporation both contribute 15% to the total evaporation (Sutanto, Wenninger, Coenders-Gerrits, and Uhlenbrook, 2012; Wenninger, Beza, and Uhlenbrook, 2010; Zhang, Shen, Sun, and Gates, 2011; Wang et al., 2010).

2.2 Soil moisture

Transpiration is the largest evaporative flux that directly connects the subsurface with the atmosphere which size is controlled by the subsurface soil moisture. The subsurface is divided into the saturated and the unsaturated zone, separated by the groundwater table. In the saturated zone, water flows slowly towards an area of discharge. However, in the unsaturated zone water is stored for shorter time-periods before it percolates to the groundwater or is transported back to the atmosphere through vegetation's roots. The part in the unsaturated zone where plants have developed their roots is the rootzone. The volume of water present in the rootzone is determining the transpiration flux.

The ability of vegetation to take up water from the soil depends on the soil moisture content, which is a function of soil type. Figure 2.2 presents a soil moisture retention curve that represents the negative pressure (suction) in the subsurface in relation to the moisture content (Lan Wang-Erlandsson et al., 2016). The shape of this curve is dependent on the soil type. Close to saturation, the soil water is held by capillary forces and the moisture above field capacity (θ_{cap}) drains under gravity and percolates to the groundwater. When soil moisture decreases, the suction becomes larger and water is bounded stronger to the soil grains. Moisture below the wilting point (θ_{pwp}) is held too strong by the soil matrix that vegetation's root are not able to extract the water. The moisture in between θ_{cap} and θ_{pwp} is accessible to vegetation. The Van Genuchten model is a commonly applied model to describe the shape of the water retention curve, depending on soil characteristics (Van Genuchten, 1980).

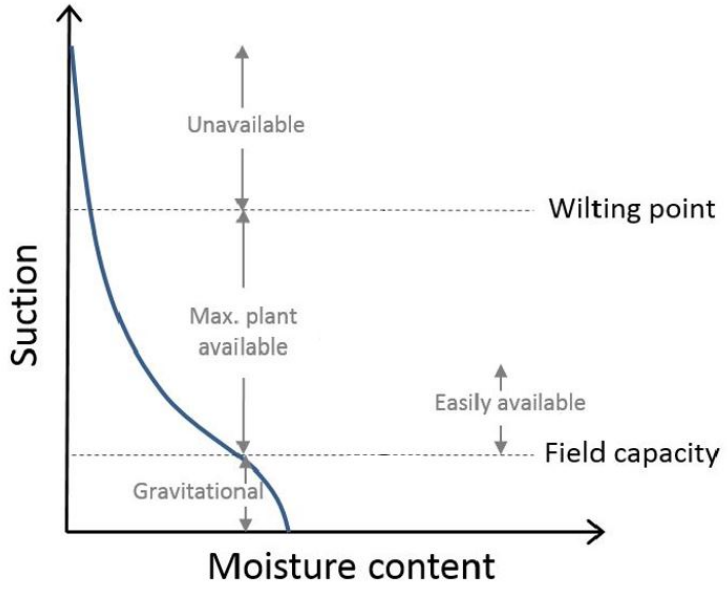

Figure 2.2: Soil moisture retention curve (Lan Wang-Erlandsson et al., 2016)

2.3 Climate classification

Climate is defined as the average weather over a 30 years period (WMO, 1989). The size of the rootzone storage reservoir is dependent on climatic conditions and ordering climatic regions is therefore important in the analysis of land surface water and energy fluxes (Guswa, 2008; Kleidon, 2004).

2.3.1 Budyko framework

The Budyko framework relates soil moisture and evaporation rates and provides insight in a catchment's water balance. It describes empirically the partitioning of precipitation in evaporation and runoff as a function of climate. The ratio between annual potential evaporation and precipitation is the aridity index, which is related to actual evaporation rates by the Budyko framework (Budyko, Miller, & Miller, 1974). Figure 2.3 presents the Budyko model with the theoretical curve based on observations and the water and energy limited regimes (Budyko et al., 1974). In catchments with aridity indices below 1, the annual precipitation exceeds annual potential evaporation, indicating that a catchment could evaporate following potential rates, but energy is limiting the actual evaporation rates in this regime. In catchments with aridity indices above 1, actual evaporation is limited by water availability because the annual actual evaporation cannot exceed annual precipitation. Catchments worldwide follow the theoretical Budyko curve (Gentine et al., 2012). However, vertical and horizontal deviations from this curve occur indicating changes in water partitioning and changes in climate, respectively. Water balance changes could be related to changes in vegetation, topography and soils, water losses by groundwater or adaptation to climate change.

2.3.2 Aridity index

The aridity index (AI) is measure for the dry or wetness of a region and is defined by Equation 2.4. $\overline{E_\mathrm{p}}$ and $\overline{P}$ represent the annual mean potential evaporation and precipitation, respectively. The Budyko framework, explained in section 2.3.1, is based on the aridity index.

$$\mathrm{AI} = \frac{\overline{E_\mathrm{p}}}{\overline{P}} \tag{2.4}$$

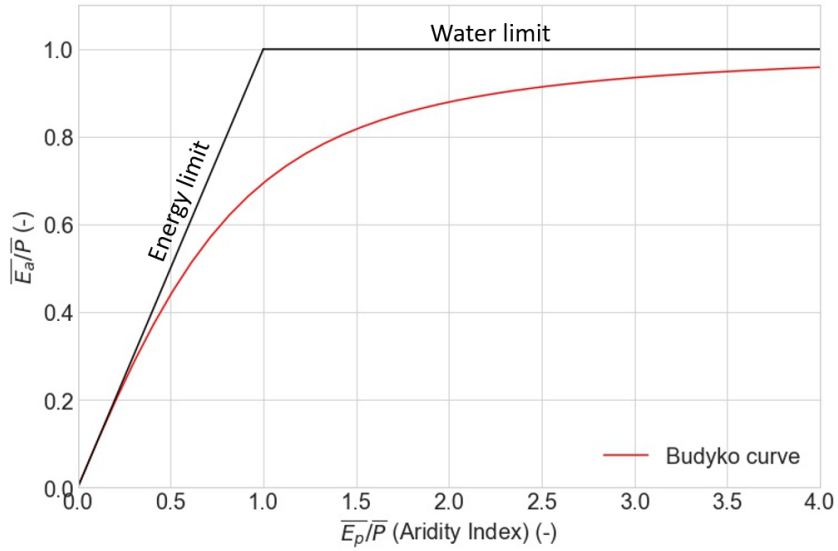

Figure 2.3: The solid line represents energy and water limited regimes and the red line represents the Budyko's theoretical curve (Budyko, Miller, & Miller, 1974)

2.3.3 Seasonality index

Seasonality of precipitation describes to what extent the precipitation is spread over the year. The seasonality index (SI) is defined by Equation 2.5 (Gao et al., 2014).

$$\mathrm{SI} = \frac{1}{\overline{P_\mathrm{a}}} \sum_{m=1}^{m=12} |\overline{P_\mathrm{m}} - \frac{\overline{P_\mathrm{a}}}{12}| \tag{2.5}$$

with $\overline{P_\mathrm{a}}$ the annual mean precipitation and $\overline{P_\mathrm{m}}$ the monthly mean precipitation of month m. The values of SI vary between 0 and 1. A high SI indicates that most of the annual precipitation falls within a few months. A SI close to 0, however, indicates year-round precipitation.

2.3.4 Time lag

The time lag between precipitation and potential evaporation is an indicator for energy and water availability within a year. The time-lag is defined as the time difference in months between the maximum monthly-mean E_p and P (Yang et al., 2016).

2.4 Climate modelling

Worldwide many Earth system models have been developed for describing and understand past and future climates. The models represent the natural components in the Earth's system and are subdivided into four main sub-models: atmosphere, land-surface, oceans and sea-ice. Although the global models are improving, there is still a lot of variation in the prediction between the models (Kattsov et al., 2013). Global climate simulations are performed in a coupled mode of the four sub-models. However, in model development the models are isolated and run in offline mode. Offline simulations provide more detailed information about the performance of a single model and simulation times are reduced due to less complexity (Balsamo et al., 2015).

3 HTESSEL model description

The land surface model used in this research is the HTESSEL scheme which is part of EC-EARTH climate simulations and the Integrated Forecasting System (IFS) of the European Centre for Medium-Range Weather Forecasts (ECMWF). This chapter presents model characteristics. Section 3.1 presents information on the development of the HTESSEL model. Section 3.2 describes the main structure of the model and the parameterisations related to soil hydrology. Section 3.3 presents the coding structure of the model.

3.1 Model development

The model described by Blondin (1991) discretises the soil in three layers, with vegetation roots in the two upper layers and soil type, hydraulic conductivity and diffusivity are fixed over the model domain. This model resulted in a large positive bias of surface temperatures in summer. Moreover, evaporation rates were too high in wet conditions and too low in dry conditions (Blondin, 1991). The inaccurate model results were attributed to the representation of land surface hydrology and Viterbo and Beljaars (1995) described changes to the hydrology representation. He stated that the summer temperature bias and the too low evaporation rates in dry periods in the scheme of Blondin (Blondin, 1991) were due to a lack of subsurface water storage in the model. Therefore, a fourth soil layer was added and roots were distributed equally over the upper three layers. The fourth model layer acts in this model as a recharge reservoir to supply water to the upper layers in extensive dry spells. The total available water for root extraction increased from 41 mm in the model of Blondin (1991) to 152 mm in the model of Viterbo and Beljaars (1995). Besides the changed layers and root representation, the Clapp and Hornberger soil scheme was adopted and conductivity and diffusivity were described as a function of soil moisture. Even though the total available water increased significantly, the evaporation rates predicted with the new model were still underestimated in dry periods. This issue was assigned to a single soil type in all gridpoints (Viterbo & Beljaars, 1995).

Major changes in the land surface parameterisation were made by B. J. van den Hurk, Viterbo, Beljaars, and Betts (2000). Figure 3.1a presents the schematics of the land surface as represented in this research, later referred to as TESSEL (Tiled ECMWF Scheme for Surface Exchanges over Land). The four tiled gridbox (vegetation, bare soil, interception and snow (Viterbo & Beljaars, 1995)) was replaced by eight subgrid fractions with separately calculated surface fluxes. The eight tiles are: high and low vegetation, snow on bare soil/low vegetation and snow underneath high vegetation, open and frozen water, bare soil and an interception reservoir. Furthermore, a global vegetation database (Section 4.2.4) was applied to describe 18 different vegetation types. The specification of vegetation type leads to a more realistic representation of reality but it comes with estimation of many internal model parameters leading to an increased degree of freedom in the model. Instead of the equal root distribution over the three upper layers in Viterbo (Viterbo & Beljaars, 1995), the soil was discretised in four model layers with a root distribution dependent on vegetation type in TESSEL, resulting in an increase in total available water for root extraction. Offline model simulations were executed for different regions and it was concluded that evaporation is still underestimated in some regions while in other regions the transpiration levels in the dry season were too high compared to estimates. This overestimation was assigned to inappropriate soil characteristics and a lack of surface runoff (B. J. van den Hurk et al., 2000).

In 2008, the TESSEL scheme for land surface fluxes was replaced by HTESSEL (Hydrology TESSEL). TESSEL's main shortcomings were a global uniform soil texture and a lack of surface runoff. Therefore, a global soil map was implemented and a new hydrology schematisation was introduced in HTESSEL (B. van den Hurk et al., 2008). Moreover, the Clapp and Hornberger scheme for

soil hydrology was replaced by the Van Genuchten formulation. Figure 3.1b presents the changed surface hydrology in the revised land surface model HTESSEL. The figure presents two gridcells with similar incoming precipitation fluxes. Spatial variable soil type and orography lead to different surface and subsurface runoff fluxes. The tiled structure presented in figure 3.1a is similar in HTESSEL.

Alessandri et al. (2017) developed a seasonal varying subgrid effective vegetation coverage, as a function of LAI in order to include seasonal dynamics of vegetation. In summer season, when the LAI of vegetation is the largest, the effective vegetation coverage is larger than in winter season and evaporation fluxes are larger. Model experiments applying this method have shown improvements of vegetation impacts in global scale climate simulations and predictions over land (Alessandri et al., 2017).

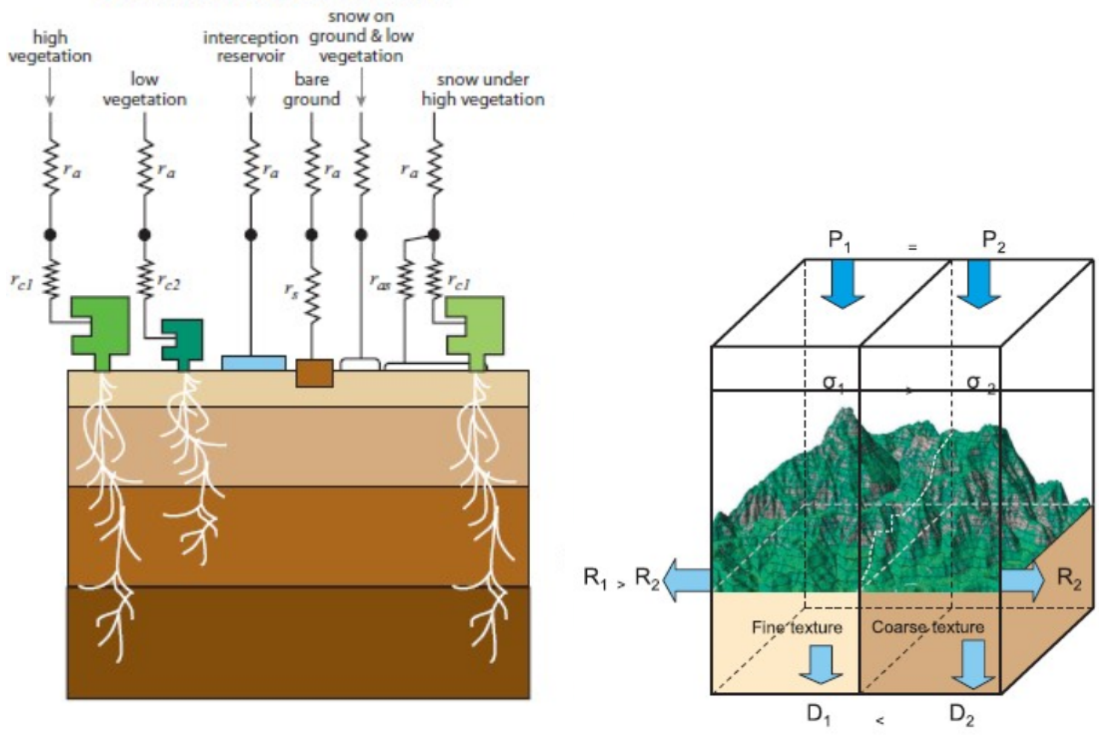

Figure 3.1: Tiled model structure in TESSEL (a) and the introduced subgrid runoff scheme in HTESSEL (b) (ECMWF, 2016)

3.2 Model structure

The IFS documentation of cycle CY43RI (2016) and the model codes itself are used as a reference for the model structure (ECMWF, 2016).

3.2.1 Surface parameterisation

As mentioned in Section 3.1 each gridcell is subdivided into eight tiles, with six tiles on land. This research focuses on the vegetation covered tiles. The vegetation cover of a gridcell is derived from the GLCC database (Section 4.2.4). The 20 vegetation classes in HTESSEL are presented in Table 3.1 and the vegetation dependent parameter values that are presented in Appendix A.1.

For each gridcell, four vegetation parameters are derived: Dominant vegetation type T_{H} and T_{L} and area fraction A_{H} and A_{L} for high and low vegetation, respectively. Equation 3.1 describes the areal coverage of low and high vegetation and bare soil. c_{veg} is a fixed vegetation dependent coverage

Table 3.1: HTESSEL vegetation indices and corresponding vegetation types. H/L refers to high or low vegetation (ECMWF, 2016)

Index	Vegetation type	H/L
1	Crops, mixed farming	L
2	Short grass	L
3	Evergreen needleleaf trees	H
4	Deciduous needleleaf trees	H
5	Deciduous broadleaf trees	H
6	Evergreen broadleaf trees	H
7	Tall grass	L
8	Desert	-
9	Tundra	L
10	Irrigated crops	L

Index	Vegetation type	H/L
11	Semidesert	L
12	Ice caps and glaciers	-
13	Bogs and marshes	L
14	Inland water	-
15	Ocean	-
16	Evergreen shrubs	L
17	Deciduous shrubs	L
18	Mixed forest/woodland	H
19	Interrupted forest	H
20	Water and land mixtures	L

that represents the bare soil fraction in between plants. The seasonal dynamic c_{veg} developed by Alessandri et al. (2017) is not applied in this research. Evergreen broadleaf trees for example have a vegetation coverage of 0.99, while deciduous shrubs only cover 50% of the vegetated area fraction. The tile fractions are a function of the areal coverages c_{H}, c_{L} and c_{B} and the dynamically chaging interception and snow coverage.

$$\begin{aligned} c_{\text{H}} &= A_{\text{H}} c_{\text{veg}}(T_{\text{H}}) \\ c_{\text{L}} &= A_{\text{L}} c_{\text{veg}}(T_{\text{L}}) \\ c_{\text{B}} &= 1 - c_{\text{L}} - c_{\text{H}} \end{aligned} \tag{3.1}$$

3.2.2 Soil discretisation

In the vertical the soil depth is 289 cm, divided into four layers with depths from the top to the bottom layer of 7, 21, 72 and 189 cm. These depths have shown to provide a good balance between computational costs and time scale representations between one day and one year (Deardorff, 1978). The model defines separate model layer depths for temperature, moisture and sea ice. However, all depths are similar for simplicity of the code. Fluxes are defined at the layer interfaces, states are defined at full layers.

3.2.3 Surface fluxes

The main fluxes between the land-surface and the atmosphere are the water and energy fluxes. The energy fluxes can be subdivided into latent and sensible heat fluxes. The total latent (E) and sensible (H) heat fluxes are a weighted average of the fluxes in the different tiles and are expressed by:

$$E = \sum_{i=1}^{8} C_i E_i$$

$$H = \sum_{i=1}^{8} C_i H_i$$

where C_i is the coverage of tile i that depends both on the vegetated area and on snow and intercepted water coverage. In this research only the latent heat fluxes are considered.

The latent heat flux for high and low vegetation is given by Equation 3.2.

$$E_i = \frac{\rho_\mathrm{a}}{(|U_\mathrm{L}|C_{\mathrm{H},i})^{-1} + r_\mathrm{c}}[q_\mathrm{L} - q_\mathrm{sat}(T_{\mathrm{sk},i})] \tag{3.2}$$

with ρ_a the air density, c_p the heat capacity of moist air, g the acceleration of gravity, r_c the canopy resistance, $C_{\mathrm{H},i}$ the turbulent exchange coefficient for the given tile, $|U_\mathrm{L}|$, T_L, z_L and q_L the wind speed, temperature, height of the lowest atmospheric model level and humidity. q_sat is the saturated humidity which is a function of is the mean skin temperature $T_{\mathrm{sk},i}$ for the given tile.

The canopy resistance is a function of downward short-wave radiation R_s, leaf area index LAI, average unfrozen root soil water θ, atmospheric water vapour deficit D_a and a minimum stomatal resistance $r_{\mathrm{S,min}}$.

$$r_\mathrm{c} = \frac{r_{\mathrm{S,min}}}{\mathrm{LAI}} f_1(R_\mathrm{s}) f_2(\bar{\theta}) f_3(D_\mathrm{a}) \tag{3.3}$$

f_1 is a function of incoming shortwave radiation R_s, described by Equation 3.4 with $a = 0.81$, $b = 0.004\,\mathrm{W^{-1}m^2}$ and $c = 0.05$.

$$\frac{1}{f_1(R_\mathrm{s})} = \min[1, \frac{bR_\mathrm{s} + c}{a(bR_\mathrm{s} + 1)}] \tag{3.4}$$

f_3 describes the dependence on atmospheric humidity deficit depending on vegetation type.

$$\frac{1}{f_3(D_\mathrm{a})} = \exp(-g_\mathrm{D} D_\mathrm{a}) \tag{3.5}$$

f_2 is dependent on soil moisture and the vegetation dependent root distribution as described in equation 3.6 to 3.8.

$$\frac{1}{f_2(\bar{\theta})} = \begin{cases} 0 & \bar{\theta} \le \theta_\mathrm{pwp} \\ \frac{\bar{\theta} - \theta_\mathrm{pwp}}{\theta_\mathrm{cap} - \theta_\mathrm{pwp}} & \theta_\mathrm{pwp} \le \bar{\theta} \le \theta_\mathrm{cap} \\ 1 & \bar{\theta} > \theta_\mathrm{cap} \end{cases} \tag{3.6}$$

$$\bar{\theta} = \sum_{k=1}^{4} R_k \max[f_{\mathrm{liq},k}\theta_k, \theta_\mathrm{pwp}] \tag{3.7}$$

$$R_k = 0.5[\exp(-a_\mathrm{r} z_{k-1/2}) + \exp(-b_\mathrm{r} z_{k-1/2}) - \exp(-a_\mathrm{r} z_{k+1/2}) - \exp(-b_\mathrm{r} z_{k+1/2})] \tag{3.8}$$

θ_pwp is the soil moisture at permanent wilting point and θ_cap the soil moisture at field capacity. These parameters are dependent on soil type and are based on the Van Genuchten soil water equations. Appendix A.2 presents the Van Genuchten soil characteristics values applied in HTESSEL. $\bar{\theta}$ is the weighted average of the unfrozen soil water. R_k is the fraction of roots in each layer and is the sum of exponential functions of the depth of the bottom of the layer ($z_{k\pm1/2}$) and attenuation coefficients a_r and b_r. The root distribution for different vegetation types is presented in Table 3.2. $f_{\mathrm{liq},k}$ represents the fraction of unfrozen soil water that is dependent on soil temperature. The available soil moisture is limited by lower boundary θ_pwp and by upper boundary θ_cap.

Table 3.2: Fraction of roots (%) in each layer for different vegetation types. Vegetation indices refer to vegetation types in Table 3.1 (ECMWF, 2016)

Vegetation index	**1**	**2**	**3**	**4**	**5**	**6**	**7**	**8**	**9**	**10**	**11**	**13**	**16**	**17**	**18**	**19**
Layer 1	24	35	26	26	24	25	27	100	47	24	17	25	23	23	19	19
Layer 2	41	38	39	38	38	34	27	0	45	41	31	34	36	36	35	35
Layer 3	31	23	29	29	31	27	27	0	8	31	33	27	30	30	36	36
Layer 4	4	4	6	7	7	14	9	0	0	4	19	11	11	11	10	10

3.2.4 Soil water budget

The water in the subsurface determines the canopy resistance (Equation 3.3) and thereby the transpiration flux in the vegetation covered tiles. The infiltrating water moves through the four subsurface model layers obeying Darcy's law which is described by Equation 3.9.

$$F_{\mathrm{w}} = \rho_{\mathrm{w}}(\lambda \frac{\partial \theta}{\partial z} - \gamma) \tag{3.9}$$

The water flux F_{w} [$\mathrm{kgm^{-2}s^{-1}}$] in the soil is a positive downward flux and a function of the change in soil moisture (θ) over depth (z). In this equation ρ_{w} is the density of water in [$\mathrm{kgm^{-3}}$], λ the hydraulic diffusivity [$\mathrm{m^2s^{-1}}$] and γ the hydraulic conductivity [$\mathrm{ms^{-1}}$].

The change of soil moisture over time is described by Equation 3.10 where the volumetric sink term S_θ [$\mathrm{m^3m^{-3}s^{-1}}$], representing root extraction, is added.

$$\rho_{\mathrm{w}} \frac{\partial \theta}{\partial t} = -\frac{\partial F_{\mathrm{w}}}{\partial z} + \rho_{\mathrm{w}} S_\theta \tag{3.10}$$

Combining Equations 3.9 and 3.10 and defining $S_\theta = S_\theta(\theta, z)$, the general partial differential equation 3.11 is obtained. A similar equation is also applied for soil and ice temperature computations. This differential equation is numerically integrated applying an upper and lower boundary. The upper boundary is defined by the difference between incoming (precipitation) and outgoing (evaporation and surface runoff) water fluxes. At the bottom of layer four free drainage is assumed.

$$\frac{\partial \theta}{\partial t} = \frac{\partial}{\partial z}(\lambda \frac{\partial \theta}{\partial z} - \gamma) + S_\theta \tag{3.11}$$

The soil water calculation depends on two soil properties determining the vertical movement of water through the soil (hydraulic conductivity and diffusivity) and three water fluxes determining the upper model boundary (interception, runoff and transpiration).

Soil hydraulic conductivity and diffusivity (γ and λ in Equation 3.11) are a function of the soil moisture content. The TESSEL land-surface model applies the Clapp and Hornberger formulation to define these soil characteristic values, considering one global loamy soil type (Clapp & Hornberger, 1978). In HTESSEL the Van Genuchten formulation was adopted which deals with spatial variable soil textures (Van Genuchten, 1980). Implementing soil moisture dependent hydraulic soil properties lead to an improvement of HTESSEL's ability to predict runoff (B. van den Hurk et al., 2008). In the Van Genuchten scheme, the hydraulic conductivity (γ) is dependent on the hydraulic head (h) and soil-type dependent parameters (α, n and l). The Van Genuchten soil parameters applied for the HTESSEL soil textures are presented in Appendix A.3.

The interception reservoir is modelled as a small layer that collects water from precipitation and

dew on top of the soil and vegetation. The tile coverage of the interception reservoir is a function of the LAI area contributions from high and low vegetation tiles. The capacity of the interception reservoir is approximately 1 mm and intercepted water evaporates with potential rates. At each timestep three parameters are calculated: interception storage, throughfall and interception evaporation. The throughfall is the part of the precipitation that recharges the soil water.

Surface runoff is generated when the surface water flux exceeds the maximum infiltration rate into the soil. Surface runoff is described by Equation 3.12.

$$R = T + M - I_{\max} \tag{3.12}$$

T is the throughfall of precipitation, M snowmelt and $I_{\max}$ the maximum infiltration rate. HTESSEL describes a variable infiltration rate $I_{\max}$ within a gridpoint as a function of the soil moisture in the top 50 cm of the soil(the effective depth for surface runoff), soil type and orography. Subsurface runoff is the water that leaves the system by drainage from layer four which is defined by the hydraulic conductivity of this layer. Besides, all moisture above the saturation of a model layer generates subsurface runoff.

The transpiration flux is a function of canopy resistance, that is a function the unfrozen soil moisture content and rooting distribution (Equation 3.3 and 3.6). The soil moisture is recharged by infiltration from precipitation and diffusion between the layers and is depleted by subsurface drainage and root extraction. Root extraction is defined by Equation 3.13. The contribution of each layer to the root extraction is a function of the root fraction (R_k), the unfrozen soil moisture (θ_k) and the layer thickness (D_k) and the total tile evaporation rate E and tile coverage C. The evaporation rate is calculated by Equation 3.2 and distributed over the four model layers for root extraction calculation. The total root extraction from each layer is the sum of the different tiles that contribute to transpiration (dry low vegetation, dry high vegetation and snow underneath high vegetation).

$$\rho_{\mathrm{w}} S_{\theta,k} = \sum_i C_i \frac{E_i}{D_k} \frac{R_k \theta_k}{\sum_j R_j \theta_j} \tag{3.13}$$

Equation 3.11 is numerically solved applying an upper and lower model boundary: precipitation minus runoff minus evaporation at the top and free drainage at the bottom. The water flux in Equation 3.11 is defined at the interface between the layers ($F_{k+1/2}$) and the states θ_k and $S_{\theta,k}$ at full layers. The differential equation is solved by a triadiagonal system of equations. For details of this solution refer to Chapter 8.11 of the IFS Documentation and the related model codes (ECMWF, 2016).

3.2.5 Rootzone storage capacity

The total rootzone storage capacity (S_{R}) is not a modelling parameter in HTESSEL. However, $S_{\mathrm{R,HTESSEL}}$ can be derived from the plant available soil water ($\theta_{\mathrm{cap}} - \theta_{\mathrm{pwp}}$) and the total depth of vegetation's roots (Equation 3.14). All vegetation types except desert and tundra (index 8 and 9) have roots in all four model layers, which means that eventually all the water in the four model layers can be extracted by the roots. Rootzone depth z in Equation 3.14 is therefore equal to the total modelling depth, except for desert and tundra. Soil type is the only spatial variable defining the total rootzone storage capacity in HTESSEL because the model depth is fixed. Figure 3.2 schematises rootzone parameterisation in HTESSEL with red lines representing boundaries of roots influence area. The left image represents a model layer as a water bucket. All water below the wilting point and above the field capacity is not available to roots. The middle figure represents the available water bucket with instantaneous root extraction which is dependent on the root distribution and the soil moisture in a model layer. The right image represents the total available water, which represents $S_{\mathrm{R,HTESSEL}}$ and is calculated by Equation 3.14.

$$S_{\mathrm{R,HTESSEL}} = z(\theta_{\mathrm{cap}} - \theta_{\mathrm{pwp}}) \tag{3.14}$$

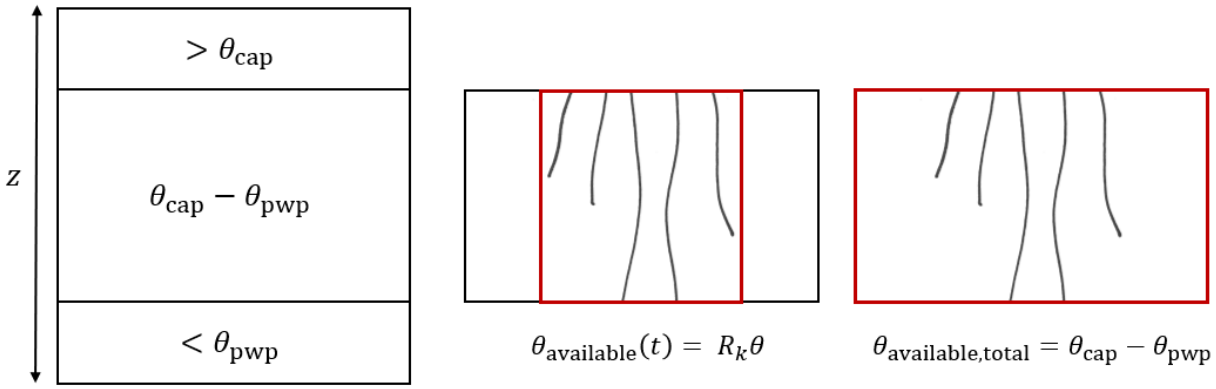

Figure 3.2: Water bucket representation of a modelling layer. Left: full model layer with water contents. Middle: instantaneous root available water. Right: Long-term root available water.

3.3 Model code

The surface code of the offline HTESSEL model contains several modules that describe the parameterisation of the land-surface, all coded in Fortran90. The relevant technical information about the different modules in the offline HTESSEL model is presented in this section.

The SUSURF module initialises land-surface constants before model integration. SUSSOIL and SUSVEG are the two relevant initialised modules called by SUSURF. In SUSSOIL the Van Genuchten soil properties are described and in SUSVEG the vegetation characteristics (e.g. stomatal resistance, albedo and vegetation coverage).

The land-surface parameterisation is described by two main routines: SURFEXCDRIVER and SURFTSTP. SURFEXCDRIVER computes tile fluxes and skin temperatures and is part of the vertical diffusion scheme. It calls three relevant routines:

- VSURF: this module prepares surface boundary conditions. The resistance functions for evaporation are described here.
- VEVAP: this module computes the evapotranspiration of each tile. It sums the interception evaporation, high and low vegetation evaporation and bare soil evaporation fluxes.
- VSFLX: this module computes the surface fluxes for each tile (momentum, heat and moisture flux).

In SURFTSTP land values of temperature, moisture and snow are updated. It uses several subroutines that compute separate elements of the model. The relevant subroutines are:

- SRFROOTFR: this module computes the fraction of roots for each soil layer, for each vegetation type applying Equation 3.8.
- SRFWL: this module computes the changes in the interception reservoir. It computes the next time step interception layer storage, throughfall and tile evaporation from the interception layer.
- SRFWEXC-VG: this module is part of the soil water budget equations, based on the Van Genuchten scheme. Soil moisture, soil temperature, throughfall, snowmelt, tile evaporation

are inputs for this routine. Surface runoff, root extraction for the different soil layers and hydraulic soil properties are calculated. It returns modified diffusivities and the right hand side of the tridiagonal system of equations.

- SRFWDIF: this module solves the tridiagonal system of equations for soil moisture.
- SRFWINC: this module computes the next timestep soil moisture by solving the system of soil moisture equations.
- SRFWNG: this module computes corrections in the interception layer and the soil water. The intercepted water should be non-negative and is bounded by the maximum interception capacity. Soil water should also be non-negative and is bounded by soil saturation. The excessive water drains and is accounted for as subsurface runoff.

The model generates six output files with fixed parameters, water fluxes, energy fluxes, evaporative fluxes, 2 meters atmospheric parameters and internal model parameters.

4 Methodology

This chapter presents the methodology applied in this research. Section 4.1 describes the study area and Section 4.2 the data sources used. In Section 4.3 the catchment characteristics are presented. Section 4.4 and Section 4.5 present the mass balance approach and the model approach.

4.1 Study area

The research is performed for 15 river catchments in Australia. Australia is a country with different climatic regions which is of interest for this research because vegetation coverage and rootzone storage development are dependent on climatic conditions. Moreover, the Australian Bureau of Meteorology (BoM) provides easily accessible streamflow data for 222 hydrological reference stations (BoM, 2015).

River catchments were selected based on the following three criteria:

Size: catchment area is of the order of magnitude of a gridpoint of 0.5° x 0.5° $\sim 2500\,\mathrm{km}^2$;

Location: catchments are spread around Australia covering different climatic regions with different vegetation types;

Streamflow: available streamflow timeseries of at least 25 years, no data gaps and realistic rainfall-runoff characteristics.

Figure 4.1 presents spatial variation in annual mean precipitation in Australia and the location of the 15 selected river catchments. Table 4.1 presents the study catchment names, short names, hydrological reference stations from BoM, coordinates and areas (BoM, 2015).

Table 4.1: Study catchments and their characteristics (BoM, 2015)

Catchment name	**Catchment short name**	**Hydrological station**	**Coordinates**	**Area (km^2)**
Abercrombie River	A	412028	149.325°E, 33.955°S	2631
Avoca River	Av	408200	143.299°E, 36.438°S	2677
Dogwood Creek	D	422202B	150.179°E, 26.709°S	2882
East Alligator River	EA	G8210010	133.332°E, 12.717°S	2398
East Baines River	EB	G8110004	130.034°E, 15.766°S	2443
Gregory River	G	912101A	139.252°E, 18.643°S	12652
Herbert River	He	116006B	145.922°E, 18.491°S	7487
Kent River	K	604053	117.087°E, 34.888°S	1786
Mitchell River	Mi	919003A	144.290°E, 16.472°S	7734
Murrumbidgee River	Mu	410761	149.101°E, 35.540°S	5158
Namoi River	Na	419005	150.778°E, 30.678°S	2532
Normanby River	No	105101A	144.839°E, 15.281°S	2306
Paroo River	P	424201A	144.786°E, 28.689°S	22885
Reedy Creek	R	403209A	146.345°E, 36.332°S	5506
Wenlock River	W	925001A	142.638°E, 12.454°S	3290

4.2 Data collection

4.2.1 Reanalysis data

In climate studies historical and present-day weather observations are important for future predictions. However, weather observation stations are not evenly distributed around the globe and

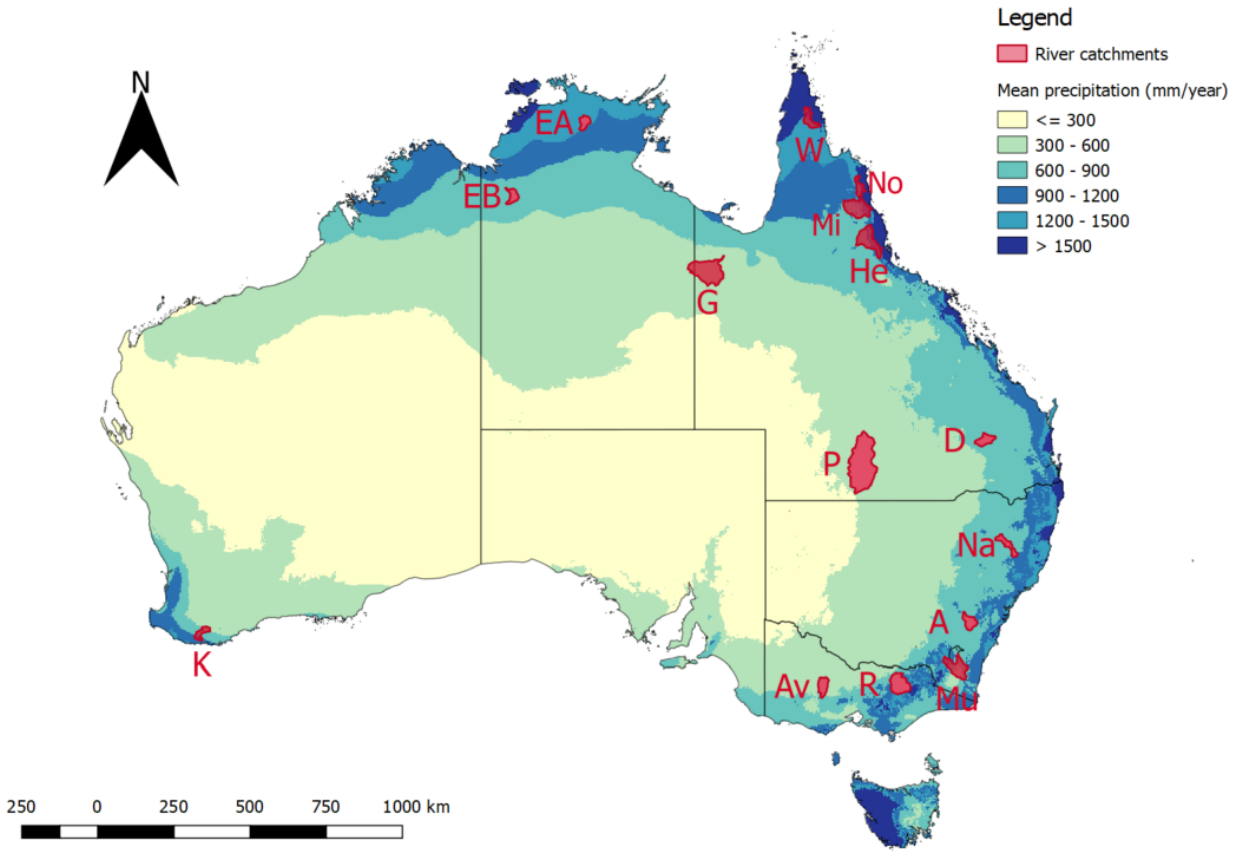

Figure 4.1: Spatial variation in annual mean precipitation (1961-1990) in Australia and the location of the study catchments (BoM, 2015).

historical records are limited. Reanalysis data provides a solution for this limitation of observations in space and time. Past observations are reanalysed using forecasting models and data assimilation systems to create historical datasets. These datasets describe climate variables for the atmosphere, the land surface and oceans on a global scale (Keeley, 2019).

The Global Soil Wetness Project is a research program providing providing global historical data on hydro-energy-eco systems. The third phase of GSWP (GSWP-3) is a recently developed dataset by Hyungjun Kim that describes atmopsheric boundary conditions (e.g. precipitation, air temperature and wind speed) on a 3 hourly timescale from 1901-2010 for a 0.5° x 0.5° grid (Kim, 2017). This dataset is used as input for the mass balance approach and the HTESSEL land surface model.

4.2.2 Energy flux data

The Fluxcom dataset provides a gridded product of energy fluxes based on Fluxnet eddy covariance towers, satellite observations and meteorological data (Jung et al., 2019). The three data sources are interpolated using machine learning techniques and monthly variations in net radiation, latent and sensible heat fluxes are estimated. In this research, the RS+METEO dataset that is based on meteorological data from GSWP-3 is used for analysing latent heat fluxes. Global mean and seasonal energy fluxes are compared to global energy datasets and large similarities were found. Therefore the dataset is considered as a promising tool for land model evaluations (Jung et al., 2019).

Reliability Fluxcom dataset

A water balance analysis is performed in order to check the reliability of this dataset in the study catchments. Latent heat fluxes can be converted into evaporation fluxes by Equation 4.1 with E the total evaporation flux in ms^{-1}, LE the latent heat flux in Wm^{-2}, λ_{E} the latent heat of vaporization which is equal to $2.26 \times 10^6\,\mathrm{Jkg}^{-1}$ and ρ the density of water which is $1000\,\mathrm{kgm}^{-3}$.

$$E = \frac{\mathrm{LE}}{\rho \lambda_{\mathrm{E}}} \tag{4.1}$$

The water balance is calculated for the 15 study catchments with GSWP-3 precipitation, Fluxcom derived evaporation and observed river discharge for the time-period 1973-2010.

4.2.3 Hydrological data

Precipitation

Daily precipitation is derived from the GSWP-3 dataset for the 15 study catchments. Snowfall is not considered because snowfall is very rare in the studied areas. Conversion from gridded data to catchment data is performed applying weighted averaging.

Streamflow

Streamflow data is obtained from the Australian BoM (BoM, 2015). The 15 stations and the abbrevation names are presented in Figure 4.1. The length of the streamflow timeseries vary per station. The longest time-series for which station data and GSWP-3 data are available is 1973-2010.

Evaporation

It is complex to directly measure evaporation fluxes, in contrary to for example precipitation, streamflow and temperature. Different methods that directly measure actual evaporation rates exist (e.g. lysimeters and eddy covariance method). These direct measurements require costly instrumentation or intense fieldwork activities and available data is therefore limited. Global gridded evaporation datasets are not used because they either contain information on the vegetation's rootzone (reanalysis data) or describe point scale measurements that are not representative on catchment scales (Fluxnet) (Keeley, 2019; US Department of Energy, 2019). Due to the lack of useful data, potential evaporation fluxes are estimated indirectly based on meteorological data. Actual evaporation rates are derived from potential evaporation rates based on the water balance.

Potential evaporation models provide a solution to the lack of observational data. These models differ in data requirements and complexity. Comparison studies based on Fluxnet tower fluxes provide insight in the performance of different modelled potential evaporation estimates. It was found that simple formulations based on temperature and radiation data provide better potential evaporation estimates than the complex Penman-Monteith equation that requires a lot of data (Maes, Gentine, Verhoest, and Miralles, 2019; Oudin et al., 2005). In this study the Hargreaves and Samani formulation is applied for estimating potential evaporation rates. This method only requires temperature and top of the atmosphere radiation data and was used in the study of Gao et al. (2014) on mass balance derived rootzone storage estimates. Temperature data is obtained from the GSWP-3 dataset and top of the atmosphere radiation data from Mines ParisTech (Mines ParisTech, 2014).

Equation 4.2 describes the Hargreaves and Samani potential evaporation formulation. λ_{E} is the latent heat of vaporization, α a constant, equal to 0.00023, R_{e} is the top of the atmosphere radiation and T_{a}, T_{min} and T_{max} the average, minimum and maximum daily temperatures.

$$\lambda_E E_p = \alpha R_e (T_a + 17.8)\sqrt{T_{max} - T_{min}} \tag{4.2}$$

Annual actual evaporation rates are based on the water balance. Assuming the change in storage of a long time period is zero, the long-term average actual evaporation is estimated by Equation 4.3. Daily evaporation rates are derived from the ratio between long term mean actual and potential evaporation. Detailed formulations for the derivation of actual evaporation are described in Section 4.2.3.

$$\overline{E_a} = \overline{P} - \overline{Q} \tag{4.3}$$

4.2.4 Geographical data

Topography

Topography is driving land surface water fluxes. Steep terrains have smaller water retention than flat terrains. Digital elevation maps (DEM) provide information on topography. A DEM from USGS is obtained in order to analyse the hydrological behaviour of the river catchments (USGS, 2010).

Vegetation

Vegetation is controlling the water fluxes between the land surface and the atmosphere by transpiration. Information on vegetation coverage in river catchments is needed for the understanding of hydrological processes. Dominating high and low vegetation types (T_H and T_L) and the high and low vegetation coverage (C_H and C_L) on a global 0.5° x 0.5° grid are derived from the Global Land Cover Characteristics (GLCC1.2) dataset. This dataset is based on 1 year of data of Advanced Very High Resolution Radiometer data, eco-regions, digital elevation models and map data (ECMWF, 2016). The vegetation types are based on the classification presented in Table 3.1.

Soil

Soil texture data is derived from the from the FAO/UNESCO Digital Soil Map of the World (FAO, 2003). The following six different soil types are distinguished: Coarse, Medium, Medium-fine, Fine, Very fine and Organic.

4.3 Catchment characteristics

Tabulated catchment characteristics are presented in Appendix B, with hydrological, climatic, vegetation and soil characteristics. Appendix C presents the monthly mean precipitation and potential evaporation rates based on GSWP-3 and Hargreaves and Samani for the study catchments. The figure clearly illustrates rainfall and potential evaporation seasonalities.

Figure 4.2 presents the different catchments in the Budyko framework. The figure shows that the aridity index is larger than 1 in all study catchments which indicates that water availability is limiting the evaporation rates. Based on the catchment characteristics, the study catchments are divided into three climatic subgroups: tropical, temperate and mediterranean.

Catchments EA, EB, G, He, Mi, No and W are classified as tropical catchments. These catchments have strong rainfall seasonality with a dry season from May to October. In the Budyko curve (Figure 4.2) these catchments, except EB and G, are clustered with aridity indices in between 1 and 2 and $\overline{E_a}/\overline{P}$ smaller than 0.85. Catchments EB and G are covered with low vegetation and receive less rainfall than the other tropical catchments and have therefore higher aridity indices

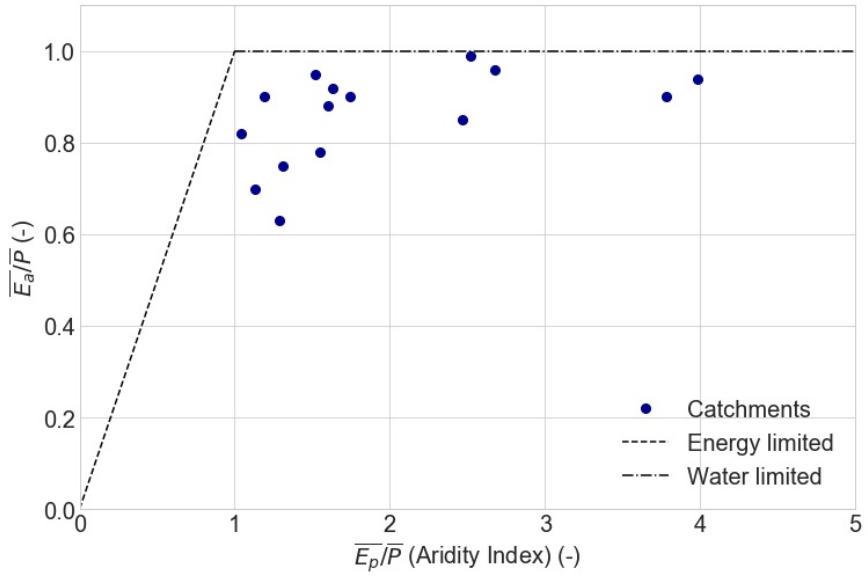

Figure 4.2: Study catchments plotted in the Budyko framework applying long term average water fluxes (1973-2010)

(AI > 2). Though, the catchments are considered as tropical catchments due to similar rainfall and potential evaporation patterns as EA, He, Mi, No and W.

Catchments A, D, Na, Mu and P are classified as temperate catchments. Precipitation seasonality indices are maximum 0.40 indicating year-round rainfall. The dry and wet seasons are variable for the different catchments. Aridity indices are higher than in the tropical catchments but $\overline{E_a}/\overline{P}$ is higher due to smaller annual rainfall rates. Catchment P has an aridity index of 4.38 and is thereby the driest river catchment in this study. It is covered by low vegetation and receives little precipitation during the year with more rain in summer than in winter.

Catchments Av, K and R are classified as mediterranean catchments. Aridity and seasonality indices are similar to the temperate catchments but the hydrological signal is different. The time-lag between maximum precipitation and potential evaporation is 5 or 6 months, which distinguishes these catchments from the temperate and tropical regions. As presented in Appendix C, precipitation rates are higher in May to October when potential evaporation rates are low. The other months of the year, rainfall and actual evaporation rates are limited, even though potential evaporation is high.

4.4 Mass balance approach

4.4.1 Hydrological year

In hydrology it is common to define hydrological years instead of calender years. In this study the hydrological year starts the month after the wettest month. The wettest month is determined by the difference between monthly mean precipitation and potential evaporation. It is assumed that the storage deficit at the end of the hydrological year - the last day of the wettest month - is at its minimum. All calculations are performed from the start of the hydrological year in 1973 to the end of the hydrological year in 2010.

4.4.2 Transpiration

Long term actual evaporation is derived from the water balance. However, for shorter timescales the storage term in the water balance ($\frac{dS}{dt}$) is not negligible. Therefore, actual evaporation rates are

derived from potential evaporation rates for daily and monthly timescales. Section 4.2.3 describes the calculation of potential evaporation. As mentioned in Section 2.1 actual evaporation can be divided into four different evaporation fluxes (interception, open water and soil evaporation and transpiration). Transpiration is the only flux that transports water from the root zone to the atmosphere and is therefore of interest in this research. Open water evaporation is not relevant because this flux is not related to vegetation. Interception and soil evaporation are accounted for in one interception flux. This flux can be calculated assuming a maximum interception storage capacity for each catchment ($S_{\mathrm{i,max}}$). It is assumed that all intercepted water is directly transported back to the atmosphere, following potential evaporation rates, without recharging the soil water. When cumulative precipitation exceeds the interception storage capacity, water infiltrates and recharges the soil water. The part of the precipitation that reaches the subsurface storage is the effective precipitation (P_e) and is responsible for recharging the soil water.

The water balance for interception storage is described by Equation 4.4.

$$\frac{dS_{\mathrm{i}}}{dt} = P - E_{\mathrm{i}} - P_{\mathrm{e}} \tag{4.4}$$

with S_{i} the interception storage in mm, dt the timestep in days, P the precipitation in mm/day, E_{i} the interception evaporation in mm/day and P_{e} the effective precipitation in mm/day.

The interception evaporation and the effective precipitation for each timestep (dt is 1 day) are described by Equations 4.5 and 4.6.

$$E_{\mathrm{i}} = \begin{cases} E_{\mathrm{p}} & \text{if } E_{\mathrm{p}}dt < S_{\mathrm{i}} \\ \frac{S_{\mathrm{i}}}{dt} & \text{if } E_{\mathrm{p}}dt \geq S_{\mathrm{i}} \end{cases} \tag{4.5}$$

$$P_{\mathrm{e}} = \begin{cases} 0 & \text{if } S_{\mathrm{i}} \leq S_{\mathrm{i,max}} \\ \frac{S_{\mathrm{i}} - S_{\mathrm{i,max}}}{dt} & \text{if } S_{\mathrm{i}} > S_{\mathrm{i,max}} \end{cases} \tag{4.6}$$

with $S_{\mathrm{i,max}}$ the maximum interception storage capacity in mm and E_{p} the potential evaporation in mm/day.

The longterm average transpiration flux for the timeseries (1973-2010) can be calculated with a water balance where the effective precipitation is the incoming flux and discharge and transpiration are the outgoing fluxes (Equation 4.7 and 4.8).

$$\frac{dS}{dt} = \overline{P_{\mathrm{e}}} - \overline{Q} - \overline{E_{\mathrm{t}}} = 0 \tag{4.7}$$

$$\overline{E_{\mathrm{t}}} = \overline{P_{\mathrm{e}}} - \overline{Q} \tag{4.8}$$

Daily transpiration rates are estimated following the approach applied by Nijzink et al. (2016). Daily potential evaporation is linearly scaled with the ratio of long-term transpiration and potential evaporation by Equation 4.9 (Capell et al., 2016).

$$E_{\mathrm{t}} = E_{\mathrm{p}} \frac{\overline{E_{\mathrm{t}}}}{\overline{E_{\mathrm{p}}}} \tag{4.9}$$

with $\overline{E_{\mathrm{t}}}$ and $\overline{E_{\mathrm{p}}}$ the long term average evaporation rates and E_{t} and E_{p} daily evaporation rates.

4.4.3 Storage deficits

The subsurface storage deficit (S_D) is the cumulative difference between daily effective precipitation and transpiration fluxes. It is assumed that the storage deficit is equal to zero at the start of the hydrological year. At the end of the timeseries, the storage deficit returns to zero because the long term water balance is closed. The maximum deficit over the analysed period represents the total storage volume available for vegetation to transpire in a catchment, assuming vegetation has continuous access to water. Equation 4.10 describes the storage deficits and Equation 4.11 the derived rootzone storage capacity. Figure 4.3 presents an explanatory example of the storage deficit estimation. This figure presents the storage deficits for 50 days in the Abercrombie catchment. The estimated total rootzone storage capacity of this catchment is 54.2 mm for the selected 20 days.

$$S_\mathrm{D}(t) = \int_{t_0}^{t_1} (P_\mathrm{e} - E_\mathrm{t})dt \tag{4.10}$$

$$S_\mathrm{R}^* = \max(S_\mathrm{D}(t)) \tag{4.11}$$

S_D is the daily storage deficit calculated over timeseries t_0 to t_1 in mm. S_R^* (mm) is the total rootzone storage capacity of the catchment, which is equal to the maximum storage deficit over the studied timeseries.

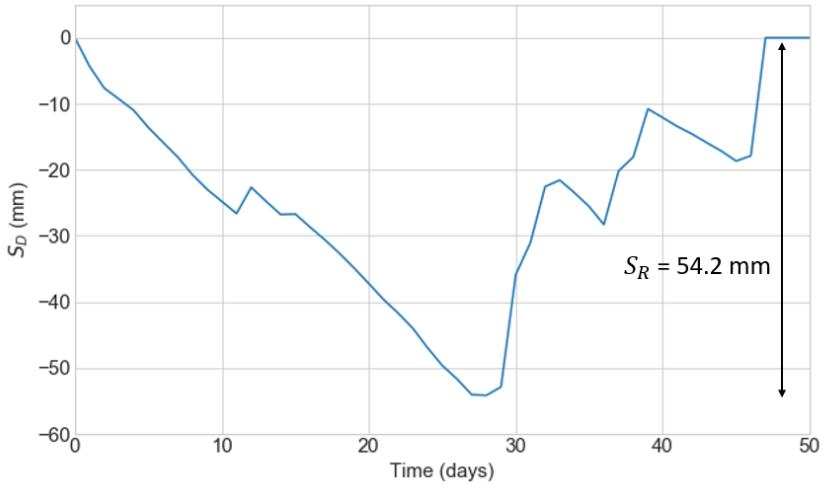

Figure 4.3: Storage deficits of the Abercrombie Catchment (01-01-1973 - 20-02-1973). The rootzone storage capacity S_R^* is estimated as the maximum storage deficit over the presented timeseries

Figure 4.4 presents the result of the storage deficit calculation of the Abercrombie catchment over the timeseries 1973-2010. The daily storage deficits show a remarkable result because multi-year droughts are observed between 1978 and 1983 and between 2001 and 2010 (Australia's Millennium drought) van Dijk et al., 2013). These two multi-year decreases in storage deficits correspond to periods with less than average precipitation. Transpiration rates are close to constant over the entire timeseries when estimated by Equation 4.9. It is however expected that the transpiration is lower in years with low precipitation rates due to a water shortage. In wet years, the transpiration flux is expected to be closer to the potential evaporation because there is more water available. In order to represent the dynamic character of transpiration on annual scales, an iterative approach in estimating the transpiration flux is applied instead of the initial approach given by Equation 4.9. This approach is explained in Section 4.4.4.

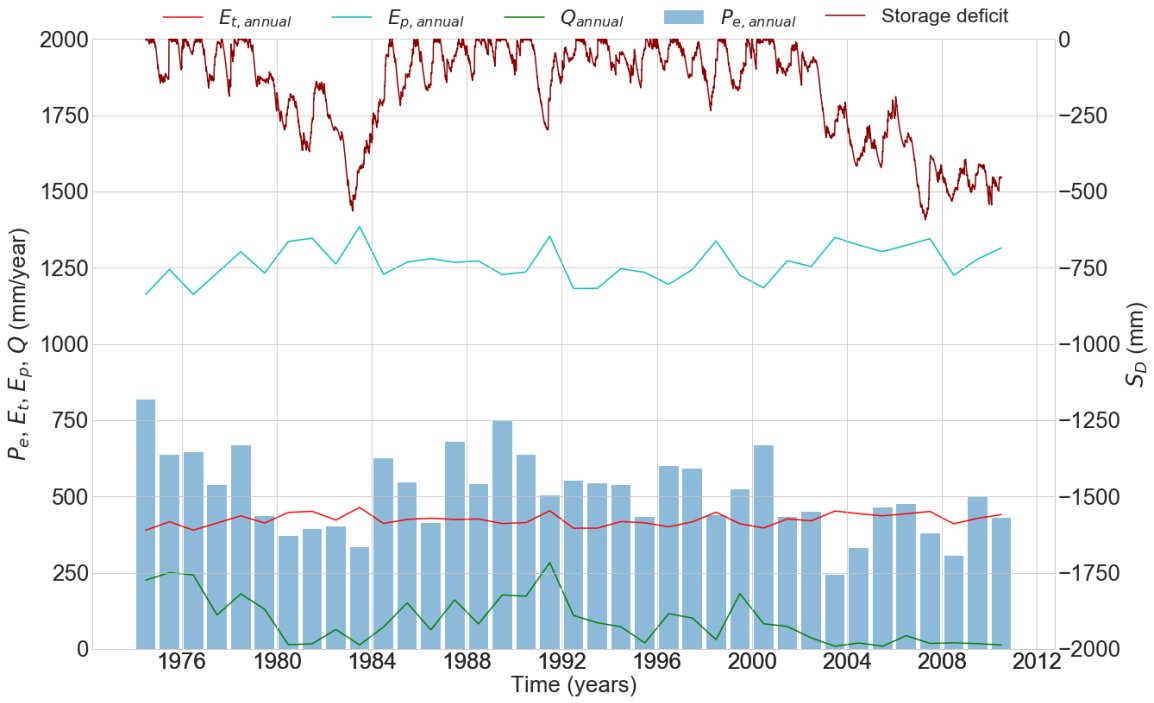

Figure 4.4: Storage deficits based on transpiration rates estimated with Equation 4.9 for the Abercrombie Catchment from 1973-2010

4.4.4 Storage deficit iteration method

An iterative approach is applied in order to account for the annual dynamics of the transpiration flux. It is assumed that the storage change over the entire timeseries (1973-2010) is zero. Initially, the storage deficits are based on Equation 4.9. The iterative method is based on the annual water balance, which is in contrary to the long term water balance not closed. The following iteration steps describe the storage deficit iteration method. Step 3 to 6 are executed iteratively. The symbols a and d represent daily and annual values, t_0 and t_1 represent the start and end of the hydrological year.

1. Calculate E_t and corresponding storage deficits with Equation 4.9 and 4.10.
2. Calculate the storage change over each hydrological year in the timeseries.

$$\frac{dS_\mathrm{a}}{dt} = S_\mathrm{D}(t_0) - S_\mathrm{D}(t_1) \tag{4.12}$$

3. Calculate annual total transpiration following the water balance.

$$\overline{E_\mathrm{t,a}} = \overline{P_\mathrm{e,a}} - \overline{Q_\mathrm{a}} - \frac{dS_a}{dt} \tag{4.13}$$

4. Calculate daily transpiration rates.

$$E_\mathrm{t,d} = \frac{\overline{E_\mathrm{t,a}}}{\overline{E_\mathrm{p,a}}} E_\mathrm{p,d} \tag{4.14}$$

5. Calculate storage deficits.

$$S_\mathrm{D} = \int_{t_0}^{t_1} (P_\mathrm{e} - E_\mathrm{t}) dt \tag{4.15}$$

6. The input storage deficit of iteration i is the average of iteration $i-1$ and $i-2$

$$S_{\mathrm{D},i} = \frac{S_{\mathrm{D},i-1} + S_{\mathrm{D},i-2}}{2} \tag{4.16}$$

Different modelling constraints are set to the iterative method in order to optimise the estimated storage deficits.

First, a water balance constraint is set because the water balance should close over the entire timeseries, as preliminary assumed. The water balance is defined as $\mathrm{WB} = \sum P_{\mathrm{e}} - \sum Q - \sum E_{\mathrm{t}}$ over the studied timeseries. A shortage or surplus of water of 2% of the total effective precipitation over the timeperiod 1973-2010 is accepted (Equation 4.17). In case the water balance after an iteration does not fulfill this requirement, the excess or lacking water is distributed over the timeseries proportional to the estimated transpiration in order to close the water balance.

$$\frac{\mathrm{WB}_{1973-2010}}{\sum P_{\mathrm{e},1973-2010}} > 2\% \tag{4.17}$$

Secondly, two constraints were set to the estimated transpiration rates.

- The annual transpiration should be larger than zero because negative transpiration is physically not possible (constraint a).

$$\frac{\overline{E_{\mathrm{t,a}}}}{\overline{E_{\mathrm{p,a}}}} > 0 \tag{4.18}$$

- The daily transpiration is bounded by a fraction f of 25% (constraint b) and 50% (constraint c) of the initial transpiration estimated with Equation 4.9.

$$\frac{\overline{E_{\mathrm{t}}}}{\overline{E_{\mathrm{p}}}} - f\frac{\overline{E_{\mathrm{t}}}}{\overline{E_{\mathrm{p}}}} < \frac{\overline{E_{\mathrm{t,a}}}}{\overline{E_{\mathrm{p,a}}}} < \frac{\overline{E_{\mathrm{t}}}}{\overline{E_{\mathrm{p}}}} + f\frac{\overline{E_{\mathrm{t}}}}{\overline{E_{\mathrm{p}}}} \tag{4.19}$$

The storage deficits obtained when applying the different constraints are analysed. Table 4.2 presents an overview of the advantages and disadvantages of the different constraints based on the results of ten iterations. The goal of the iteration method is to account for transpiration dynamics. All three constraints lead to a different amount in variation of the annual transpiration flux. Constraint (a) leads to the largest variations, followed by constraint (c) and (b) that constrict the variations more strongly. The main disadvantage of constraints (a) and (c) is the fact that the multiyear droughts, as observed in Figure 4.4, completely disappear. The smoothening of the storage deficits in constraints (a) and (c) leads to a loss of the extremes, that are defining a catchments S_{R}. Therefore, the rootzone storage capacities obtained with constraint (b) are applied in this research, even though the variation in E_t for constraint (b) is limited.

Table 4.2: Overview of advantages and disadvantages of different constraints in the storage deficit iteration method

Constraint	**Advantages**	**Disadvantages**
(a) $\frac{\overline{E_{\mathrm{t,a}}}}{\overline{E_{\mathrm{p,a}}}} > 0$	No boundaries to E_{t}	Multiyear droughts disappear
(b) $f = 25\%$	Variation in E_{t}	E_{t} goes to model boundaries
(c) $f = 50\%$	Variation in E_{t}	Multiyear droughts disappear

4.4.5 Return periods

The return period of an event is defined as the time interval in which it is likely that the event will occur. In Section 4.4.3 the total rootzone storage capacity (S_{R}^{*}) is described as the maximum storage deficit over a certain time period, assuming the E_t estimate is perfect and ecosystems avoid water stress. Ecosystems design their rooting system in order to overcome dry periods with certain return periods, dependent on vegetation type (Gao et al., 2014; Lan Wang-Erlandsson et al., 2016). It is likely that the drought return periods are lower for low vegetation (e.g. grasses) than for high vegetation (e.g. forests) because low vegetation develop smaller rooting systems. Grasses and other low vegetation types go dormant during extreme droughts while forests invest in their rooting system (Arend, Brunner, Dawes, Sperisen, & Herzog, 2015).

The S_{R} corresponding to drought return periods are estimated using the Gumbel extreme value distribution (Gumbel, 1941). The reduced variate y is defined by Equation 4.20.

$$y = -\ln(-\ln(1 - \frac{1}{T})) \tag{4.20}$$

T is the return period of annual maximum S_{D} estimates. The reduced variate y is linearly related to the annual extreme storage deficits, defined as the difference between the maximum and minimum storage deficit in a single hydrological year. This linear relation results in S_{R} estimates that correspond to different drought return periods for the studied ecosystem.

4.4.6 Catchment rootzone storage capacities

The method applied for estimating rootzone storage capacities is explained in sections 4.4.1 to 4.4.5. This section presents the final assumptions made in estimating S_{R}.

The rootzone storage capacities of each catchment are estimated based on the storage deficit iteration method and drought return periods. HTESSEL makes a distinction between high and low vegetation. Therefore, the rootzone storage capacities estimated with the mass balance approach are divided into $S_{\mathrm{R,low}}$ and $S_{\mathrm{R,high}}$. The low and high vegetation S_{R} are based on drought return periods T_{low} and T_{high} of 2 and 40 years, respectively. Return periods of 1.5 and 3 and 20 and 60 years for low and high vegetation, respectively, are applied for sensitivity analysis. Table 4.3 presents the three combinations of model assumptions applied in this research.

Table 4.3: Input parameters for low, average and high rootzone storage capacity estimation

Parameter	**Low**	**Average**	**High**
$S_{\mathrm{i,max}}$[mm]	3.5	2.5	1.5
f [%]	±35%	±25%	±15%
T_{low} [years]	1.5	2	3
T_{high} [years]	20	40	60

S_{R} represents the total water storage capacity in the rootzone in the catchment. The fractions of the dominant high and low vegetation types determine the catchments storage capacity following Equation 4.21. The high and low vegetation type fractions (C_{low} and C_{high}) are obtained from the vegetation dataset described in Section 4.2.4.

$$S_{\mathrm{R,catchment}} = C_{\mathrm{low}} S_{\mathrm{R,low}} + C_{\mathrm{high}} S_{\mathrm{R,high}} \tag{4.21}$$

4.5 Model approach

The total rootzone storage capacity in the HTESSEL model is described by Equation 3.14. Mass balance S_R estimates can be implemented by changing modelling depths and available water.

4.5.1 Modelling depth

HTESSEL describes three different model layer depths: RDAT, RDAW and RDAI for temperature, moisture and sea ice, respectively. In the current model, all three layer thicknesses are the same. Viterbo and Beljaars (1995) states that the soil discretisation is based on modelling the soil temperature budget and moisture depths are the same for simplicity of the code. Sea ice depths are not relevant in the study area of this research.

Method

Changing the moisture depths (RDAW) leads to a change in total soil water storage. Figure 4.5 presents the same water bucket schematisation as in Figure 3.2 but with a modified moisture depth. The left image represents the total rootzone storage capacity in a model layer in the current HTESSEL model. The middle figure represents the same layer, with a modified depth z_2. Instantaneous root extraction is a function of the rooting distribution in this layer. The right figure represents the total rootzone storage capacity in the layer with modified depth z_2.

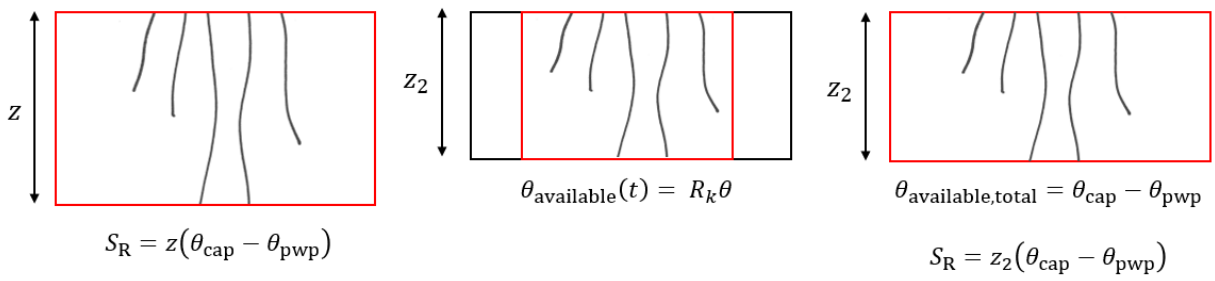

Figure 4.5: Water bucket representation of a modelling layer with a modified moisture depth. The red lines represent the boundaries of root available water. Left: total root available water in the base model. Middle: instantaneous root available water with depth z_2. Right: Long-term root available water with depth z_2.

Modified depths directly influence the soil water budget by Equation 3.11. The total water storage in the system changes, leading to a change evaporation rates and subsurface water fluxes.

$$\frac{\partial\theta}{\partial t} = \frac{\partial}{\partial z}(\lambda\frac{\partial\theta}{\partial z} - \gamma) + S_\theta \tag{4.22}$$

For the study catchments the total model depths (z_{total}) are calculated with Equation 4.23.

$$z_{total} = \frac{S_{R,MB}}{\theta_{cap}} - \theta_{pwp} \tag{4.23}$$

The modified depth of layer 4 is calculated with Equation 4.24.

$$z_4 = z_{total} - z_1 - z_2 - z_3 \tag{4.24}$$

In case this formulation leads to $z_4 < 0$, z_4 is set to 0.2 and z_3 is calculated by Equation 4.25.

$$z_3 = z_{\text{total}} - z_1 - z_2 - 0.2 \tag{4.25}$$

Appendix G.1 presents the modified model depths for the study catchments.

Model code

Modelling depths are defined in the SUSSOIL module. Moisture depths (RDAW) are modified in this module. Appendix D presents the adapted SUSSOIL module.

Limitations

Changing the moisture depths but not the temperature depths leads to a mismatch between temperature and moisture layers. In the heat budget calculations in module SRFT, soil temperature is a function of soil moisture. A mismatch between the layers could lead to inconsistencies in the calculation of soil temperatures. Moreover, the fraction of frozen soil, calculated in module SRFWEXC-VG, is a function of soil temperatures. It was chosen to change the depth of the bottom layer, and if needed also layer 3 in order to minimise the inconsistencies in model layers.

4.5.2 Moisture availability

The total rootzone storage capacity in HTESSEL is a function of the available soil moisture for root extraction ($\theta_{\text{cap}} - \theta_{\text{pwp}}$). The values for θ_{cap} and θ_{pwp} are derived from soil type dependent soil porosity (θ_{sat}) and Van Genuchten parameters (Appendix A.3). $S_{\text{R,MB}}$ can be implemented in HTESSEL by changing these soil parameters. Modification of θ_{sat}, leading to changed θ_{cap} and θ_{pwp}, directly changes the available soil moisture for transpiration. Soil parameters also influence other model processes than transpiration such as surface runoff, hydraulic conductivity and diffusivity and thermal diffusivity. Besides this, unrealistic soil parameters are obtained when θ_{sat} is modified. For example, to represent the total rootzone storage capacity of low vegetation in Abercrombie catchment of 134 mm, a porosity of 0.11 is calculated, instead of the medium soil porosity of 0.44. This value for porosity occurs in rocky subsurfaces which is not realistic (Fitts, 2002). This approach, where model parameters are modified from the top, is not considered further in this research due to unrealistic representation of the subsurface and the influence on other model processes than transpiration. The HTESSEL parameterization allows for changes in root available water in the formulation of root extraction only. This method does not influence other processes than root extraction.

Method

HTESSEL describes the available water for root extraction by the liquid water content (ZLIQ) that is computed by Equation 4.26. ZLIQ depends on relative soil moisture (θ), bounded by field capacity and wilting point, and the fraction of frozen soil (ZF), that depends soil temperatures.

$$\text{ZLIQ}_k = \max(\theta_{\text{pwp}}, \min(\theta_{\text{cap}}, \theta_k(1 - \text{ZF}))) \tag{4.26}$$

ZLIQ is used in two model formulations: canopy resistance and root extraction rate.

Canopy resistance is calculated in the V-SURF module. Equations 4.27 to 4.29 present the calculation of canopy resistance in this module. The different functions in Equation 4.29 are explained in Section 3.2. The canopy resistance is linearly dependent on the water that is available for root extraction (ZLIQ).

$$\overline{\theta} = \sum_{k=1}^{4} R_k \mathrm{ZLIQ}_k \tag{4.27}$$

$$f_2 = \frac{\overline{\theta} - \theta_{\mathrm{pwp}}}{\theta_{\mathrm{cap}} - \theta_{\mathrm{pwp}}} \tag{4.28}$$

$$r_{\mathrm{c}} = \frac{r_{\mathrm{S,min}}}{\mathrm{LAI}} f_1(R_{\mathrm{s}}) f_2(\bar{\theta}) f_3(D_{\mathrm{a}}) \tag{4.29}$$

Root extraction rates in vegetation covered tiles are calculated in the SRFWEXC-VG module by Equations 4.30 and 4.31. Equation 4.31 distributes the transpiration flux over the four model layers, based on available moisture and roots in the layers. The root extraction rates provide the boundary condition for the soil water budget in the next timestep.

$$\theta_k = \mathrm{ZLIQ} - \theta_{\mathrm{pwp}} \tag{4.30}$$

$$\rho_{\mathrm{w}} S_{\theta,k} = \sum_i C_i \frac{E_i}{D_k} \frac{R_k \theta_k}{\sum_j R_j \theta_j} \tag{4.31}$$

ZLIQ represents the liquid soil water that is available for root extraction. For implementation of $S_{\mathrm{R,MB}}$, an extra model parameter is introduced in the formulation of ZLIQ, defined as the Moisture Availability Factor (MAF). The MAF represents a reduction in water volume that is accessible to the roots. Figure 4.6 presents a schematisation of the the effects of the MAF on the soil water. The middle figure shows instantaneous root available water limited by MAF. The right figure represents the total root available water, bounded by MAFθ_{cap} and θ_{pwp}.

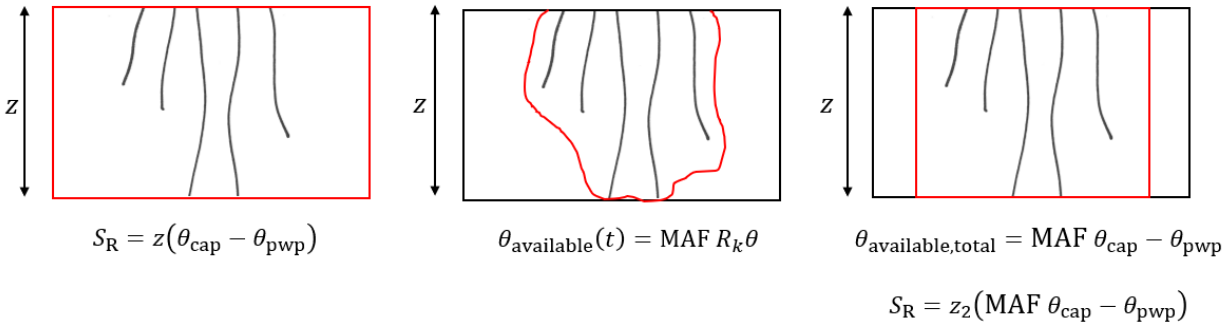

Figure 4.6: Water bucket representation of a modelling layer with a modified moisture availability. The red lines represent the boundaries of root available water. Left: total root available water in the base model. Middle: instantaneous root available water limited by MAF. Right: Long-term total root available water limited by MAF.

Surface fluxes are, in contrary to the modelled subsurface, calculated separately for high and low vegetation tiles. Therefore, the MAF is calculated separately for high and low vegetation following Equation 4.32, applying the mass balance S_{R} estimates for high and low vegetation.

$$\mathrm{MAF} = \frac{\theta_{\mathrm{pwp}} + \frac{S_{\mathrm{R,MB}}}{z}}{\theta_{\mathrm{cap}}} \tag{4.32}$$

Equation 4.33 describes the modified ZLIQ equations in the VSURF and the SRFWEXC-VG modules.

$$\mathrm{ZLIQ}_k = \max(\theta_{\mathrm{pwp}}, \min(\mathrm{MAF}\theta_{\mathrm{cap}}, \theta_k(\mathrm{MAF} - \mathrm{ZF}))) \tag{4.33}$$

Model code

The VSURF module describes the resistance functions for evaporation, including canopy resistance. MAF is introduced in this module in the formulation of ZLIQ following Equation 4.33. Module SRFWEXC-VG describes the soil water budget. In this module the root extraction is formulated. MAF is introduced similarly as in the VSURF module. The model codes are presented in Appendices F and E.

Limitations

It is not possible to create storage above field capacity or below wilting point due to the limits of the model water moisture above θ_{cap} drains and water below θ_{pwp} is not accessible to roots. For regions with $S_{\mathrm{R,MB}} > S_{\mathrm{R,HTESSEL}}$ the moisture availability method cannot be applied and MAF≤ 1.

4.5.3 Root distribution

The rooting distribution, presented in Table 3.2, describes per vegetation type the percentage of roots in each modelling layer. The table shows that all vegetation types except desert and tundra, root in all four layers and are therefore able to extract all the available water present in those layers. The amount of roots in a certain layer only influences the time it takes to extract the soil water and not the total rootzone storage capacity, unless the amount of roots in the bottom layer(s) is reduced to zero. Changing the layer 4 roots to zero means that the vegetation is not able to extract the water in layer 4 and the total rootzone storage capacity is a function of the depths of layers 1, 2 and 3. Since the percentage of roots in layer 4 is small compared to the other layers, especially in low vegetation types, it is expected that the storage in this layer is not actively used by the vegetation. Therefore, the root distribution is set to 33% in all layers and is combined with the previously described moisture depth method.

Method

Root distributions are set to 33% in the top three layers and 0% in the fourth layer for all vegetation types. Moisture depths were changed as described in Equation 4.23, while only considering the top three layers. The depth of layer 4 is set to 500 mm. Appendix G.3 presents the moisture depths for the study catchments applying a 33% rooting distribution.

Model code

Root distributions are changed in the SRFROOTFR module.

Limitations

This method cannot be applied together with the moisture availability approach. When considering the depths of the top three layers, the MAF is larger than 1 for all study catchments which is not possible. Therefore, the method is only applied in combination with the moisture depth approach.

4.5.4 Canopy resistance scaling

The canopy resistance described by Equation 3.3 is a function of vegetation specific parameters, incoming radiation, humidity and soil moisture. In order to analyse the effect of the vegetation

specific parameters, this method describes a combination of canopy resistance scaling and the moisture depth and moisture availability methods.

Method

The canopy resistance is scaled by the long-term evaporation derived from the water balance and the long-term evaporation calculated by the base model. Equations 4.34 and 4.35 describes the modified canopy resistance equation applied in the VSURF module, in which EF represents the evaporation factor. This method is applied in combination with the base model, the moisture depth model and the moisture availability model for catchments EA, He and A with EF-coefficients of 1.23, 1.26 and 1.07, respectively.

$$\mathrm{EF} = \frac{\overline{E}_{\text{base model}}}{\overline{E}_{\text{water balance}}} \tag{4.34}$$

$$r_{\mathrm{c}} = \mathrm{EF}\frac{r_{\mathrm{S,min}}}{\mathrm{LAI}} f_1(R_{\mathrm{s}}) f_2(\bar{\theta}) f_3(D_{\mathrm{a}}) \tag{4.35}$$

Model code

The Evaporation factor (EF) is added to the calculation of canopy resistance in the VSURF module.

Limitations

The method is not independent from the model, because modelled evaporation is used for estimating the EF value.

4.5.5 Model simulations

Model specifications

Table 4.4 presents the relevant model specifications. Documentation of downloading and running the offline land surface model is obtained from: https://docs.google.com/document/d/1yvjvte7_xMe8rste9VSn-TRY-Hz7j4l2NLPVogbVHUg/edit#. The model is run in the cca environment of the ECMWF computing systems.

Table 4.4: Model specifications

Model version	EC-EARTH v3.3 cycle CY43R1
Forcing data	GSWP-3
Temporal resolution	3-hourly
Model timeseries	1970-2010
Spin-up period	1970-1973
Spatial resolution	Reduced gaussian global grid (N128)
Initial conditions	ERA-interim 1970

Overview simulations

The base simulation is run with the model properties as presented in Table 4.4. The three model approaches described in Section are run for the 15 study catchments separately with different values for model depths and moisture availability factors. Appendices G.1, G.2 and G.3 provide the values

for modified moisture depths, MAF values and modified moisture depths with the modified root distribution, respectively, for the study catchments applied in this research.

Table 4.5 presents an overview of the performed model simulations with the abbreviations that are referred to in the following chapters.

Table 4.5: Model simulations with abbreviations.

Model simulation	**Abbreviation**
Base model	Base
Moisture depth approach	MD
Moisture availability approach	MA
Moisture depth approach and 33% root distribution	MD-33
Base model and canopy resistance scaling	Base-EF
Moisture depth and canopy resistance scaling	MD-EF
Moisture availability and canopy resistance scaling	MA-EF

4.5.6 Model validation

The model is validated on water and energy fluxes, on different time-scales. Modelled surface and subsurface fluxes are compared to long-term annual mean observed river discharge and evaporation fluxes derived from the water balance. Monthly modelled runoff terms are compared to monthly observed river discharge. The Nash Sutcliffe Efficiency (NSE) is used as a performance metric that is largely applied for evaluating hydrological models (McCuen, Knight, & Cutter, 2006). Equation 4.36 describes the formulation of NSE. With Q_{o} observed flows, $\overline{Q_{\mathrm{o}}}$ the mean of the observed flows and Q_{m} modelled flows. This metric is applied on both flows and on logarithm of the flows. The NSE of the logarithmic flows provides more insight in the low flows.

$$\mathrm{NSE} = 1 - \frac{\sum_{i=1}^{n}(Q_{\mathrm{o},i} - Q_{\mathrm{m},i})^2}{\sum_{i=1}^{n}(Q_{\mathrm{o},i} - \overline{Q_{\mathrm{o}}})^2} \tag{4.36}$$

The model performance is described by relative model errors. The relative difference between modelled and observed fluxes provides insight in the magnitude of the error in relation to the base model. Equation 4.37 presents the formulation of relative model errors with x representing the water or energy fluxes.

$$\text{Relative error} = \left|\frac{x_{\mathrm{model}} - x_{\mathrm{observed}}}{x_{\mathrm{observed}}}\right| \tag{4.37}$$

Modelled latent heat fluxes are compared to the Fluxcom dataset for long-term, seasonal and monthly time-scales (Jung et al., 2019). Root mean square errors are calculated for analysing monthly model performances (4.38).

$$\mathrm{RMSE} = \sqrt{(\overline{x_{\mathrm{model}} - x_{\mathrm{observed}}}^2)} \tag{4.38}$$

5 Results

In this chapter the results and the discussion of the results are presented. Section 5.1 presents the results of the mass balance approach. Section 5.2 presents the model results regarding water fluxes (5.2.1), energy fluxes (5.2.2), describes inter-model comparisons (5.2.3) and the results from the canopy resistance scaling method (5.2.4). Section 5.3 presents an overview of the results.

5.1 Rootzone storage capacity estimates

The total rootzone storage capacity in HTESSEL overestimates the mass balance S_{R} in all catchments except in catchment No. Table 5.1 presents $S_{\mathrm{R,MB}}$ and $S_{\mathrm{R,HTESSEL}}$ in the three climatic regions. On average, $S_{\mathrm{R,MB}}$ is larger in tropical catchments than in temperate and mediterranean catchments, but $S_{\mathrm{R,HTESSEL}}$ is the largest in temperate regions due to finer soil types. Rootzone storage capacity estimates of the individual catchments are included in Appendix H. The results presented in this chapter are based on the average model situation from Table 4.3.

Table 5.1: Average mass balance rootzone storage capacity estimates and HTESSEL rootzone storage capacities in the three climatic regions.

Climate region	$\boldsymbol{S}_{\mathrm{R,MB}}$ **(mm)**	$\boldsymbol{S}_{\mathrm{R,HTESSEL}}$ **(mm)**
Temperate	194	630
Mediterranean	321	609
Tropical	437	553

Figure 5.1 presents $S_{\mathrm{R,MB}}$ and $S_{\mathrm{R,HTESSEL}}$ in relation to aridity and seasonality indices and the timelag between E_{p} and P in the study catchments. There is no clear trend between $S_{\mathrm{R,HTESSEL}}$ and the three parameters, because the storage capacities in HTESSEL only depend on soil type and model layer depth which are not related to climatic characteristics. However, mass balance S_{R} shows a slight increasing trend in relation to rainfall seasonality indices. Tropical ecosystems have designed larger rootzone storage capacities in order to overcome dry periods than temperate ecosystems with year-round precipitation. EB and G have a lower S_{R} (EB:300 mm, G:194 mm) than the other tropical catchments which is due to 100% coverage of low vegetation, resulting in lower S_{R}. Catchment R has a seasonality index of 0.25 but a relatively large S_{R} of 487 mm which is related to a large coverage with high vegetation.

The relation between storage capacity and aridity index is presented in Figure 5.1b. A study on the relation between effective rooting depths and AI found a large peak in effective rooting depths for 0.8 <AI< 1.5 but a constant pattern when aridity indices increased (Yang et al., 2016). The mass balance S_{R} estimates show a similar pattern with high S_{R} in wet tropical regions and constantly lower S_{R} in the dryer regions. The tropical catchments have relatively low aridity indices but large storage capacities due to strong rainfall seasonality. In warm and dry catchments (P and G), the aridity index is high because of high potential evaporation and low precipitation rates. However, S_{R} estimates are relatively low because transpiration fluxes are low due to limited water availability.

It was found that effective rooting depths increase with the time-lag between energy and water availability (Yang et al., 2016). This pattern is also observed in Figure 5.1c. Mediterranean catchments K and R have developed larger water storage reservoirs than temperate catchments A, D and Na with a time-lag of zero.

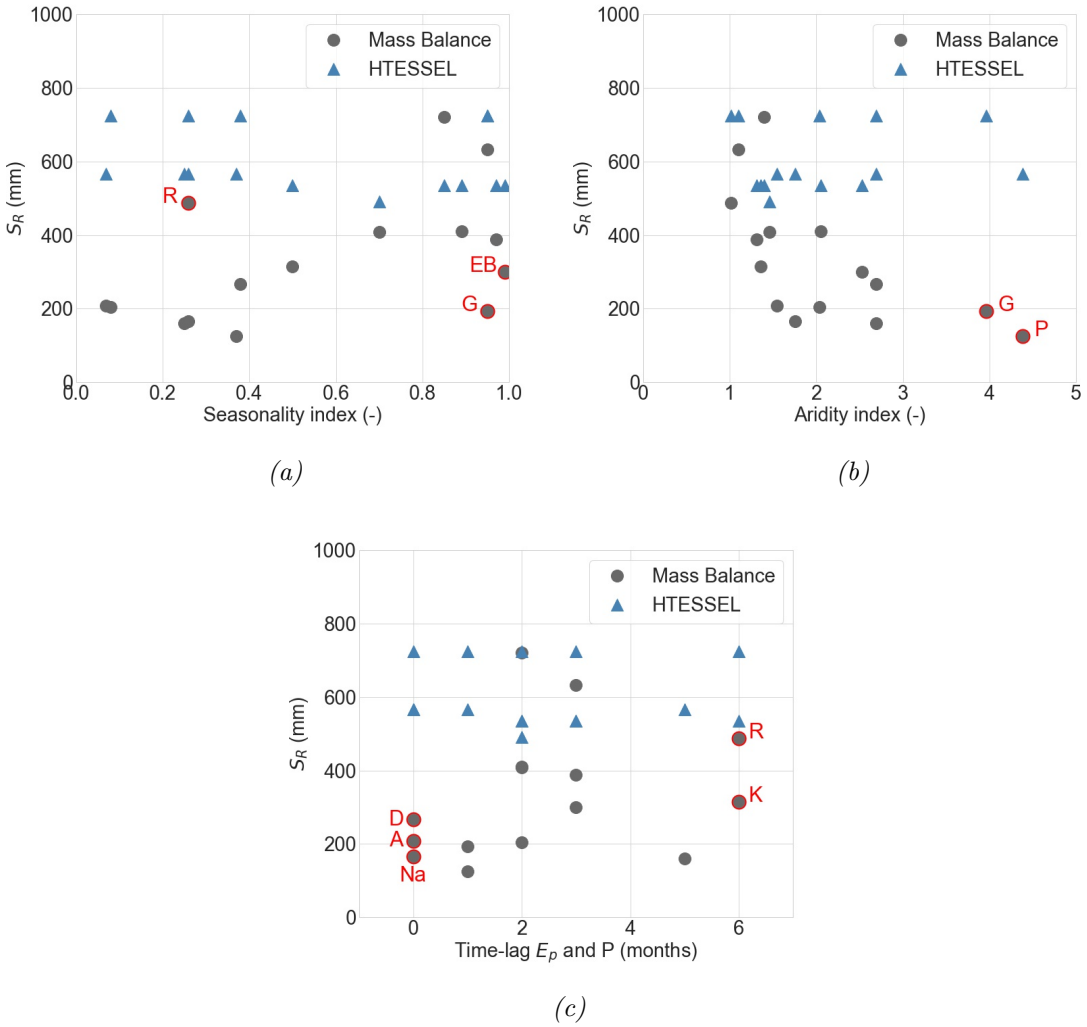

Figure 5.1: $S_{\mathrm{R,MB}}$ and $S_{\mathrm{R,HTESSEL}}$ in relation to rainfall seasonality index (a), aridity index (b) and E_{p} and P time-lag (c)

5.1.1 S_{R} uncertainty

Table 4.3 presents three different combinations of model assumptions, leading to low, average and high $S_{\mathrm{R,MB}}$ estimates. On average, the upper and lower S_{R} estimates deviate 45 mm from the average $S_{\mathrm{R,MB}}$ estimates.

The sensitivity of the S_{R} estimates to different $S_{\mathrm{i,max}}$ assumptions is small. However, the effect of variable f that bounds the variation in annual transpiration on the rootzone storage estimate is larger, especially for catchments with large inter-annual variations in storage deficits. The larger the allowed variation in annual transpiration, the smaller the S_{R} estimate. The largest differences between $S_{\mathrm{R,low}}$, $S_{\mathrm{R,avg}}$ and $S_{\mathrm{R,high}}$ are observed in the catchments with the largest inter-annual S_{D} variability and therefore this factor strongly influences the S_{R} estimates. Drought return period assumptions also directly influence the S_{R} estimates. Catchments dominated by low vegetation, with relatively small return periods, result in much lower S_{R} estimates than catchments dominated by high vegetation, with larger return periods. The order of magnitude of the return period, and thereby the difference between high and low vegetation, has a stronger influence on the S_{R} estimates than the different T_{low} and T_{high} assumptions between the low, average and high models.

5.2 Model simulations

5.2.1 Water fluxes

Long term model performance

Figure 5.2 presents long term mean evaporation fluxes derived from the water balance and calculated with the base HTESSEL model. The mass balance S_{R} estimates (Section 5.1) indicate that the model would overestimate evaporation in all catchments, except in catchment No. However, the base model also underestimates water balance evaporation in K and R. Observed and modelled long term annual mean discharges provide a similar picture as evaporation but with opposite signs. Although the difference between $S_{\mathrm{R,\ MB}}$ and $S_{\mathrm{R,\ HTESSEL}}$ is smaller in tropical regions, the relative base model errors in long-term evaporation simulation are larger than in temperate and mediterranean catchments.

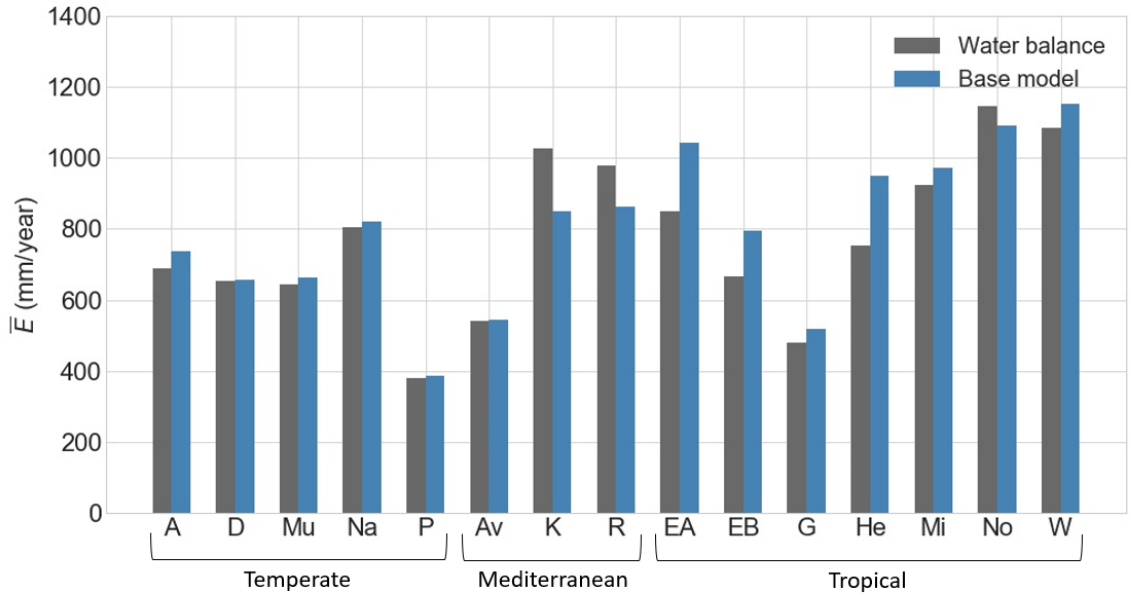

Figure 5.2: Long term mean (1973-2010) total actual evaporation derived from the water balance and calculated by the base model for the study catchments

Table 5.2 presents the absolute long term mean evaporation rates in the three climatic regions for the base, MD and MA models. The table shows that in the three regions both MA and MD models are reducing the annual mean evaporation flux compared to the base model, as expected from the S_{R} estimates. The MD model results in a small reduction of relative $\overline{E}$ error (1%) compared to the base model in all tropical and temperate catchments but on average not in mediterranean catchments due to the inconsistent results in catchments K and R. The MA model results in a stronger reduced long term mean evaporation than the MD model. In tropical catchments, this leads on average to a relative model error reduction, but the results are variable for individual catchments. In temperate and mediterranean catchments the MA model leads to an underestimation of $\overline{E}$ and strong overestimation of $\overline{Q}$. MA modelled $\overline{Q}$ is 185 mm/year in temperate catchments while the observed $\overline{Q}$ is only 55 mm/year.

Seasonal model performance

In temperate and tropical catchments, the dry season relative base model discharge error (130%) is larger than the wet season relative base model discharge error (51%). Relative model errors in mediterranean catchments are of another order of magnitude (1962% in dry season, 232% in wet

Table 5.2: Average long term mean (1973-2010) evaporation flux (mm/year) derived from the water balance and calculated by the HTESSEL model for the three climatic regions and the base, moisture availability and moisture depth models.

$\overline{E}$ (mm/year)	Water balance	Base	MD	MA
Tropical	843	932	924	864
Temperate	635	653	649	556
Mediterranean	848	752	749	665

season).

Temperate catchments
Figure 5.3 presents monthly mean river discharges for temperate catchment Mu. The figure shows that the MA model overestimates river flows during all months but that the MD model is able to simulate the observed seasonal discharge pattern better than the base model. Figures 5.6a and 5.6b present boxplots of wet and dry season relative monthly mean discharge model errors. The MD model leads to median relative model errors of 30% and 26% in the wet and dry season respectively, which is smaller than in the base model (38% and 27%).

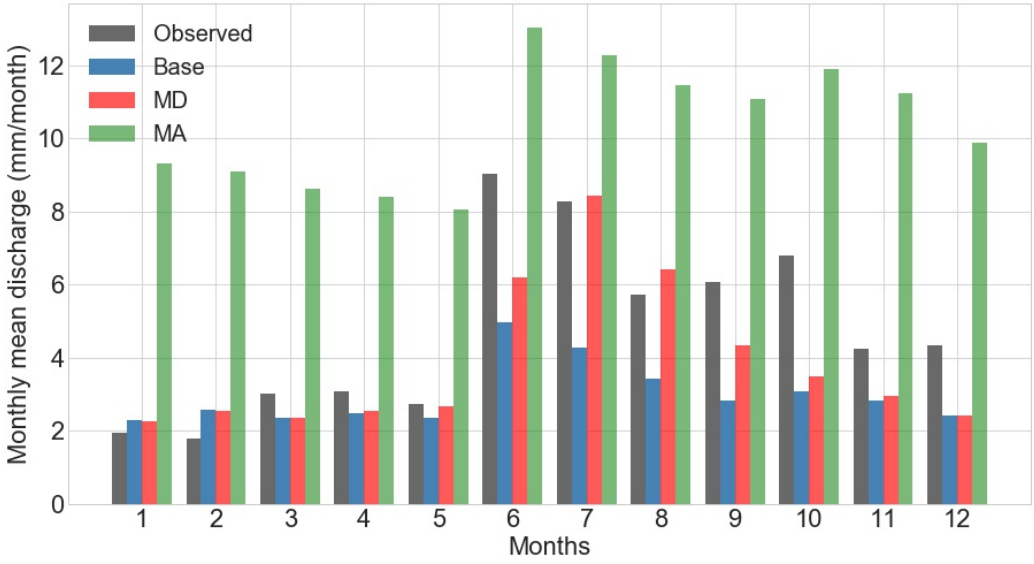

Figure 5.3: Monthly mean river discharge observed and modelled with the base model (Base), moisture depth model (MD) and moisture availability model (MA) in the **temperate** catchment Murrumbidgee (Mu).

Mediterranean catchments
In the mediterranean catchment Av, the base model overestimates dry season discharge with a relative model error of 141%. The MD model results in a reduction of dry season discharge and a relative model error of 122%. The base model underestimates wet season discharge. The MD model results in an increase in wet season river discharge, which leads to an overestimation of the flows and larger relative model errors (base: 43%, MD: 61%). The MA model overestimates river discharge in all months in all three mediterranean catchments.

Tropical catchments
The base model shows variable results in tropical catchments regarding seasonal discharge simulations. Figure 5.4 presents modelled and observed monthly mean river discharge in tropical

catchment Mi and clearly shows that the model is missing the discharge extremes in January and February while dry season flows are overestimated by the model. This is likely due to large elevation differences in four tropical catchments which leads to a fast response to extreme rainfall events (USGS, 2010). HTESSEL does not describe water routing with elevation differences and is therefore missing the extreme flows. Figure 5.4 shows that both the MD and MA models lead to a more realistic wet season discharge simulation than the base model. However, dry season flows are only better represented by the MD model. Figures 5.10a and 5.10b present boxplots of the wet and dry season model performance in tropical catchments. Wet season median relative model errors are 70%, 65% and 74% in the base, MD and MA model respectively. Dry season median relative model errors are 90%, 76% and 66% in the base, MD and MA model respectively. Even though the dry season median model error in the MA model is the smallest, the spread in results is large. The outlier datapoint observed in Figure 5.10b is catchment No. In this catchment, $S_{\mathrm{R,MB}}$ is larger than $S_{\mathrm{R,HTESSEL}}$ and long-term observed $\overline{E}$ is smaller than modelled $\overline{E}$. However, seasonal variations show that the base model overestimates dry season discharge, but due to the large underestimation of discharge in the wet season the annual discharge simulation is too large. As the modelled depth in the MD model is larger than in the base model, dry season discharge increases with the MD model, leading to large discharge simulation errors in the dry season.

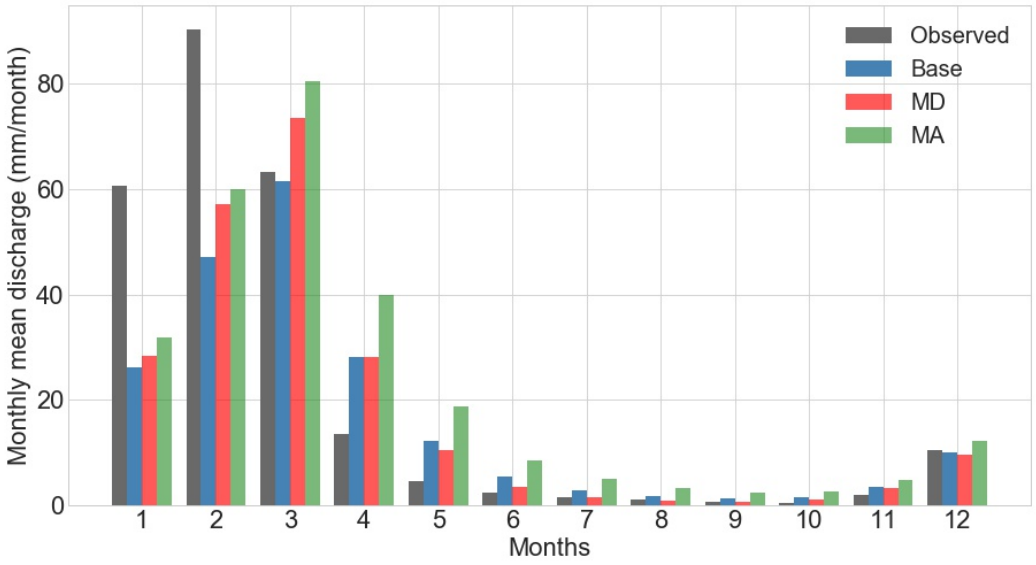

Figure 5.4: Monthly mean river discharge observed and modelled with the base model (Base), moisture depth model (MD) and moisture availability model (MA) in the **tropical** catchment Mitchell (Mi).

Monthly model performance

Temperate catchments

Figure 5.5 presents the observed and modelled rainfall-runoff relation in temperate catchment A and Figure 5.6 presents a boxplot of the NSE performance of river flows and logarithmic river flows in all temperate catchments. Figure 5.5 shows that base and MD model runoff simulations are similar, except during discharge peaks (winter 1990 and 1998) when the MD model simulates a runoff closer to the observed value than the base model. Median NSE of monthly river flows increases from 0.46 with the base model to 0.49 with the MD model, averaged over the temperate catchments. In low flow periods the base and MD models underestimate river discharge, but low flow model performance also slightly increases with the MD model (base: 0.28, MD: 0.31). The MA model constantly overestimates river discharges, leading to low NSE performance.

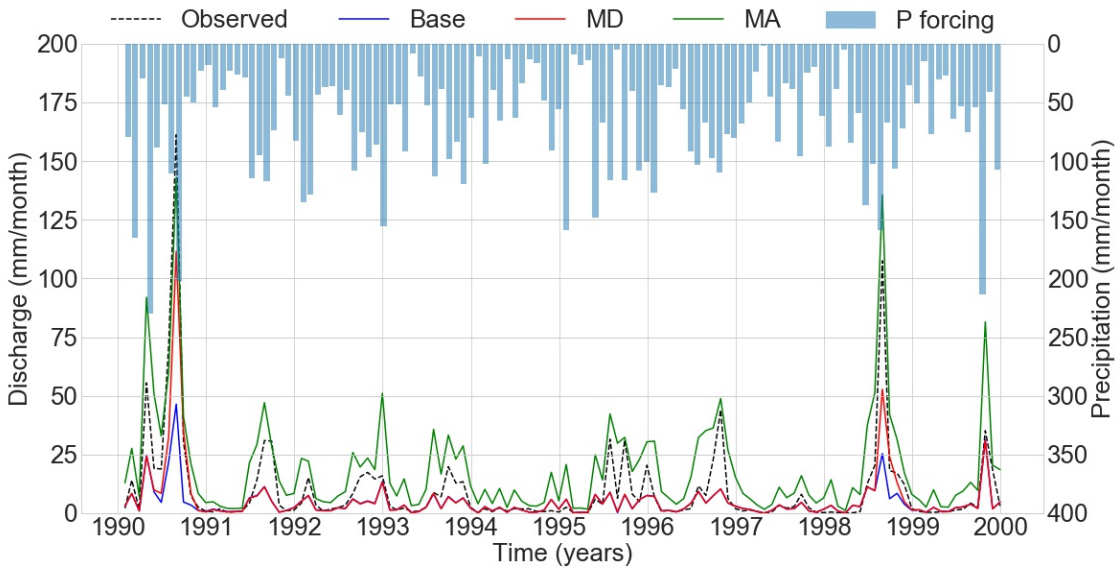

Figure 5.5: Monthly precipitation and monthly modelled river discharge in the **temperate** catchment A for the timeseries 1990-2000.

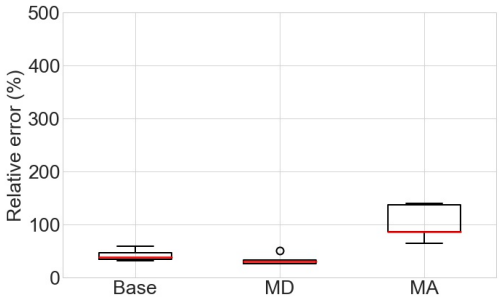

(a) Wet season relative errors (Q)

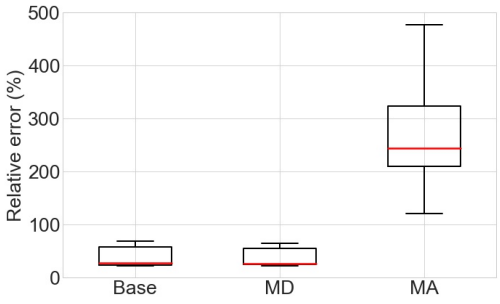

(b) Dry season relative errors (Q)

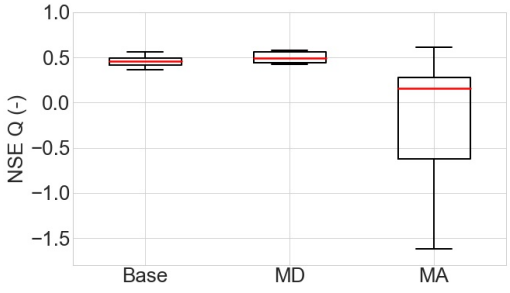

(c) NSE Q

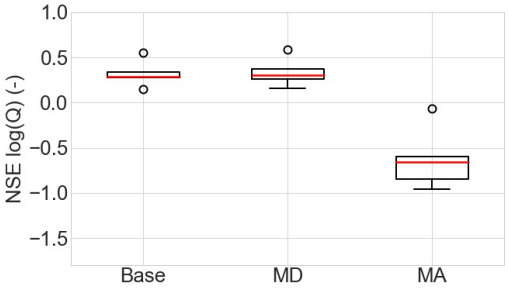

(d) NSE $\log(Q)$

Figure 5.6: Wet and dry season relative model errors regarding discharge simulations and NSE of the modelled monthly discharge (Q) and the logarithmic modelled monthly discharge ($\log(Q)$) averaged over the **temperate** catchments (1973-2010). The red line presents the median, the box is bounded by the first (Q1) and third (Q3) quartile, the whiskers are bounded by the upper and lower data-point within the inter-quartile-range (IQR=Q3−Q1), data-points outside the whisker boundaries are marked as dots.

Mediterranean catchments

Figures 5.7 and 5.8 present the monthly rainfall-runoff relation of the mediterranean catchment K and the NSE model performance in all mediterranean catchments. Note that the axis scales of Figure 5.8a and 5.8b are not the same because of large differences in NSE values. The rainfall-runoff relation in Figure 5.7 clearly shows the overestimation of modelled discharges. The base model shows the highest NSE performance regarding flows in mediterranean catchments (NSE= 0.18). However, the MD model performs better than the base model for low flows (NSE-log base= −0.13, NSE-log MD= 0.05).

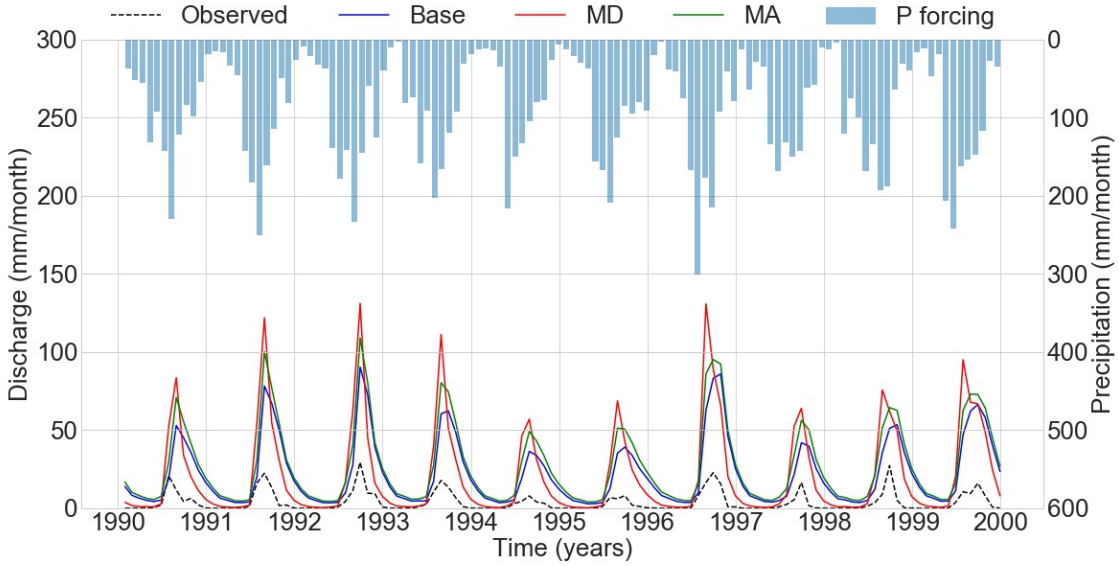

Figure 5.7: Monthly precipitation and monthly modelled river discharge in the **mediterranean** catchment K for the timeseries 1990-2000.

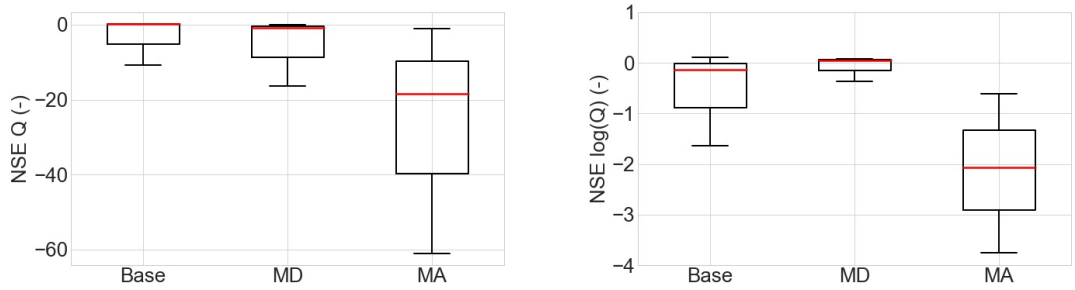

(a) NSE Q *(b)* NSE $\log(Q)$

Figure 5.8: NSE of the modelled monthly discharge (Q) and the logarithmic modelled monthly discharge ($\log(Q)$) averaged over the **mediterranean** catchments (1973-2010). The boxplots are defined similar to Figure 5.6

Tropical catchments
Figure 5.9 presents the monthly rainfall-runoff relation of the tropical catchment EA and Figure 5.10 presents tropical NSE values. The three models underestimate river discharges in this catchment. The base model simulates the lowest flows, which is clearly visible in 1994 and 1996. The median NSE in the tropical catchments is 0.52 with the base model and increases for both MD and MA models to 0.60 and 0.61, respectively. However, the MD and MA models NSE-log values are lower than in the base model. The outlier datapoints observed in Figure 5.10c and Figure 5.10d are catchments EB and G, respectively.

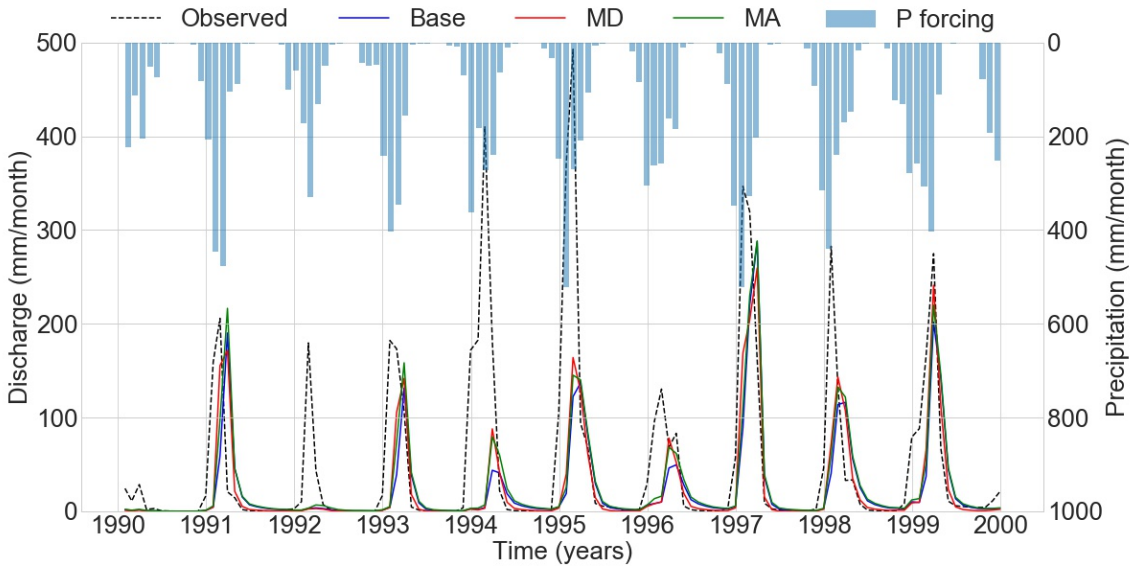

Figure 5.9: Monthly precipitation and monthly modelled river discharge in the **tropical** catchment EA for the timeseries 1990-2000.

Model performance by land cover

The tile fraction of high and low vegetation and the vegetation types are influencing the modelled water fluxes. There is no clear relation observed between model NSE performance and the fractional coverage of vegetation. From seasonal discharge variations in catchments with predominantly low vegetation (EB, G and P) it is observed that modelled dry season discharge is too low. This is in contrast to catchments with predominantly high vegetation where modelled discharge is too low in the wet season, but too high in the dry season. Low vegetation such as grasses stop transpiring in the dry season, which leads to larger river flows. HTESSEL is not able to describe this process and therefore underestimates observed dry season river flows.

5.2.2 Energy fluxes

Reliability Fluxcom dataset

Table 5.3 presents the relative water balance deviation ($\frac{\sum P-E-Q}{\sum P}$) applying GSWP-3 precipitation, Fluxcom derived evaporation and observed discharge in the study catchments for the time-period 1973-2010. The table shows that Fluxcom derived evaporation does not provide realistic data for the seven catchments where the relative water balance is larger than 10%. Therefore, a qualitative analysis is only performed in the catchments with realistic water balances (WB deviation$<$ 10%).

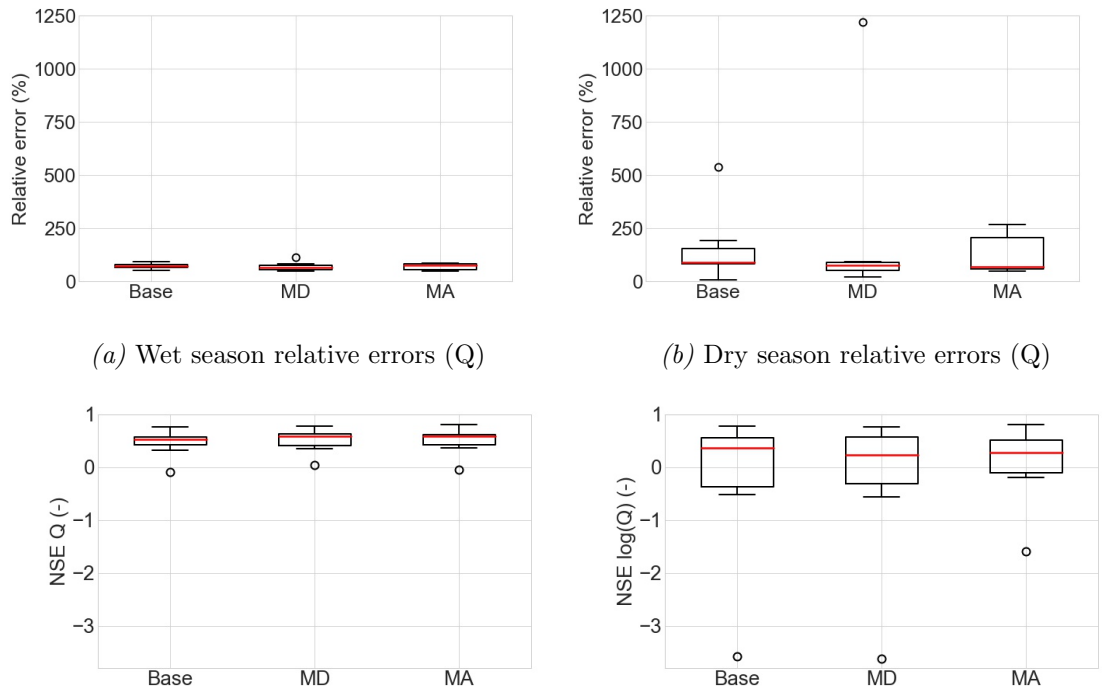

(a) Wet season relative errors (Q)

(b) Dry season relative errors (Q)

(c) NSE (Q)

(d) NSE log(Q)

Figure 5.10: Wet and dry season relative model errors regarding discharge simulations and NSE of the modelled monthly discharge (Q) and the logarithmic modelled monthly discharge (log(Q)) averaged over the **tropical** catchments (1973-2010). The boxplots are defined similar to Figure 5.6

Table 5.3: Relative water balance deviation applying GSWP-3 precipitation, Fluxcom derived evaporation and observed discharge for the time period 1973-2010.

Catchment	WB deviation
A	3%
D	5%
Mu	21%
Na	14%
P	4%

Catchment	WB deviation
Av	10%
K	26%
R	20%
EA	2%
EB	6%

Catchment	WB deviation
G	2%
He	1%
Mi	23%
No	23%
W	9%

Longterm model performance

Latent heat flux averages over the period 1973-2010 show that base model overestimates latent heat fluxes compared to Fluxcom latent heat fluxes. Relative errors in latent heat flux simulation in the base, MD and MA models averaged over the representative catchments are 26%, 25% and 17%, respectively. Relative errors in latent heat simulations are larger in tropical regions than in temperate and mediterranean regions.

Seasonal model performance

In temperate regions, the base model dry season relative error in latent heat flux simulation is larger (36%) than the wet season error (8%). MD and MA model errors increase in the wet season but decrease in the dry season compared to the base model, with larger improvements with the MA model than the MD model. In tropical catchments the latent heat base model relative simulation errors are larger than in the temperate catchments. MA model relative errors reduce during all months while MD model relative errors increase in the dry months compared to the base model. Mediterranean catchments are not qualitatively analysed due to non-closure of the water balance.

However, it was found that the monthly mean modelled latent heat flux signal in mediterranean regions is out-of-phase with the Fluxcom latent heat flux signal.

Monthly model performance

On monthly timescales, the average root mean squared errors (RMSE) is 29 Wm^{-2}, which is large considering an average latent heat flux of 49 Wm^{-2}. Larger RMSE are found in the tropics than in the temperate regions. However, the correlation between modelled and Fluxcom latent heat fluxes is larger in tropical regions (0.81) than in temperate regions (0.42). The MA model results in a reduction of relative errors and an increase in correlation, while the MD model results in larger or equal errors in the representative river catchments and decreased correlations.

5.2.3 Inter-model comparison

Evaporation fluxes

The model calculates the four evaporation fluxes described in Section 2.1 separately. Table 5.4 presents the four evaporation fluxes with the abbreviations used in HTESSEL and the relative contributions to the total evaporation in the three models averaged over the study catchments.

Table 5.4: Evaporation fluxes with relative long-term mean contributions to the total evaporation in the base, MD and MA models averaged over the catchments (1973-2010).

Evaporation flux	**Abbreviation**	**Base**	**MD**	**MA**
Canopy evaporation	E_c	22%	22%	22%
Soil evaporation	E_s	25%	25%	33%
Transpiration	E_t	53%	53%	43%
Water evaporation	E_w	0%	0%	0%

The canopy evaporation (interception evaporation) is in HTESSEL directly related to the fixed LAI of the vegetation coverage. Therefore, canopy evaporation contributes less to the total evaporation in catchments with predominantly low vegetation than in catchments with predominantly high vegetation. The different models do not result in changes in canopy evaporation rates.

Soil evaporation is a function of the bare ground fraction of the model tile and the soil water fraction in the top soil layer. The larger the vegetation coverage, defined by c_veg, the lower the soil evaporation fraction. Fractional long term averaged soil evaporation varies from 14% in EA, covered with tall grass ($c_\mathrm{veg} = 0.70$) and interrupted forest ($c_\mathrm{veg} = 0.90$), to 59% in P, covered with semidesert-vegetation ($c_\mathrm{veg} = 0.10$). Absolute soil evaporation in the MD model is similar to the base model but increases in the MA model with on average 40 mm/year compared to the base model. The relative contribution of E_s in the MA model increases compared to the base model with 3% in tropical catchments and 18% in temperate catchments, due to lower MAF values and higher bare ground fractions in the temperate catchments.

Transpiration fluxes contribute the most to the total base and MD model evaporation flux, with the largest rates in tropical catchments. Implementation of S_R estimates lead to an average reduction in transpiration flux of 6 mm/year and 116 mm/year in the MD and MA models compared to the base model, with larger reductions in temperate catchments due to smaller S_R estimates. The MA model E_s increase and E_t decrease result in the changed evaporation contributions presented in Table 5.4.

Runoff fluxes

Modelled runoff fluxes are separated into surface (Q_s) and subsurface (Q_{sb}) runoff. Figure 5.11 presents long term mean observed runoff and the averaged long term runoff contributions of Q_s and Q_{sb} in the three different climatic regions for the three models. In tropical catchments (Figure 5.11a), the MD and MA models lead to increased surface and subsurface runoff fluxes compared to the base model. In temperate catchments, subsurface runoff contributes little to the total runoff in the base and the MD models (Figure 5.11b) and the MA model results in a large increase in both surface and subsurface runoff fluxes. Figure 5.11c shows that the MD model leads to a small increase in subsurface runoff in the mediterranean catchments, whereas subsurface runoff fluxes have doubled in the MA model compared to the base model.

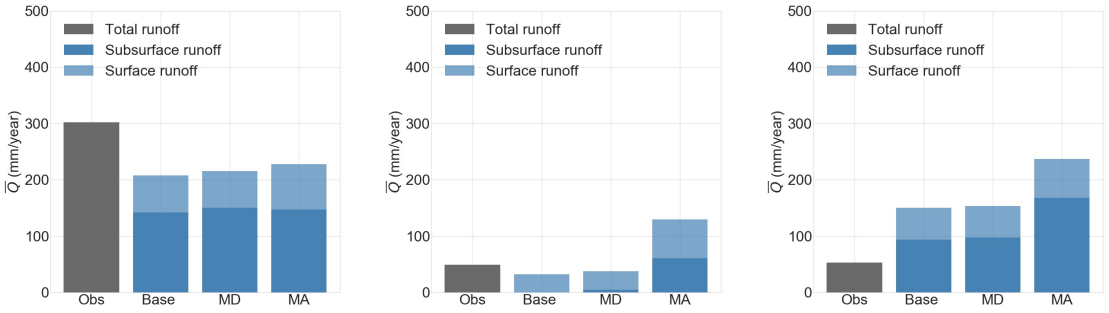

(a) Tropical *(b)* Temperate *(c)* Mediterranean

Figure 5.11: Long term (1973-2010) annual mean total observed runoff (Obs) and modelled surface and subsurface runoff fluxes averaged over the catchments in the three models.

Soil moisture

The model provides information on the soil moisture in the four layers. The MD model does not lead to changes in relative soil moisture compared to the base model but absolute soil moisture changes in the bottom layers due to the modified moisture depths. The MA model results show that soil moisture increases in all layers compared to the base model in all catchments, except A, Na, P and Av.

Root distribution

Changes in root distribution are applied to the MD model as described in Section 4.5.3. Compared to the MD model, the MD-33 model results in a decrease in long term average river discharge and an increase in long term average evaporation rates in all catchments except K and R. The increase in MD-33 total evaporation is due to larger dry season transpiration in tropical catchments and larger soil evaporation in temperate catchments compared to the MD model. The MD-33 NSE model performance is lower than in the MD and base model in all catchments except EB, G and He.

5.2.4 Canopy resistance scaling model performance

The Base-EF, MD-EF and MA-EF models are tested for tropical catchments EA and He and temperate catchment A. Table 5.5 presents NSE model performance of the different models with and without canopy resistance scaling averaged for the three catchments. The EF model results in a consistent reduction in monthly evaporation and increase in monthly river discharge compared to the models without the scaling factor. This leads to similar NSE performance but consistently higher NSE-log performance in the three catchments, compared to the models without canopy resistance scaling. Averaged over the three catchments, the MD-EF model has the highest NSE

performance. Moreover, RMSE of latent heat flux simulations reduce with the EF-model compared to the models without canopy resistance scaling.

Table 5.5: NSE and NSE-log from the base, MD and MA models with and without canopy resistance scaling averaged for catchments He, EA and A.

	Base	**Base-EF**	**MD**	**MD-EF**	**MA**	**MA-EF**
NSE (-)	0.41	0.44	0.57	0.57	0.44	0.42
NSE-log (-)	0.11	0.20	0.13	0.23	0.04	0.09

5.3 Overview results

The results show that the model results are consistent with the S_{R} estimates, except in catchments K and R. The difference between $S_{\mathrm{R,\,MB}}$ and $S_{\mathrm{R,\,HTESSEL}}$ is the largest in temperate regions. The long term mean water and energy fluxes simulated by the base model show that relative errors are larger in tropical regions than in temperate regions. However, NSE base model performance and latent heat flux correlations are larger in temperate than in tropical regions. In the base model, dry season relative errors in water and energy flux simulations are on average larger than wet season relative errors and log-NSE values are lower than NSE values. This indicates that the inadequate total rootzone storage capacities are likely a source of dry season modelling errors. Wet season simulation errors are more likely related to inadequate runoff formulations.

The MD model simulations lead to smaller long-term model relative errors regarding water and energy fluxes than the base model, but the changes are small. Seasonal and monthly discharge simulation performance increases, but latent heat flux simulation performance decreases compared to the base model.

The MA model has stronger effects on modelled water fluxes than the MD model which leads to strong discharge overestimations in temperate and mediterranean river catchments. Figure 5.11 shows that this overestimation is due to increased surface and subsurface runoff fluxes compared to the base model. In tropical catchments, the MA model does not lead to unrealistic river flows because MAF values are on average larger (MAF= 0.8) than in temperate and mediterranean regions (MAF= 0.6). The lower the MAF value, the larger the change in moisture levels and higher moisture levels lead to larger subsurface and surface runoff fluxes. Moreover, the low MAF values lead to high, unrealistic, soil evaporation rates. The combination of low MAF values and high bare soil fractions lead to unrealistic discharge and evaporation fluxes in the temperate catchments. However, model performance regarding latent heat flux simulations is higher in the MA model than in the base and MD models.

The canopy resistance scaling approach forces an increase in canopy resistance resulting in a decrease in evaporation. Combining this method with the implementation of rootzone storage capacity has larger effects on the model performance than the S_{R} implementation itself, resulting in higher model performance. These results indicate that, besides hydrology dynamics, the fixed vegetation dependent parameters $r_{\mathrm{s,min}}$ and LAI strongly influence the modelled evaporation.

The results show that the MD model provides a consistent improvement in water flux simulations while the MA model results in variable model performances. Figure 5.12 presents the MD model performance compared to the base model based on long term mean $\overline{E}$ and NSE coefficients in the 9 catchments that are considered to show representative model results. The mediterranean catchments are excluded because the model results are not consistent with the $S_{\mathrm{R,MB}}$ estimates in catchments K and R. Moreover, tropical catchments No and G are excluded because dry season modelled discharge errors are strongly deviating from the median in these tropical catchments. Figure 5.12a shows that the MD model leads in all catchments to a small improvement in modelled $\overline{E}$ compared to the base model. Figure 5.12b presents NSE coefficients of the flows and the

logarithmic flows of the base and the MD model. In 6/10 catchments both coefficients improve with the MD model compared to the base model. NSE coefficients of the flows increase in 8/10 catchments with the MD model compared to the base model.

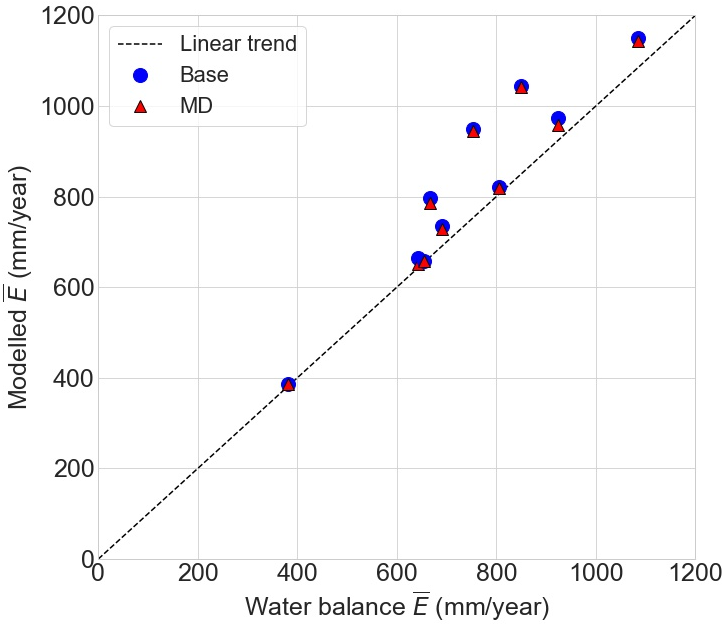

(a) Modelled and water balance long term mean evaporation

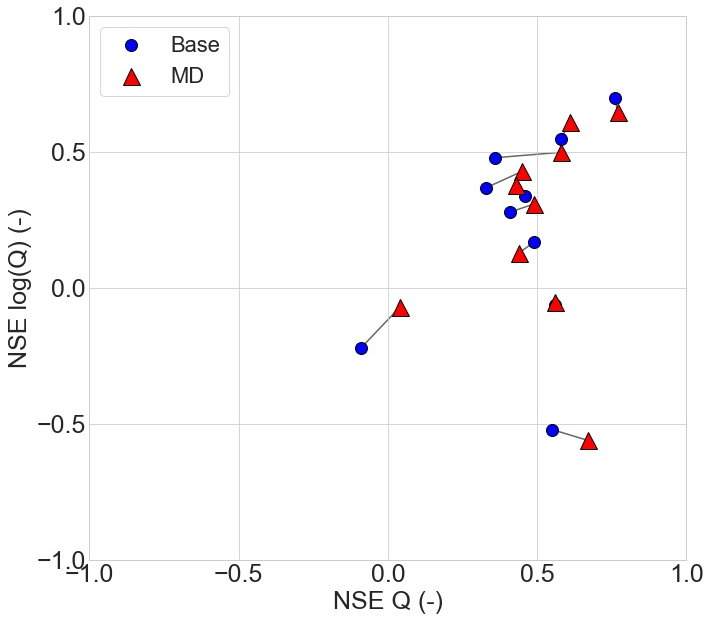

(b) NSE model performance

Figure 5.12: Model performance of base and the MD model in the representative river catchments for time period 1973-2010. Water balance $\overline{E}$ is derived from long term mean GSWP-3 precipitation and observed river discharge. NSE efficiency is based on monthly observed and modelled discharge. The lines in Figure 5.12b connect the base and MD model performance of similar catchments. The presented catchments are A, D, Mu, Na, P, EA, EB, He, Mi, W

6 Discussion

In this chapter the methodology of this research is discussed. Section 6.2 presents uncertainties in the used datasets. Section 6.3 describes the limitations of the mass balance approach and Section 6.4 presents uncertainties in the modelling approach.

6.1 Study area

The study is based on 15 Australian river catchments with the corresponding grid-cells. This is a small subset and the results provide therefore only an indication of the model performance on larger scales. The assumption is made that the river catchment is representative for the entire model grid-cell but inconsistencies could be present related to different vegetation coverage, elevation differences and groundwater dynamics. The HTESSEL model is developed for European climate predictions, while this research focuses on Australia which is characterised by different climatic conditions than Europe. The larger errors found in tropical regions could be related to the inability of HTESSEL to predict in tropical regions, which are not present in Europe.

6.2 Data

The data described in Chapter 4.2 is carefully selected, however, uncertainties are still present. The GSWP-3 dataset is used as input for both the mass balance approach and the HTESSEL model and biases in the described atmospheric variables could result in modelling errors. Due to the high spatial variability of precipitation, grid-cell averaged precipitation input could be unrepresentative for the catchment resulting in errors in the S_{R} estimates and hydrological model validation because measured streamflow accounts for this variability. Large errors in streamflow data are not expected because streamflow is directly measured and only complete datasets that showed logical discharge behaviour in relation to precipitation were selected. Potential evaporation is based on an empirical formulation based on temperature and radiation. More complex formulations could be used, but these require more data which leads to more degrees of freedom.

This vegetation input map from GLCC is a dataset which describes global vegetation types in 1990 which is considered to be representative for the studied time-period of 1973-2010. However, vegetation coverage is variable due to anthropogenic activities and climate change and it would be more realistic to have a dynamic representation of vegetation coverage in order to account for vegetation-climate interactions. Global soil maps are in contrast to vegetation coverage less variable in time. However, the Van Genuchten soil parameters are based on empirical formulations which could be a source of error. Moreover, soil types and the corresponding parameters are assumed to be constant over the vertical model profile.

The Fluxcom latent heat fluxes showed unrealistic results in seven study catchments. This dataset has shown the ability to reproduce energy fluxes on continental and global scales (Jung et al., 2019). However, this study found that the results on local scales are not realistic regarding water balances.

6.3 Mass balance approach

Total rootzone storage capacities are estimated with a mass balance approach. The main difficulty in this method is the estimation of actual evaporation fluxes. Evaporation fluxes are derived from catchment's water balances and potential evaporation estimates. In this study, it is assumed that actual evaporation has a similar seasonal variation as potential evaporation. However, this is not the case in the analysed mediterranean catchments Av, K and R, where E_{p} and P are out of

phase. From a hydrological perspective it is likely that the actual evaporation follows a trend similar to seasonal precipitation in water limited catchments, with higher evaporation rates in winter than in summer due to a water shortage in summer. This evaporation signal is also obtained from HTESSEL model simulations in mediterranean regions. However, directly applying the E_p seasonality leads to overestimated summer evaporation and underestimated winter evaporation rates. Applying a seasonal evaporation pattern based on the HTESSEL model output in the mass balance approach in catchment K results in a smaller S_R estimate (252 mm) than the initial estimate (315 mm). Applying smaller S_R estimates in the mediterranean catchments would lead to even larger modelling errors than with the currently applied S_R estimate. Total catchment S_R estimates are dependent on the vegetation coverage and selected return periods that represent time-scales of vegetation's adaptation. Where high vegetation invests in root growth, low vegetation can go dormant in periods of water shortage. The assumptions made for estimating the transpiration flux are not valid for dormant low vegetation. Transpiration fluctuations of low vegetation are better represented by NDVI data (Normalised Difference Vegetation Index), that directly shows when vegetation is dormant and not transpiring.

The iterative approach described in Section 4.4.4 accounts for intra-annual variations in evaporation. This method was not used in previous studies and is a promising development of the mass balance approach. However, it is largely dependent on assumptions. The factor f that limits the variation in annual evaporation fluxes influences storage deficits significantly. Without limits, the estimated annual evaporation can go to zero with this approach, which is not realistic. Annual evaporation limits could be verified by independent datasets describing inter-annual evaporation variability.

The method describes water storage in the rootzone assuming that all the water available for transpiration origins from precipitation and is stored in this reservoir. However, vegetation could have other water sources than precipitation supplying water to the roots, for example groundwater or irrigation. Vegetation that roots in deep groundwater and vegetation rooting in wetlands with high water tables are not dependent on rootzone water storage and are able to transpire more than expected with the currently used method. Deep roots tapping water from the groundwater could be a large issue in Australia as Eucalyptus forests, a species that can develop deep roots, contribute for 74% to the total forest area (Australian Government, 2018; Le Maitre, Scott, and Colvin, 1999). Agricultural crops could be supplied with irrigation water that is not covered in precipitation datasets. Furthermore, crops are harvested every season and do not develop a root system based on long-term optimisation principles. According to Table 3.1, four catchment gridpoints are for a significant amount covered by crops which could lead to S_R estimates that are not representing the natural processes in these regions.

The main limitations of the mass balance approach are its data dependency and the scale. Data is scarce and is always prone to errors. Moreover, there is a mismatch between climate model global scales and the catchment-scale estimates from the mass balance approach. Remote-sensing data could provide a solution to the data and scale issues, but data should be selected carefully and should be independent of rootzone parameterisations. Furthermore, classification maps could be developed that relate S_R to for example climatic parameters, land-use or topography, based on a catchment-scale S_R dataset covering regions worldwide. However, this is challenging because ecosystems are unique and root development is a product of ecosystem optimisation which is dependent on many unknown variables.

6.4 Model approach

6.4.1 Model limitations

HTESSEL describes 20 fixed vegetation types with many vegetation-dependent parameters that lead to many degrees of freedom in the model. Vegetation coverage influences the timing of root extraction and transpiration, but total rootzone storage capacities are only a function of modelling depth and soil type.

The HTESSEL root distribution implicitly describes the depth of the rootzone, but since all vegetation types root in all four layers, the total S_{R} is not dependent on rooting distributions. Root depths are limited to the 2.89 m modelling depth while it was found that vegetation can root much deeper (Canadell et al., 1996). Moreover, even though the contribution of roots in the fourth layer to the total is limited (e.g. 4% for short grass), all water in the fourth layer can eventually be accessed by this little amount of roots. $S_{\mathrm{R,\ HTESSEL}}$ values in regions with low vegetation and low rainfall seasonality are likely to be overestimated because the fourth layer is hydrologically not active due to the small amount of roots. HTESSEL describes rooting density indirectly by the vegetation type dependent c_{veg} parameter. However, different c_{veg} values do not lead to different rootzone storage capacities because it does not limit the total accessible water to roots. c_{veg} only influences the timing of transpiration but not the total water volume. Alessandri et al. (2017) added a seasonal variable effective vegetation density fraction based on LAI to the model, in order to account for seasonal variations in transpiration rates. The model used in this research does not contain this variable parameter and vegetation density is fixed. It would be interesting to explore the effect of a seasonal variable vegetation density on seasonal variations in predicted river discharge and evaporation fluxes.

6.4.2 Moisture depth method

The moisture depth method directly changes the total rootzone water storage by modifying the modelling soil moisture depth. A limitation of this method is inconsistent layer representation that could lead to errors in soil temperature calculations. It was found that relative soil moisture does not significantly change with the MD model in all layers. Therefore it is concluded that the inconsistent layers do not lead to issues in modelling soil temperatures. However, it is recommended to modify the model in a way that different layer depths for temperature and moisture layers are consistently parameterised.

Modelling depths are modified in the fourth layer in order to minimise the effect of layer inconsistencies. However, it is more realistic to modify the depths proportionally to the current layer depths because the root distribution is parameterised based on the current depth distribution. Moreover, the model issue in catchments where the depths of both layer 3 and 4 were reduced is solved applying proportional depth changes.

6.4.3 Moisture availability method

The moisture availability method reduces the total rootzone water storage by limiting the water that is available for root extraction. This method does not allow for increasing total rootzone storage capacities (MAF$>$ 1) without modifying the modelling soil depth. A combination of the MD and MA model approaches could be tested and optimised in order to improve modelling performance.

The results show that soil evaporation strongly increases applying this method, which could be avoided by exponentially decreasing MAF with depth. This would be more realistic because the root density follows an exponential profile over depth and extraction from deep layers requires more suction by the vegetation than extraction from shallow layers.

6.4.4 Canopy resistance scaling method

The canopy resistance scaling method is only applied in three river catchments and the results can therefore not be generalised. The scaling factor is applied to the canopy resistance equation because this parameter is directly related to the ability of vegetation to transpire. The evaporation scaling factor could also be applied to the formulation of total evaporation. In this case, the total evaporation is directly scaled towards the water balance derived evaporation. This solution would result in more realistic average evaporation rates. Combining this with the implementation of mass balance rootzone water storage capacities would result in more adequate seasonal and long term evaporation simulations.

6.4.5 Model validation

The base, MD and MA models are validated with catchment discharge data and Fluxcom latent heat flux data. The use of discharge data is not fully independent as long-term annual observed river discharge is also used in the estimation of S_{R}. However, seasonal and monthly discharge variations were not used in the S_{R} estimates. Water balance comparisons are very useful for analysing model performance because evaporation and discharge are directly linked on the long-term. Seasonal variations in discharge provide an insight in the model performance regarding runoff simulations but cannot be directly linked to seasonal evaporation fluxes. However, comparison of monthly modelled latent heat fluxes to Fluxcom latent heat fluxes provides a direct insight in model performance regarding evaporation. Local water balance calculations show that latent heat fluxes from this dataset are not reliable in all catchments. This dataset is considered as a promising tool in land surface model evaluations, but based on this study it is questionable whether this dataset should be applied on local scales.

6.4.6 Model simulations

The results are based on offline model simulations which is preferred in model development since isolated models provide more insight in the individual model processes. However, in future works, coupled simulations could provide more information on the effect of modified evaporation fluxes on global climate processes.

7 Conclusion

This research investigates the effects of the climate-based mass balance method for estimating the maximum water storage capacity in the vegetation's rootzone on the representation of water and energy fluxes in the HTESSEL land surface model.

Based on an analysis of the model structure, implementing mass balance-based total rootzone storage capacity estimates in the model and evaluating model performance, the conclusion is drawn that climate-based mass balance total rootzone water storage capacities have small effects on the representation of water and energy fluxes by the model, but contribute to an improvement in simulating these fluxes. It was found that model depth modifications, based on rootzone storage capacities derived from mass balances, result in consistent model improvements (Table 7.1).

Table 7.1: NSE and NSE-log of monthly modelled discharge in the base model and the moisture depth model averaged over the 10 representative river catchments.

	Base model	**Moisture depth model**
NSE (-)	0.44	0.51
NSE-log (-)	0.21	0.23

The results indicate that the current model strongly overestimates evaporation fluxes with larger relative errors in the dry season than in the wet season, which suggests that the modelling errors could be caused by the inadequate representation of root available water. However, the small model improvement when climate-based rootzone water storage capacities are implemented indicate that other factors, such as input data, parameter estimations and other hydrological process representations, are also contributing to the modelling bias. This was confirmed by the canopy resistance scaling approach which shows that changing internal model parameters have larger effects on flux simulations than the implementation of modified rootzone water storage capacities only.

This research contributes to the development of land surface models by investigating the potential of a holistic modelling approach for estimating rootzone water storage capacities. In future research, the mass balance method could be used to develop an adaptive modelling scheme that represents vegetation dynamics. Furthermore, it would be valuable to focus future studies on the representation of all hydrological processes in land surface models and on the effects the large amount of internal model variables have on the modelling performance. In order to continue developing land surface models it is paramount to invest in collaborations between hydrologists and climate scientists.

References

Alessandri, A., Catalano, F., De Felice, M., Van Den Hurk, B., Reyes, F. D., Boussetta, S., ... Miller, P. A. (2017). Multi-scale enhancement of climate prediction over land by increasing the model sensitivity to vegetation variability in ec-earth. *Climate Dynamics*, *49*(4), 1215–1237.

Arend, M., Brunner, I., Dawes, M. A., Sperisen, C., & Herzog, C. (2015). How tree roots respond to drought. *Frontiers in Plant Science*, *6*(July), 1–16. doi:10.3389/fpls.2015.00547

Australian Government. (2018). *Australia's State of the Forests Report 2018*.

Balsamo, G., Albergel, C., Beljaars, A., Boussetta, S., Brun, E., Cloke, H., ... Vitart, F. (2015). ERA-Interim/Land: A global land surface reanalysis data set. *Hydrology and Earth System Sciences*, *19*(1), 389–407. doi:10.5194/hess-19-389-2015

Blondin, C. (1991). Parameterization of land-surface processes in numerical weather prediction. In *Land surface evaporation* (pp. 31–54). Springer.

BoM. (2015). Hydrologic reference stations. Retrieved from http://www.bom.gov.au/water/hrs/index.shtml

Brunner, I., Herzog, C., Dawes, M. A., Arend, M., & Sperisen, C. (2015). How tree roots respond to drought. *Frontiers in plant science*, *6*, 547.

Budyko, M. I., Miller, D. H., & Miller, D. H. (1974). *Climate and life*. Academic press New York.

Canadell, J., Jackson, R., Ehleringer, J., Mooney, H., Sala, O., & Schulze, E. (1996). Max rooting depth of veg types at global scale Talks about boreal. *Oecologia*, *108*, 583–595. doi:10.1007/BF00329030. arXiv: AR00038244

Capell, R., Hrachowitz, M., Savenije, H., Han, D., Arheimer, B., Pechlivanidis, I., ... Wagener, T. (2016). The evolution of root-zone moisture capacities after deforestation: a step towards hydrological predictions under change? *Hydrology and Earth System Sciences*, *20*(12), 4775–4799. doi:10.5194/hess-20-4775-2016

Clapp, R. B. & Hornberger, G. M. (1978). Empirical equations for some soil hydraulic properties. *Water resources research*, *14*(4), 601–604.

De Boer-Euser, T., McMillan, H. K., Hrachowitz, M., Winsemius, H. C., & Savenije, H. H. (2016). Influence of soil and climate on root zone storage capacity. *Water Resources Research*, *52*(3), 2009–2024. doi:10.1002/2015WR018115

Deardorff, J. W. (1978). Efficient prediction of ground surface temperature and moisture, with inclusion of a layer of vegetation. *Journal of Geophysical Research*, *83*(C4), 1889. doi:10.1029/jc083ic04p01889

ECMWF. (2016). Ifs documentation cycle cy34r1, part iv: Physical processes.

FAO. (2003). *Digital soil map of the world (dsmw)*. Food and Agricultural Organization of the United Nations, re-issued version.

Fitts, C. R. (2002). *Groundwater science*. Elsevier.

Gao, H., Hrachowitz, M., Schymanski, S. J., Fenicia, F., Sriwongsitanon, N., & Savenije, H. H. (2014). Climate controls how ecosystems size the root zone storage capacity at catchment scale. *Geophysical Research Letters*, *41*(22), 7916–7923. doi:10.1002/2014GL061668

Gentine, P., D'Odorico, P., Lintner, B. R., Sivandran, G., & Salvucci, G. (2012). Interdependence of climate, soil, and vegetation as constrained by the Budyko curve. *Geophysical Research Letters*, *39*(19), 2–7. doi:10.1029/2012GL053492

Gumbel, E. J. (1941). The return period of flood flows. *The annals of mathematical statistics*, *12*(2), 163–190.

Guswa, A. J. (2008). The influence of climate on root depth: A carbon cost-benefit analysis. *Water Resources Research*, *44*(2), 1–11. doi:10.1029/2007WR006384

Jackson, R. B., Canadell, J., Ehleringer, J. R., Mooney, H. A., Sala, O. E., & Schulze, E. D. (1996). A global analysis of root distributions for terrestrial biomes. *Oecologia*, *108*(3), 389–411. doi:10.1007/BF00333714

Jung, M., Koirala, S., Weber, U., Ichii, K., Gans, F., Camps-Valls, G., ... Reichstein, M. (2019). The FLUXCOM ensemble of global land-atmosphere energy fluxes. *Scientific data*, *6*(1), 74. doi:10.1038/s41597-019-0076-8. arXiv: 1812.04951

Kattsov, V., Federation, R., Reason, C., Africa, S., Uk, A. A., Uk, T. A., ... Uk, A. S. (2013). Evaluation of climate models. *Climate Change 2013 the Physical Science Basis: Working Group I Contribution to the Fifth Assessment Report of the Intergovernmental Panel on Climate Change*, *9781107057*, 741–866. doi:10.1017/CBO9781107415324.020

Keeley, S. (2019). Climate reanalysis. Retrieved from https://www.ecmwf.int/en/research/climate-reanalysis

Kim, H. (2017). Global Soil Wetness Project Phase 3 Atmospheric Boundary Conditions (Experiment 1) [Data set]. *Data Integration and Analysis System (DIAS)*. doi:https://doi.org/10.20783/DIAS.501

Kleidon, A. (2004). Max-Planck Institute for Biogeochemistry Global datasets of rooting zone depth inferred from inverse methods. *Journal of Climate*, 2714–2722.

Kleidon, A. & Heimann, M. (1998). A method of determining rooting depth from a terrestrial biosphere model and its impacts on the global water and carbon cycle. *Global Change Biology*, *4*(3), 275–286. doi:10.1046/j.1365-2486.1998.00152.x

Le Maitre, D. C., Scott, D. F., & Colvin, C. (1999). A review of information on interactions between vegetation and groundwater. *Water SA*, *25*(2), 137–152.

Maes, W. H., Gentine, P., Verhoest, N. E., & Miralles, D. G. (2019). Potential evaporation at eddy-covariance sites across the globe. *Hydrology and Earth System Sciences*, *23*(2), 925–948. doi:10.5194/hess-23-925-2019

McCuen, R. H., Knight, Z., & Cutter, A. G. (2006). Evaluation of the Nash-Sutcliffe Efficiency Index. *Journal of Hydrologic Engineering. 11(6)*(December), 631–635. doi:10.1061/(ASCE)1084-0699(2006)11

Milly, P. C. (1994). Climate, soil water storage, and the average annual water balance. *Water Resources Research*, *30*(7), 2143–2156. doi:10.1029/94WR00586

Mines ParisTech. (2014). Radiation data. Retrieved from soda-pro.com

Oudin, L., Hervieu, F., Michel, C., Perrin, C., Andréassian, V., Anctil, F., & Loumagne, C. (2005). Which potential evapotranspiration input for a lumped rainfall-runoff model? Part 2 - Towards a simple and efficient potential evapotranspiration model for rainfall-runoff modelling. *Journal of Hydrology*, *303*(1-4), 290–306. doi:10.1016/j.jhydrol.2004.08.026

Pachauri, R. K., Allen, M. R., Barros, V. R., Broome, J., Cramer, W., Christ, R., ... Dasgupta, P., et al. (2014). *Climate change 2014: Synthesis report. contribution of working groups i, ii and iii to the fifth assessment report of the intergovernmental panel on climate change*. Ipcc.

Pitman, A. J. (2003). The evolution of, and revolution in, land surface schemes designed for climate models. *International Journal of Climatology*, *23*(5), 479–510. doi:10.1002/joc.893

Savenije, H. H. & Hrachowitz, M. (2017). HESS Opinions "catchments as meta-organisms - A new blueprint for hydrological modelling". *Hydrology and Earth System Sciences*, *21*(2), 1107–1116. doi:10.5194/hess-21-1107-2017

Schenk, H. & Jackson, R. B. (2002a). Rooting depths , lateral root spreads and below-ground / allometries of plants in water-limited. *Society*, *90*(3), 480–494.

Schenk, H. & Jackson, R. B. (2002b). The Global Biogeography of Roots. *72*(3), 311–328.

Schmied, H. M., Eisner, S., Franz, D., Wattenbach, M., Portmann, F. T., Flörke, M., & Döll, P. (2014). Sensitivity of simulated global-scale freshwater fluxes and storages to input data, hydrological model structure, human water use and calibration. *Hydrology and Earth System Sciences*, *18*(9), 3511–3538. doi:10.5194/hess-18-3511-2014

Seneviratne, S. I., Corti, T., Davin, E. L., Hirschi, M., Jaeger, E. B., Lehner, I., ... Teuling, A. J. (2010). Investigating soil moisture-climate interactions in a changing climate: A review. *Earth-Science Reviews*, *99*(3-4), 125–161. doi:10.1016/j.earscirev.2010.02.004. arXiv: WebofScience

Sivandran, G. & Bras, R. L. (2013). Dynamic root distributions in ecohydrological modeling: A case study at Walnut Gulch Experimental Watershed. *Water Resources Research*, *49*(6), 3292–3305. doi:10.1002/wrcr.20245

Sutanto, S. J., Wenninger, J., Coenders-Gerrits, A. M., & Uhlenbrook, S. (2012). Partitioning of evaporation into transpiration, soil evaporation and interception: A comparison between isotope measurements and a hydrus-1d model. *Hydrology and Earth System Sciences*, *16*(8), 2605–2616. doi:10.5194/hess-16-2605-2012

US Department of Energy. (2019). The data portal serving the fluxnet community. Retrieved from https://fluxnet.fluxdata.org/

USGS. (2010). Usgs eros archive - digital elevation - global multi-resolution terrain elevation data 2010 (gmted2010). Retrieved from https://www.usgs.gov/centers/eros/science/usgs-eros-archive-digital-elevation-global-multi-resolution-terrain-elevation?qt-science_center_objects=0#qt-science_center_objects

van den Hurk, B. J., Viterbo, P., Beljaars, A., & Betts, A. (2000). *Offline validation of the era40 surface scheme*. European Centre for Medium-Range Weather Forecasts.

van den Hurk, B., Viterbo, P., Scipal, K., Betts, A. K., Beljaars, A., Hirschi, M., & Balsamo, G. (2008). A Revised Hydrology for the ECMWF Model: Verification from Field Site to Terrestrial Water Storage and Impact in the Integrated Forecast System. *Journal of Hydrometeorology*, *10*(3), 623–643. doi:10.1175/2008jhm1068.1

Van Genuchten, M. T. (1980). A closed-form equation for predicting the hydraulic conductivity of unsaturated soils 1. *Soil science society of America journal*, *44*(5), 892–898.

van Dijk, A. I., Beck, H. E., Crosbie, R. S., de Jeu, R. A., Liu, Y. Y., Podger, G. M., ... Viney, N. R. (2013). The millennium drought in southeast australia (2001–2009): Natural and human causes and implications for water resources, ecosystems, economy, and society. *Water Resources Research*, *49*(2), 1040–1057.

Viterbo, P. & Beljaars, A. C. (1995). An Imprvoved Land Surface Parameterization Scheme in the ECMWF Model and Its Validation. *Journal of Climate*, *8*.

Wang, L., Caylor, K. K., Villegas, J. C., Barron-Gafford, G. A., Breshears, D. D., & Huxman, T. E. (2010). Partitioning evapotranspiration across gradients of woody plant cover: Assessment of a stable isotope technique. *Geophysical Research Letters*, *37*(9), 1–7. doi:10.1029/2010GL043228

Wang-Erlandsson, L. [L.], Van Der Ent, R. J., Gordon, L. J., & Savenije, H. H. (2014). Contrasting roles of interception and transpiration in the hydrological cycle - Part 1: Temporal characteristics over land. *Earth System Dynamics*, *5*(2), 441–469. doi:10.5194/esd-5-441-2014

Wang-Erlandsson, L. [Lan], Bastiaanssen, W. G., Gao, H., Jagermeyr, J., Senay, G. B., Van Dijk, A. I., ... Savenije, H. H. (2016). Global root zone storage capacity from satellite-based evaporation. *Hydrology and Earth System Sciences*, *20*(4), 1459–1481. doi:10.5194/hess-20-1459-2016

Wenninger, J., Beza, D. T., & Uhlenbrook, S. (2010). Experimental investigations of water fluxes within the soil-vegetation-atmosphere system: Stable isotope mass-balance approach to partition evaporation and transpiration. *Physics and Chemistry of the Earth*, *35*(13-14), 565–570. doi:10.1016/j.pce.2010.07.016

Winsemius, H., Schaefli, B., Montanari, A., & Savenije, H. (2009). On the calibration of hydrological models in ungauged basins: A framework for integrating hard and soft hydrological information. *Water Resources Research*, *45*(12).

WMO. (1989). Calculation of monthly and annual 30-year standard normals. World Meteorological Organization [Washington].

Yang, Y., Donohue, R. J., & McVicar, T. R. (2016). Global estimation of effective plant rooting depth: Implications for hydrological modelling. *Journal of the American Water Resources Association*, *5*(3), 2–2. doi:10.1111/j.1752-1688.1969.tb04897.x

Zhang, Y., Shen, Y., Sun, H., & Gates, J. B. (2011). Evapotranspiration and its partitioning in an irrigated winter wheat field: A combined isotopic and micrometeorologic approach. *Journal of Hydrology*, *408*(3-4), 203–211. doi:10.1016/j.jhydrol.2011.07.036

A HTESSEL model parameters

Table A.1: Vegetation indices, vegetation types and model parameter values. H/L refer to high or low vegetation. $r_{s,min}$ is a minimum canopy resistance, c_{veg} represents vegetation coverage, g_D describes the dependence of canopy resistance on water vapor pressure deficit and a_r and b_r are attenuation coefficients describing root distribution (ECMWF, 2016)

Index	**Vegetation type**	**H/L**	$\mathbf{r_{s,min}}$ **(sm^{-1})**	$\mathbf{c_{veg}}$	$\mathbf{g_D}$**(hPa^{-1})**	$\mathbf{a_r}$	$\mathbf{b_r}$
1	Crops, mixed farming	L	100	0.9	0	5.558	2.614
2	Short grass	L	100	0.85	0	10.739	2.608
3	Evergreen needleleaf trees	H	250	0.9	0.03	6.706	2.175
4	Deciduous needleleaf trees	H	250	0.9	0.03	7.066	1.953
5	Deciduous broadleaf trees	H	175	0.9	0.03	5.99	1.955
6	Evergreen broadleaf trees	H	240	0.99	0.03	7.344	1.303
7	Tall grass	L	100	0.7	0	8.235	1.627
8	Desert	-	250	0	0	4.372	0.978
9	Tundra	L	80	0.5	0	8.992	8.992
10	Irrigated crops	L	180	0.9	0	5.558	2.614
11	Semidesert	L	150	0.1	0	4.372	0.978
12	Ice caps and glaciers	-	-	-	-	-	-
13	Bogs and marshes	L	240	0.6	0	7.344	1.303
14	Inland water	-	-	-	-	-	-
15	Ocean	-	-	-	-	-	-
16	Evergreen shrubs	L	225	0.5	0	6.326	1.567
17	Deciduous shrubs	L	225	0.5	0	6.326	1.567
18	Mixed forest/woodland	H	250	0.9	0.03	4.453	1.631
19	Interrupted forest	H	175	0.9	0.03	4.453	1.631
20	Water and land mixtures	L	150	0.6	0	-	-

Table A.2: Volumetric soil moisture (m^3m^{-3}) parameters based on Van Genuchten (ECMWF, 2016)

Soil Texture	$\theta_{\mathbf{sat}}$	$\theta_{\mathbf{cap}}$	$\theta_{\mathbf{pwp}}$	$\theta_{\mathbf{res}}$	$\theta_{\mathbf{cap}} - \theta_{\mathbf{pwp}}$
Coarse	0.403	0.244	0.059	0.025	0.185
Medium	0.439	0.347	0.151	0.01	0.196
Medium fine	0.43	0.383	0.133	0.01	0.251
Fine	0.52	0.448	0.279	0.01	0.17
Very fine	0.614	0.541	0.335	0.01	0.207
Organic	0.766	0.663	0.267	0.01	0.396

Table A.3: Van Genuchten soil parameters (ECMWF, 2016)

Soil type	α **(m^{-1})**	**l (-)**	**n (-)**	γ_{sat} **($10^{-6} ms^{-1}$)**
Coarse	3.83	1.25	1.38	6.94
Medium	3.14	-2.342	1.28	1.16
Medium-Fine	0.83	-0.588	1.25	0.26
Fine	3.67	-1.977	1.10	2.87
Very-Fine	2.65	2.5	1.10	1.74
Organic	1.30	0.4	1.20	0.93

B Catchment characteristics

Table B.1: Hydrological and climatic characteristics of the study catchments.

Catchment	$\overline{Q}$ (mm/year)	$\overline{P}$ (mm/year)	$\overline{E_a}$ (mm/year)	T (°C)	$\overline{E_p}$ (mm/year)	RC (-)	AI (-)	SI (-)	Time-lag (months)
A	94	787	693	12.7	1223	0.12	1.55	0.07	0
Av	8	505	497	14.2	1358	0.02	2.69	0.25	5
D	24	661	637	19.8	1776	0.04	2.69	0.38	0
EA	586	1539	953	26.3	2014	0.38	1.31	0.97	3
EB	134	879	745	27.4	2227	0.15	2.53	0.99	3
G	55	509	453	25.8	2013	0.11	3.96	0.95	1
He	326	1140	814	21.4	1667	0.29	1.46	0.70	2
K	41	889	848	15.1	1207	0.05	1.36	0.50	6
Mi	251	854	603	22.8	1748	0.29	2.05	0.89	2
Mu	59	588	530	10.9	1198	0.10	2.04	0.08	2
Na	84	802	718	14.6	1415	0.10	1.76	0.26	0
No	288	1207	920	24.7	1686	0.24	1.40	0.85	2
P	26	417	392	21.7	1828	0.06	4.38	0.37	1
R	109	1243	1133	12.5	1264	0.09	1.02	0.26	6
W	472	1577	1105	26.3	1728	0.30	1.10	0.95	3

Table B.2: Soil types, vegetation types and vegation coverage in the study catchments.

Catchment	Soil Type	Low vegetation type	High vegetation type	Low vegetation coverage	High vegetation coverage
A	Medium	Crops, mixed farming	Interrupted forest	0.23	0.77
Av	Medium	Crops, mixed farming	Interrupted forest	0.79	0.21
D	Medium fine	Tall grass	Evergreen broadleaf	0.14	0.86
EA	Coarse	Tall grass	Interrupted forest	0.68	0.32
EB	Coarse	Semidesert	-	1.00	0.00
G1	Fine	Short grass	-	1	0
G2	Coarse	Short grass	-	1	0
He	Fine	Tall grass	Evergreen broadleaf	0.01	0.99
K	Coarse	Crops, mixed farming	Interrupted forest	0.65	0.35
Mi	Coarse	Tall grass	Interrupted forest	0.43	0.57
Mu	Medium fine	Tall grass	Interrupted forest	0.16	0.84
Na	Medium	Crops, mixed farming	Interrupted forest	0.33	0.67
No	Coarse	Tall grass	Interrupted forest	0.01	0.99
P	Medium	Semidesert	-	1.00	0.00
R	Medium fine	Crops, mixed farming	Evergreen broadleaf	0.02	0.98
W	Medium fine	Tall grass	Interrupted forest	0.00	1.00

C Catchment monthly mean precipitation and potential evaporation

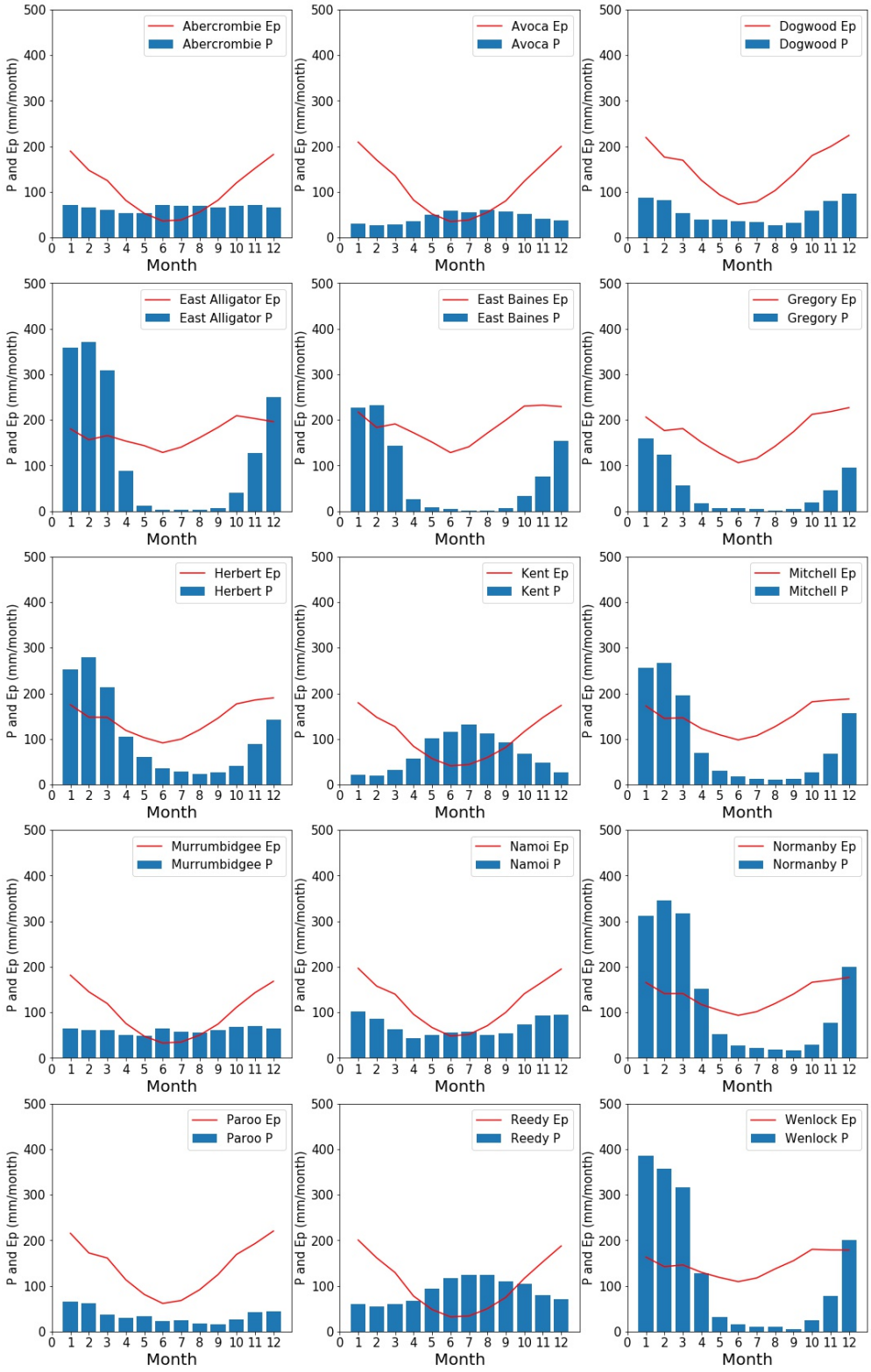

Figure C.1: Monthly mean precipitation (GSWP-3) and potential evaporation (Hargreaves and Samani) in the study catchments.

D SUSSOIL module

The changes applied to this module are marked with yellow.

```
MODULE SUSSOIL_MOD
CONTAINS
SUBROUTINE SUSSOIL(PTHRFRTI,LD_LEVGEN,LD_LESSRO,LD_LESN09)
USE PARKIND1  ,ONLY : JPIM     ,JPRB
USE YOMHOOK   ,ONLY : LHOOK,   DR_HOOK

USE YOS_DIM   , ONLY : NCSS,JPTEXT
USE YOS_SOIL  , ONLY : NSOTY    ,RRCSOIL  ,&
 & RLAMBDADRY          ,RLAMSAT1 ,RLAMBDAICE,&
 & RLAMBDAWAT          ,RKERST1  ,RKERST2  ,RKERST3,&
 & RWB      ,RCWPSIS  ,RWCONS   ,RWSAT    ,&
 & RWCAP    ,RWPWP    ,RSIMP    ,RLICE    ,RGH2O   ,&
 & RQWEVAP  ,RQWSBCR  ,RQSNCR   ,RWLMAX   ,RPSFR   ,&
 & RTF1     ,RTF2     ,RTF3     ,RTF4     ,&
 & RTFREEZSICE         ,RTMELTSICE          ,RDARSICE,&
 & RDANSICE ,RRCSICE  ,RCONDSICE,RDFSICE  ,RCIMIN  ,&
 & RHOICE   ,RLAMICE  ,&
 & RHOCI    ,RALFMINSN,RALFMINPSN,RALFMAXSN,RSNPER ,&
 & RHOMINSN ,RHOMAXSN ,&
 & RTAUF    ,RTAUA    ,RSFRESH  ,RFRSMALL ,RFRTINY ,&
 & RALAMSN  ,RDSNMAX  ,RDAT     ,RDAW     ,RDAI    ,&
 & RTHRFRTI,&
 & RCWPSISM, RMVGALPHA, &
 & RWCONSM, RMFACM, RNFACM, RLAMBDAM, RWSATM,  &
 & RWCAPM, RWPWPM, RWRESTM, RDMAXM, RDMINM, &
 & RQWEVAPM,RQWSBCRM,RLAMBDADRYM,RLAMSAT1M,RRCSOILM,&
 & LEVGEN, LESSRO,LESN09,&
 & RSRDEP, RSIGORMIN, RSIGORMAX,&
 & RLWCSWEA,RLWCSWEB,RLWCSWEC,RTEMPAMP,RHOMINSNA,&
 & RHOMINSNB,RHOMINSNC,RHOMINSND,RSNDTOVERA,RSNDTOVERB,&
 & RSNDTOVERC,RSNDTDESTA,RSNDTDESTB,RSNDTDESTC,RSNDTDESTROI,RHOMAXSN_NEW

USE YOS_CST   , ONLY : RTT, RPI

USE CPTAVE_MOD

#ifdef DOC
!**   *SUSSSOIL* IS THE SET-UP ROUTINE FOR COMMON BLOCK *YOESOIL*

!     PURPOSE
!     -------
!          THIS ROUTINE INITIALIZES THE CONSTANTS IN COMMON BLOCK
!     *YOESOIL*

!     INTERFACE.
!     ----------
!     CALL *SUSURF* FROM *SUPHEC*

!     METHOD.
!     -------

!     EXTERNALS.
!     ----------
!        *CPTAVE* IS CALLED TO GET SOIL VALUES FOR EACH OF 3 BROAD
!                                    TEXTURAL CLASSES

!     REFERENCE.
!     ----------

!     Original    A.C.M. BELJAARS         E.C.M.W.F.      89/11/02

!     MODIFICATIONS
!     -------------
!     J.-J. MORCRETTE         E.C.M.W.F.      91/07/14
!     P. VITERBO              E.C.M.W.F.       8/10/93
!     P. Viterbo     99-03-26    Tiling of the land surface
!     C. Fischer 00-12-20 Meteo-France recode initialization of rdat to avoid
!                         memory overflow on SUN workstation
!     J.F. Estrade *ECMWF* 03-10-01 move in surf vob
!        M.Hamrud      01-Oct-2003 CY28 Cleaning
!     P. Viterbo    24-05-2004      Change surface units
!     P. Viterbo   ECMWF   03-12-2004  Include user-defined RTHRFRTI
!     G. Balsamo   ECMWF   08-01-2006  Include Van Genuchten Hydro.
!     G. Balsamo   ECMWF   11-01-2006  Include sub-grid scale runoff
!     E. Dutra             12-11.2008  Include new snow parameterization
!     E. Dutra             16-11-2009  snow 2009 cleaning
```

```
!     F. Catalano A. Alessandri ENEA    10/2017     Four components soil albedo estimated from
MODIS
!     ------------------------------------------------------------------

#endif

IMPLICIT NONE

! Declaration of arguments

REAL(KIND=JPRB)   ,INTENT(IN)    :: PTHRFRTI
LOGICAL           ,INTENT(IN)    :: LD_LEVGEN
LOGICAL           ,INTENT(IN)    :: LD_LESSRO
LOGICAL           ,INTENT(IN)    :: LD_LESN09

REAL(KIND=JPRB) :: ZTHECAP(JPTEXT),ZTHEPWP(JPTEXT),ZTHESAT(JPTEXT),&
 & ZWB(JPTEXT),ZWCONS(JPTEXT),ZWPSIS(JPTEXT)
REAL(KIND=JPRB), ALLOCATABLE :: ZMVGALPHA(:),ZWCONSM(:),ZNFAC(:),&
 & ZLAMBDA(:),ZWSATM(:),ZWCAPM(:),ZWRES(:),ZWPWPM(:)

REAL(KIND=JPRB) :: ZRCGDRY, ZRHOSM, ZRHOD, ZLAMBDAQ, ZLAMBDAO, ZQ, ZLAMBDASM
REAL(KIND=JPRB) :: ZDMIN, ZDMAX, ZWFAC, ZSEMAX, ZSEMIN, ZWMAX, ZWMIN,&
 & ZFAC, ZPSIPWP, ZPSICAP
INTEGER(KIND=JPIM) :: I, JS
REAL(KIND=JPRB) :: ZHOOK_HANDLE

!     ------------------------------------------------------------------

!*         1.     SET CONSTANTS
!                 -------------

IF (LHOOK) CALL DR_HOOK('SUSSOIL_MOD:SUSSOIL',0,ZHOOK_HANDLE)
RLICE  =0.3_JPRB
RGH2O  =4.18E6_JPRB
RQSNCR =1.0_JPRB/15._JPRB
RWLMAX =0.2_JPRB
RPSFR=2._JPRB

!     LAND SURFACE CONSTANTS

LEVGEN=LD_LEVGEN
LESSRO=LD_LESSRO

!    SNOW LOGICALS

LESN09=LD_LESN09
IF (LESN09) RQSNCR =1.0_JPRB/10._JPRB

!GPB IF(.NOT.LEVGEN) &

     CALL CPTAVE(ZTHESAT,ZTHECAP,ZTHEPWP,ZWCONS,ZWPSIS,ZWB)

!     CONSTANTS DEFINING SOIL DISCRETIZATION
IF(.NOT.ALLOCATED(RDAT)) ALLOCATE(RDAT(NCSS))
IF(.NOT.ALLOCATED(RDAW)) ALLOCATE(RDAW(NCSS))
IF(.NOT.ALLOCATED(RDAI)) ALLOCATE(RDAI(NCSS))

IF (NCSS >= 1) RDAT(1)=0.07_JPRB
IF (NCSS >= 2) RDAT(2)=0.21_JPRB
IF (NCSS >= 3) RDAT(3)=0.72_JPRB
IF (NCSS >= 4) RDAT(4)=1.89_JPRB
DO I=1,NCSS
  RDAW(I)=RDAT(I)
  RDAI(I)=RDAT(I)
ENDDO

IF (NCSS >= 1) RDAW(1)=0.07_JPRB
IF (NCSS >= 2) RDAW(2)=0.21_JPRB
IF (NCSS >= 3) RDAW(3)=0.72_JPRB
IF (NCSS >= 4) RDAW(4)=1.103_JPRB

!     CONSTANTS FOR HYDRAULIC DIFFUSIVITY AND HYDRAULIC CONDUCTIVITY
!GPB IF (LEVGEN) THEN
! VAN GENUCHTEN (MV) HYDROLOGY
!
!     COMPUTE AVERAGE SOIL PROPERTIES FOR SOIL TYPES
!
```

```
!     SOIL TYPE 1 (COARSE)
!     SOIL TYPE 2 (MEDIUM)
!     SOIL TYPE 3 (MEDIUM FINE)
!     SOIL TYPE 4 (FINE)
!     SOIL TYPE 5 (VERY FINE)
!     SOIL TYPE 6 (EXT.TROP. ORGANIC SOIL)
!     SOIL TYPE 7 (TROP. ORGANIC SOIL)

  NSOTY=7
  IF(.NOT.ALLOCATED(ZMVGALPHA)) ALLOCATE (ZMVGALPHA(0:NSOTY))
  IF(.NOT.ALLOCATED(ZWCONSM)) ALLOCATE (ZWCONSM(0:NSOTY))
  IF(.NOT.ALLOCATED(ZNFAC)) ALLOCATE (ZNFAC(0:NSOTY))
  IF(.NOT.ALLOCATED(ZLAMBDA)) ALLOCATE (ZLAMBDA(0:NSOTY))
  IF(.NOT.ALLOCATED(ZWSATM)) ALLOCATE (ZWSATM(0:NSOTY))
  IF(.NOT.ALLOCATED(ZWCAPM)) ALLOCATE (ZWCAPM(0:NSOTY))
  IF(.NOT.ALLOCATED(ZWRES)) ALLOCATE (ZWRES(0:NSOTY))
  IF(.NOT.ALLOCATED(ZWPWPM)) ALLOCATE (ZWPWPM(0:NSOTY))
  IF(.NOT.ALLOCATED(RCWPSISM)) ALLOCATE (RCWPSISM(0:NSOTY))
  IF(.NOT.ALLOCATED(RMVGALPHA)) ALLOCATE (RMVGALPHA(0:NSOTY))
  IF(.NOT.ALLOCATED(RWCONSM)) ALLOCATE (RWCONSM(0:NSOTY))
  IF(.NOT.ALLOCATED(RMFACM)) ALLOCATE (RMFACM(0:NSOTY))
  IF(.NOT.ALLOCATED(RNFACM)) ALLOCATE (RNFACM(0:NSOTY))
  IF(.NOT.ALLOCATED(RLAMBDAM)) ALLOCATE (RLAMBDAM(0:NSOTY))
  IF(.NOT.ALLOCATED(RWSATM)) ALLOCATE (RWSATM(0:NSOTY))
  IF(.NOT.ALLOCATED(RWCAPM)) ALLOCATE (RWCAPM(0:NSOTY))
  IF(.NOT.ALLOCATED(RWPWPM)) ALLOCATE (RWPWPM(0:NSOTY))
  IF(.NOT.ALLOCATED(RWRESTM)) ALLOCATE (RWRESTM(0:NSOTY))
  IF(.NOT.ALLOCATED(RDMAXM)) ALLOCATE (RDMAXM(0:NSOTY))
  IF(.NOT.ALLOCATED(RDMINM)) ALLOCATE (RDMINM(0:NSOTY))
  IF(.NOT.ALLOCATED(RQWEVAPM)) ALLOCATE (RQWEVAPM(0:NSOTY))
  IF(.NOT.ALLOCATED(RQWSBCRM)) ALLOCATE (RQWSBCRM(0:NSOTY))


ZMVGALPHA(1:NSOTY)=(/3.83_JPRB,3.14_JPRB,0.83_JPRB,3.67_JPRB,2.65_JPRB,1.300_JPRB,3.14_JPRB/)
  ZWCONSM(1:NSOTY)=(/6.94E-6_JPRB,1.16E-6_JPRB,2.63E-7_JPRB,2.87E-6_JPRB,&
 &             1.740E-6_JPRB, 0.93E-6_JPRB,1.16E-6_JPRB/)

ZNFAC(1:NSOTY)=(/1.3774_JPRB,1.1804_JPRB,1.2539_JPRB,1.1012_JPRB,1.1033_JPRB,1.2039_JPRB,1.180
4_JPRB/)
  ZLAMBDA(1:NSOTY)=(/1.250_JPRB,-2.3421_JPRB,-0.5884_JPRB,-1.9772_JPRB,2.5000_JPRB,&
 &             0.40000_JPRB,-2.3421_JPRB/)

ZWSATM(1:NSOTY)=(/0.403_JPRB,0.439_JPRB,0.430_JPRB,0.520_JPRB,0.614_JPRB,0.766_JPRB,0.439_JPRB
/)

ZWRES(1:NSOTY)=(/0.025_JPRB,0.010_JPRB,0.010_JPRB,0.010_JPRB,0.010_JPRB,0.010_JPRB,0.010_JPRB/
)

! Set 0 SOILTYPE (WATER) VALUES TO 0
  ZMVGALPHA(0)=0.0_JPRB
  ZWCONSM(0)=0.0_JPRB
  ZNFAC(0)=0.0_JPRB
  ZLAMBDA(0)=0.0_JPRB
  ZWSATM(0)=0.0_JPRB
  ZWCAPM(0)=0.0_JPRB
  ZWRES(0)=0.0_JPRB
  ZWPWPM(0)=0.0_JPRB
  RCWPSISM(0)=0.0_JPRB
  RMVGALPHA(0)=0.0_JPRB
  RWCONSM(0)=0.0_JPRB
  RMFACM(0)=0.0_JPRB
  RNFACM(0)=0.0_JPRB
  RLAMBDAM(0)=0.0_JPRB
  RWSATM(0)=0.0_JPRB
  RWCAPM(0)=0.0_JPRB
  RWPWPM(0)=0.0_JPRB
  RWRESTM(0)=0.0_JPRB
  RDMAXM(0)=0.0_JPRB
  RDMINM(0)=0.0_JPRB
  RQWEVAPM(0)=0.0_JPRB
  RQWSBCRM(0)=0.0_JPRB

  ZFAC=1000._JPRB*100._JPRB/(1000._JPRB*9.8_JPRB)
  ZPSIPWP=-15._JPRB*ZFAC   ! Classic permanent wilting point
  IF (LEVGEN) THEN
    ZPSICAP=-0.10_JPRB*ZFAC  ! Value valid for sandy soil in the literature---> larger AWC
                             ! favourably compared to FC obs for medium soils (Ukraine/Russia)
```

```
                              ! produce invariant equilibrium after rescaling from TESSEL
                              ! enlarge the range of action for SM analysis (active if
PWP<W<CAP)
  ELSE
    ZPSICAP=-0.33_JPRB*ZFAC  ! Value mostly used in literature (Hillel, 1998)
  ENDIF
! ZPSICAP=-0.05_JPRB*ZFAC  ! Value used in HYPRES framework (only!)
! WRITE(NULOUT,'(/a)')'SOTYPE  RCWPSISM    RMVGALPHA     RWCONSM' &
! &     //'       RMFACM' &
! &     //'       RNFACM     RLAMBDAM       RWSATM       RWCAPM ' &
! &     //'      RWPWPM      RWRESTM       RDMAXM       RDMINM ' &
! &     //'    RQWEVAPM     RQWSBCRM'

  DO JS=1,NSOTY
    RCWPSISM(JS)=(1._JPRB/ZMVGALPHA(JS))
    RMVGALPHA(JS)=ZMVGALPHA(JS)
    RWCONSM(JS)=ZWCONSM(JS)
    RMFACM(JS)=1._JPRB-(1._JPRB/ZNFAC(JS))
    RLAMBDAM(JS)=ZLAMBDA(JS)
    RNFACM(JS)=ZNFAC(JS)
    RWSATM(JS)=ZWSATM(JS)
    ZWCAPM(JS)=ZWRES(JS)+(ZWSATM(JS)-ZWRES(JS)) &
 &           *(1._JPRB/(1._JPRB+((ABS(RMVGALPHA(JS)*ZPSICAP)) &
 &           **RNFACM(JS))))**RMFACM(JS)
    RWCAPM(JS)=ZWCAPM(JS)
    ZWPWPM(JS)=ZWRES(JS)+(ZWSATM(JS)-ZWRES(JS)) &
 &           *(1._JPRB/(1._JPRB+((ABS(RMVGALPHA(JS)*ZPSIPWP)) &
 &           **RNFACM(JS))))**RMFACM(JS)
    RWPWPM(JS)=ZWPWPM(JS)
    RWRESTM(JS)=ZWRES(JS)
    ZWMAX=.999_JPRB*RWSATM(JS)
    ZSEMAX=(ZWMAX-RWRESTM(JS))/(RWSATM(JS)-RWRESTM(JS))
    ZWFAC=(RWSATM(JS)-RWRESTM(JS))
    ZDMAX=(((1._JPRB-RMFACM(JS))*RWCONSM(JS))/ &
 &         (RMVGALPHA(JS)*RMFACM(JS)*ZWFAC)) &
 &          *(ZSEMAX**(RLAMBDAM(JS)-(1._JPRB/RMFACM(JS)))) &
 &          *(((1._JPRB-(ZSEMAX**(1._JPRB/RMFACM(JS))))**(RMFACM(JS))) &
 &          + ((1._JPRB-(ZSEMAX**(1._JPRB/RMFACM(JS))))**(-RMFACM(JS)))-2._JPRB)
    RDMAXM(JS)=ZDMAX
    ZWMIN=1.001_JPRB*RWRESTM(JS)
    ZSEMIN=(ZWMIN-RWRESTM(JS))/(RWSATM(JS)-RWRESTM(JS))
    ZDMIN=(((1._JPRB-RMFACM(JS))*RWCONSM(JS))/ &
 &         (RMVGALPHA(JS)*RMFACM(JS)*ZWFAC)) &
 &          *(ZSEMIN**(RLAMBDAM(JS)-(1._JPRB/RMFACM(JS)))) &
 &          *(((1._JPRB-(ZSEMIN**(1._JPRB/RMFACM(JS))))**(RMFACM(JS))) &
 &          + ((1._JPRB-(ZSEMIN**(1._JPRB/RMFACM(JS))))**(-RMFACM(JS)))-2._JPRB)
    RDMINM(JS)=ZDMIN

    RQWEVAPM(JS)=1._JPRB/(RWCAPM(JS)-RWPWPM(JS))
    RQWSBCRM(JS)=RPI/(1.6_JPRB*RWCAPM(JS))
!          WRITE(NULOUT,'(1X,I2,20(1X,E12.5))')JS,RCWPSISM(JS), &
! &         RMVGALPHA(JS), &
! &         RWCONSM(JS),RMFACM(JS),RNFACM(JS),RLAMBDAM(JS), &
! &         RWSATM(JS), &
! &         RWCAPM(JS),RWPWPM(JS),RWRESTM(JS), &
! &         RDMAXM(JS),RDMINM(JS), &
! &         RQWEVAPM(JS),RQWSBCRM(JS)
  ENDDO

!GPB ELSE
! CLAPP AND HORNBERGER (CH) HYDROLOGY ON A LOAMY SOIL
!        MEDIUM SOIL TYPE VALUES ARE CHOSEN EVERYWHERE

  RWB=ZWB(2)
  RWCONS=ZWCONS(2)
  RCWPSIS=ZWPSIS(2)

!     CONSTANTS FOR DEFINING THE SOIL WATER HOLDING CHARACTERISTICS

!        MEDIUM SOIL TYPE VALUES ARE CHOSEN EVERYWHERE

  RWSAT=ZTHESAT(2)
  RWCAP=ZTHECAP(2)
  RWPWP=ZTHEPWP(2)

  RQWEVAP=1.0_JPRB/(RWCAP-RWPWP)
  RQWSBCR=RPI/(RWCAP*1.6_JPRB)
```

```
!GPB ENDIF
!     CONSTANTS FOR THERMAL DIFFUSIVITY

!     VALUES TAKEN FROM Peters-Liddard et al. 1998
!     COMMON TO CH AND MV
ZRHOSM=2700._JPRB
ZLAMBDAQ=7.7_JPRB
ZLAMBDAO=2._JPRB
ZQ=0.4_JPRB
ZLAMBDASM=(ZLAMBDAQ**ZQ)*(ZLAMBDAO**(1.0_JPRB-ZQ))
ZRCGDRY=1.6E6_JPRB

RLAMBDAICE=2.2_JPRB
RLAMBDAWAT=0.57_JPRB
RKERST1=0.1_JPRB
RKERST2=1.0_JPRB
RKERST3=1.0_JPRB

!GPB IF(LEVGEN)THEN

!     VAN GENUCHTEN

  IF(.NOT.ALLOCATED(RLAMBDADRYM)) ALLOCATE (RLAMBDADRYM(NSOTY))
  IF(.NOT.ALLOCATED(RLAMSAT1M)) ALLOCATE (RLAMSAT1M(NSOTY))
  IF(.NOT.ALLOCATED(RRCSOILM)) ALLOCATE (RRCSOILM(NSOTY))
  DO JS=1,NSOTY
    ZRHOD=(1.0_JPRB-RWSATM(JS))*ZRHOSM
    RLAMBDADRYM(JS)=(0.135_JPRB*ZRHOD+64.7_JPRB)/(ZRHOSM-0.947*ZRHOD)
    RLAMSAT1M(JS)=ZLAMBDASM**(1.0_JPRB-RWSATM(JS))
!     SOIL HEAT CAPACITY

    RRCSOILM(JS)=(1.0_JPRB-RWSATM(JS))*ZRCGDRY+RWCAPM(JS)*RGH2O
  ENDDO
!GPB ELSE

!     CLAPP-HORNBERGER

  ZRHOD=(1.0_JPRB-RWSAT)*ZRHOSM
  RLAMBDADRY=(0.135_JPRB*ZRHOD+64.7_JPRB)/(ZRHOSM-0.947_JPRB*ZRHOD)
  RLAMSAT1=ZLAMBDASM**(1.0_JPRB-RWSAT)

!     SOIL HEAT CAPACITY

!     SET TO A CONSTANT REPRESENTATIVE OF THE VALUE AT FIELD CAPACITY

  RRCSOIL=(1-RWSAT)*ZRCGDRY+RWCAP*RGH2O

!GPB ENDIF

!     FORWARD TIMESTEP WEIGHTING FACTOR FOR TIME INTEGRATION

RSIMP=1._JPRB

!     CONSTANTS FOR SOIL WATER FREEZING

RTF1=RTT+1.0_JPRB
RTF2=RTT-3._JPRB
RTF3=0.5_JPRB*(RTF1+RTF2)
RTF4=RPI/(RTF1-RTF2)

!     SEA ICE RELATED CONSTANTS

RTFREEZSICE=RTT - 1.7_JPRB
RTMELTSICE=RTT
RDARSICE=1.5_JPRB
RDANSICE=1.5_JPRB
RRCSICE=1.884E06_JPRB
RCONDSICE=2.03_JPRB
RDFSICE=RCONDSICE/RRCSICE
RCIMIN=0.0_JPRB

!     SURFACE RUNOFF RELATED CONSTANTS

RSRDEP=0.5_JPRB
RSIGORMIN=100.0_JPRB
RSIGORMAX=1000.0_JPRB
```

```
!     SNOW RELATED CONSTANTS

RHOICE=920._JPRB
RLAMICE=2.22_JPRB
RHOCI=2.05E6_JPRB
RALFMINSN=0.50_JPRB
RALFMINPSN=0.80_JPRB ! Pirazzini (2004)
RALFMAXSN=0.85_JPRB
RSNPER=10000.0_JPRB
RHOMINSN=100._JPRB
RHOMAXSN=300._JPRB
RTAUF=0.24_JPRB
RTAUA=0.008_JPRB
RSFRESH=1.0_JPRB/3600._JPRB
RFRTINY =1.E-7_JPRB
RFRSMALL=10._JPRB*RFRTINY
RALAMSN=1.88_JPRB
RDSNMAX=1._JPRB

!    SNOW RELATED - NEW DENSITY PARAMETERIZATION
RLWCSWEA=200._JPRB
RLWCSWEB=0.03_JPRB
RLWCSWEC=0.1_JPRB
RTEMPAMP=4.0_JPRB

RHOMINSNA=109._JPRB
RHOMINSNB=6._JPRB
RHOMINSNC=26._JPRB
RHOMINSND=50._JPRB

RSNDTOVERA=3.7E7_JPRB
RSNDTOVERB=8.1E-2_JPRB
RSNDTOVERC=1.8E-2_JPRB

RSNDTDESTA=2.8E-6_JPRB
RSNDTDESTB=4.2E-2_JPRB
RSNDTDESTC=460.0_JPRB
RSNDTDESTROI=150.0_JPRB

RHOMAXSN_NEW=450._JPRB

! Tiles constants

RTHRFRTI=PTHRFRTI

IF (LHOOK) CALL DR_HOOK('SUSSOIL_MOD:SUSSOIL',1,ZHOOK_HANDLE)

!     ------------------------------------------------------------------

END SUBROUTINE SUSSOIL
END MODULE SUSSOIL_MOD
```

E SRFWEXC-VG module

The changes applied to this module are marked with yellow.

```
MODULE SRFWEXC_VG_MOD
CONTAINS
SUBROUTINE SRFWEXC_VG(KIDIA,KFDIA,KLON,KLEVS,KTILES,&
 & PTMST,KTVL,KTVH,KSOTY,PSDOR,PFRTI,PEVAPTI,&
 & PWSAM1M,PTSAM1M,&
 & PTSFC,PTSFL,PMSN,PEMSSN,PEINTTI,PEVAPSNW,&
 & PROS,PCFW,PRHSW,&
 & PSAWGFL,PFWEL1,PFWE234,&
 & LDLAND,PDHWLS)

USE PARKIND1  ,ONLY : JPIM     ,JPRB
USE YOMHOOK   ,ONLY : LHOOK,   DR_HOOK

USE YOS_THF   , ONLY : RHOH2O
USE YOS_SOIL  , ONLY : RSIMP    ,RPSFR    ,RDAW     ,&
 & RTF1     ,RTF2     ,RTF3     ,RTF4     ,&
 & RWPWPM, RWCAPM, RDMAXM, RDMINM, RWRESTM, RWSATM, RLAMBDAM,&
 & RMFACM, RWCONSM, RMVGALPHA, LESSRO, &
 & RSRDEP, RSIGORMIN, RSIGORMAX

USE YOS_VEG   , ONLY : RVROOTSA

#ifdef DOC
!**** *SRFWEXC_VG* -  COMPUTES THE FLUXES BETWEEN THE SOIL LAYERS AND
!                  THE RIGHT-HAND SIDE OF THE SOIL WATER EQUATIONS.
!
!     PURPOSE.
!     --------
!          THIS ROUTINE COMPUTES THE DIFFERENT COEFFICIENTS IN THE
!     SOIL MOISTURE EQUATIONS (BEFORE SNOW MELTS). THE AIM IS TO COMPUTE
!     THE MODIFIED DIFFUSIVITIES AND THE RIGHT-HAND SIDE OF THE EQUATIONS.
!     IT SHOULD BE FOLLOWED BY A CALL TO *SRFWDIF* AND *SRFWINC*.

!**   INTERFACE.
!     ----------
!          *SRFWEXC_VG* IS CALLED FROM *SURFTSTP*.

!     PARAMETER   DESCRIPTION                                     UNITS
!     ---------   -----------                                     -----
!     INPUT PARAMETERS (INTEGER):
!    *KIDIA*      START POINT
!    *KFDIA*      END POINT
!    *KLON*       NUMBER OF GRID POINTS PER PACKET
!    *KLEVS*      NUMBER OF SURFACE LAYERS
!    *KTILES*     NUMBER OF TILES (I.E. SUBGRID AREAS WITH DIFFERENT
!                 OF SURFACE BOUNDARY CONDITION)
!    *KDHVWLS*    Number of variables for soil water budget
!    *KDHFWLS*    Number of fluxes for soil water budget

!    *KTVL*       VEGETATION TYPE FOR LOW VEGETATION FRACTION
!    *KTVH*       VEGETATION TYPE FOR HIGH VEGETATION FRACTION
!    *KSOTY*      SOIL TYPE                                    (1-7)

!     INPUT PARAMETERS (REAL):
!    *PTMST*      TIME STEP                                      S
!    *PSDOR*      OROGRAPHIC PARAMETER                           m
!    *PFRTI*      TILE FRACTIONS                               (0-1)
!            1 : WATER                 5 : SNOW ON LOW-VEG+BARE-SOIL
!            2 : ICE                   6 : DRY SNOW-FREE HIGH-VEG
!            3 : WET SKIN              7 : SNOW UNDER HIGH-VEG
!            4 : DRY SNOW-FREE LOW-VEG  8 : BARE SOIL
!    *PEVAPTI*      SURFACE MOISTURE FLUX                     KG/M**2/S

!     INPUT PARAMETERS (LOGICAL):
!    *LDLAND*     LAND/SEA MASK (TRUE/FALSE)

!     INPUT PARAMETERS AT T-1 OR CONSTANT IN TIME (REAL):
!    *PWSAM1M*    MULTI-LAYER SOIL MOISTURE                   M**3/M**3
!    *PTSAM1M*    SOIL TEMPERATURE ALL LAYERS                   K
!    *PTSFC*      CONVECTIVE THROUGHFALL                      KG/M**2/S
!    *PTSFL*      LARGE SCALE THROUGHFALL                     KG/M**2/S
!    *PMSN*       SNOW MELTING                                KG/M**2/S
!    *PEMSSN*     EVAPORATIVE MISMATCH RESULTING FROM
!                  CLIPPING THE SNOW TO ZERO (AFTER P-E)      KG/M**2/S
!    *PEINTTI*    TILE EVAPORATION SEEN BY THE INTERCEPTION
!                 LAYER (INCLUDES NUMERICAL EVAPORATION
!                 MISMATCHES, FOR TILE 3, AND DEW DEPOSITION
```

```
!                FOR TILES 3,4,6,7,8)                          KG/M**2/S
!    *PEVAPSNW*  EVAPORATION FROM SNOW UNDER FOREST            KG/M**2/S

!     OUTPUT PARAMETERS (REAL):
!    *PCFW*      MODIFIED DIFFUSIVITIES                          M
!    *PRHSW*     RIGHT-HAND SIDE OF SOIL MOISTURE EQUATIONS   m**3/m**3
!    *PROS*      RUN-OFF FOR THE SURFACE LAYER                kg/m**2
!    *PFWEL1*    BARE GROUND AND TOP LAYER EXTRACTION
!                CONTRIBUTION TO EVAPORATION FROM
!                THE SKIN AND TOP LAYER                       KG/M**2/S
!    *PFWE234*   ROOT EXTRACTION FROM LAYERS 2+3+4            KG/M**2/S

!     INSTANTANEOUS DIAGNOSTIC OUTPUT PARAMETERS (REAL):
!    *PSAWGFL*   GRAVITY PART OF WATER FLUX                   KG/M**2/S
!                  (positive downwards, at layer bottom)

!     OUTPUT PARAMETERS (DIAGNOSTIC):
!    *PDHWLS*    Diagnostic array for soil water (see module yomcdh)

!     METHOD.
!     -------
!          STRAIGHTFORWARD ONCE THE DEFINITION OF THE CONSTANTS IS
!     UNDERSTOOD. FOR THIS REFER TO DOCUMENTATION.

!     EXTERNALS.
!     ----------
!          NONE.

!     REFERENCE.
!     ----------
!          SEE SOIL PROCESSES' PART OF THE MODEL'S DOCUMENTATION FOR
!     DETAILS ABOUT THE MATHEMATICS OF THIS ROUTINE.

!     ORIGINAL :
!     P.VITERBO      E.C.M.W.F.      9/02/93
!     P.VITERBO      E.C.M.W.F.      26-3-99
!        (Interface to tiling)
!     D.SALMOND      E.C.M.W.F.      000515
!     P.VITERBO      E.C.M.W.F.      17-05-2000
!        (Surface DDH for TILES)
!     J.F. Estrade *ECMWF* 03-10-01 move in surf vob
!     P. Viterbo    ECMWF    24-05-2004      Change surface units
!     G. Balsamo    ECMWF    08-01-2006      Include Van Genuchten Hydro.
!     G. Balsamo    ECMWF    11-01-2006      Include sub-grid surface runoff
!     G. Balsamo    ECMWF    03-07-2006      Add soil type
!     E. Dutra               07-07-2008      clean number of tiles dependence
!     G. Balsamo    ECMWF    15-09-2009      protect surf-runoff for occasional overshooting
!     G. Balsamo    ECMWF    12-05-2010      cleaning and unit fix in VIC
!     ------------------------------------------------------------------
#endif

IMPLICIT NONE

! Declaration of arguments

INTEGER(KIND=JPIM), INTENT(IN)   :: KIDIA
INTEGER(KIND=JPIM), INTENT(IN)   :: KFDIA
INTEGER(KIND=JPIM), INTENT(IN)   :: KLON
INTEGER(KIND=JPIM), INTENT(IN)   :: KLEVS
INTEGER(KIND=JPIM), INTENT(IN)   :: KTILES
INTEGER(KIND=JPIM), INTENT(IN)   :: KTVL(:)
INTEGER(KIND=JPIM), INTENT(IN)   :: KTVH(:)
INTEGER(KIND=JPIM), INTENT(IN)   :: KSOTY(:)

REAL(KIND=JPRB),    INTENT(IN)   :: PTMST
REAL(KIND=JPRB),    INTENT(IN)   :: PSDOR(:)
REAL(KIND=JPRB),    INTENT(IN)   :: PFRTI(:,:)
REAL(KIND=JPRB),    INTENT(IN)   :: PEVAPTI(:,:)
REAL(KIND=JPRB),    INTENT(IN)   :: PWSAM1M(:,:)
REAL(KIND=JPRB),    INTENT(IN)   :: PTSAM1M(:,:)
REAL(KIND=JPRB),    INTENT(IN)   :: PTSFC(:)
REAL(KIND=JPRB),    INTENT(IN)   :: PTSFL(:)
REAL(KIND=JPRB),    INTENT(IN)   :: PMSN(:)
REAL(KIND=JPRB),    INTENT(IN)   :: PEMSSN(:)
REAL(KIND=JPRB),    INTENT(IN)   :: PEINTTI(:,:)
REAL(KIND=JPRB),    INTENT(IN)   :: PEVAPSNW(:)
```

```
LOGICAL,   INTENT(IN)   :: LDLAND(:)

REAL(KIND=JPRB),    INTENT(INOUT):: PDHWLS(:,:,:)
REAL(KIND=JPRB),    INTENT(INOUT):: PFWEL1(:)
REAL(KIND=JPRB),    INTENT(INOUT):: PFWE234(:)

REAL(KIND=JPRB),    INTENT(OUT)  :: PROS(:)
REAL(KIND=JPRB),    INTENT(OUT)  :: PCFW(:,:)
REAL(KIND=JPRB),    INTENT(OUT)  :: PRHSW(:,:)
REAL(KIND=JPRB),    INTENT(OUT)  :: PSAWGFL(:,:)

!*         0.2    DECLARATION OF LOCAL VARIABLES.
!                 ------------ -- ------ ----------

REAL(KIND=JPRB) :: ZSAWEXT(KLON,KLEVS)
REAL(KIND=JPRB) :: ZROOTW(KLON,KLEVS,KTILES),ZEXT(KLON,KTILES)
REAL(KIND=JPRB) :: ZLIQH(KLON,KLEVS),ZLIQL(KLON,KLEVS),ZF(KLON,KLEVS),ZCONDS(KLON)
LOGICAL :: LLFREEZ

INTEGER(KIND=JPIM) :: ITYP(KLON), JK, JL, JTILE, JS

REAL(KIND=JPRB) :: Z_RHOH2O, ZD, ZEPEXT, &
 & ZEXTK, ZINFMAX, ZK, ZKM, ZPSFR, ZROC, ZROL, ZDSURF, ZKSURF, &
 & ZROT, ZINVTMST, ZW, ZWM, ZWSFL,ZEVAP, ZFF, ZFFM,ZHOH2O, ZWS, &
 & ZDMAX, ZDMIN, ZDD, ZKD, ZALPHA, ZSE, ZWFAC, ZLAM, ZMFAC, ZRMFAC, &
 & ZWCONS, ZKMD, &
 & ZRSFL, ZROEFF, ZSIGOR, ZBWS, ZB1, ZBM, ZWMAX, &
 & ZCONW1, ZLYEPS, ZLYSIC, ZVOL, ZROS, ZSUM, ZLIMRS, FH, FL

REAL(KIND=JPRB) :: ZFRK(KLEVS),ZWK(KLEVS),ZWMK(KLEVS)

REAL(KIND=JPRB) :: ZHOOK_HANDLE

!     ------------------------------------------------------------------
!*         1.    SET UP SOME CONSTANTS.
!                --- -- ---- ----------
!    SECURITY PARAMETERS

IF (LHOOK) CALL DR_HOOK('SRFWEXC_VG_MOD:SRFWEXC_VG',0,ZHOOK_HANDLE)
ZEPEXT=10._JPRB*TINY(Z_RHOH2O)

!    COMPUTATIONAL CONSTANTS.

ZHOH2O=1.0_JPRB/RHOH2O
ZPSFR=1.0_JPRB/RPSFR
ZINVTMST=1.0_JPRB/PTMST

LLFREEZ=.TRUE.

!       SET FH AND FL - FRACTIONS FOR ROOTZONE EXTRACTION
FH = 0.92_JPRB
FL = 0.73_JPRB

!     ------------------------------------------------------------------
!*          2. COMPUTATION OF THE MODIFIED DIFFUSIVITY COEFFICIENTS
!              ----------- -- --- -------- ----------- ------------
!*          2.1 Preliminary quantities related to root extraction
!               Compute first liquid fraction of soil water to
!               be used later in stress functions.
DO JK=1,KLEVS
  DO JL=KIDIA,KFDIA
    IF(PTSAM1M(JL,JK) < RTF1.AND.PTSAM1M(JL,JK) > RTF2) THEN
      ZF(JL,JK)=0.5_JPRB*(1.0_JPRB-SIN(RTF4*(PTSAM1M(JL,JK)-RTF3)))
    ELSEIF (PTSAM1M(JL,JK) <= RTF2) THEN
      ZF(JL,JK)=1.0_JPRB
    ELSE
      ZF(JL,JK)=0.0_JPRB
    ENDIF
    JS=KSOTY(JL)
    ZLIQH(JL,JK)=MAX(RWPWPM(JS),MIN(FH*RWCAPM(JS),PWSAM1M(JL,JK)*(1._JPRB*FH-ZF(JL,JK))))
    ZLIQL(JL,JK)=MAX(RWPWPM(JS),MIN(FL*RWCAPM(JS),PWSAM1M(JL,JK)*(1._JPRB*FL-ZF(JL,JK))))
  ENDDO
ENDDO

!*          2.2 Preliminary quantities related to root extraction
DO JL=KIDIA,KFDIA
  ZCONDS(JL)=0.0_JPRB
```

```
  DO JTILE=1,KTILES
    ZEXT(JL,JTILE)=0.0_JPRB
  ENDDO
ENDDO
DO JTILE=1,KTILES
  DO JK=1,KLEVS
    DO JL=KIDIA,KFDIA
      ZROOTW(JL,JK,JTILE)=0.0_JPRB
    ENDDO
  ENDDO
ENDDO

TILES: DO JTILE=1,KTILES
! no liquid evaporation contribution to soil from tile 1, 2, 5
! no root extraction from tile 3 and 8
    IF ( JTILE /= 4 .AND. JTILE /= 6 .AND. JTILE /= 7 ) CYCLE TILES
    IF (JTILE == 4) THEN
      DO JL=KIDIA,KFDIA
        ITYP(JL)=KTVL(JL)
      ENDDO
    ELSEIF (JTILE == 6.OR. JTILE == 7) THEN
      DO JL=KIDIA,KFDIA
        ITYP(JL)=KTVH(JL)
      ENDDO
    ENDIF
! Layers 1-klevs
    LAYERS: DO JK=1,KLEVS
      DO JL=KIDIA,KFDIA
        JS=KSOTY(JL)
        IF (JTILE == 7) THEN
          ZEVAP=PFRTI(JL,JTILE)*(PEVAPTI(JL,JTILE)-PEVAPSNW(JL))
        ELSE
          ZEVAP=PFRTI(JL,JTILE)*PEVAPTI(JL,JTILE)
        ENDIF
        IF (ZEVAP > 0.0_JPRB) THEN
          IF (JK == 1) THEN
            ZROOTW(JL,JK,JTILE)=1.0_JPRB
          ENDIF
        ELSE
          IF (JTILE == 4) THEN
            ZROOTW(JL,JK,JTILE)=RVROOTSA(JK,ITYP(JL))*(ZLIQL(JL,JK)-RWPWPM(JS))
          ELSEIF (JTILE == 6.OR. JTILE == 7) THEN
            ZROOTW(JL,JK,JTILE)=RVROOTSA(JK,ITYP(JL))*(ZLIQH(JL,JK)-RWPWPM(JS))
          ENDIF
        ENDIF
        ZEXT(JL,JTILE)=ZEXT(JL,JTILE)+ZROOTW(JL,JK,JTILE)
      ENDDO
    ENDDO LAYERS
    DO JL=KIDIA,KFDIA
      ZEXT(JL,JTILE)=MAX(ZEPEXT,ZEXT(JL,JTILE))
    ENDDO
ENDDO TILES

!*          2.3 COEFFICIENTS FOR TOP LAYER

DO JL=KIDIA,KFDIA
  IF (LDLAND(JL)) THEN

!           HYDRAULIC PROPERTIES.

!           VAN GENUCHTEN

    JS=KSOTY(JL)
    ZDMAX=RDMAXM(JS)
    ZDMIN=RDMINM(JS)
    ZW=MAX(MAX(PWSAM1M(JL,1),PWSAM1M(JL,2)),RWRESTM(JS))
    ZSE=(ZW-RWRESTM(JS))/(RWSATM(JS)-RWRESTM(JS))
    ZWFAC=RWSATM(JS)-RWRESTM(JS)
    ZLAM=RLAMBDAM(JS)
    ZMFAC=RMFACM(JS)
    ZRMFAC=1./ZMFAC
    ZWCONS=RWCONSM(JS)
    ZALPHA=RMVGALPHA(JS)
    IF (ZW.LE.(1.001_JPRB*RWRESTM(JS))) THEN
      ZK=0.0_JPRB
      ZD=ZDMIN
    ELSEIF ((ZW.LE.(0.999_JPRB*RWSATM(JS))).AND.(ZW.GT.(1.001_JPRB*RWRESTM(JS)))) THEN
```

```
      ZKD=ZWCONS*ZSE**ZLAM* &
     &    (1.0_JPRB-((1.0_JPRB-(ZSE**ZRMFAC))**ZMFAC))**2.0_JPRB
      ZDD=(((1.0_JPRB-ZMFAC)*ZWCONS)/(ZALPHA*ZMFAC*ZWFAC)) &
     &    *(ZSE**(ZLAM-ZRMFAC)) &
     &    *(((1.0_JPRB-(ZSE**ZRMFAC))**ZMFAC) &
     &    +((1.0_JPRB-(ZSE**ZRMFAC))**(-ZMFAC))-2.0_JPRB)
      ZK=ZKD
      ZD=ZDD
    ELSE
      ZK=RWCONSM(JS)
      ZD=ZDMAX
    ENDIF
    IF (LLFREEZ) THEN
      ZFF=MIN(ZF(JL,1),ZF(JL,2))
      ZD=ZFF*ZDMIN+(1.0_JPRB-ZFF)*ZD
! NOTE ZK = 0 for frozen soil
      ZK=ZFF*0.0_JPRB+(1.0_JPRB-ZFF)*ZK
    ENDIF
!
    IF (LESSRO) THEN

!          SURFACE RUNOFF DUE TO VARIABLE INFILTRATION CAPACITY (VIC)
!          ----------------------------------------------------------

!              Relative soil saturation is defined using
!              liquid water in upper RSRDEP layer
      DO JK=1,KLEVS
        IF (JK > 1) THEN
          ZSUM=SUM(RDAW(1:JK-1))
        ELSE
          ZSUM=0.
        ENDIF
        ZFRK(JK)=MAX(0.0_JPRB,(MIN(RSRDEP,SUM(RDAW(1:JK)))-ZSUM)/RDAW(JK))
      ENDDO
      ZRSFL=PTSFL(JL)+PMSN(JL)+PTSFC(JL)                              !Units kg/m2/s
      IF (ZRSFL.GT.0.0_JPRB)THEN
!          SUBGRID SATURATION COEFFICIENTS
        ZROEFF=MAX(0.0_JPRB,(PSDOR(JL)-RSIGORMIN))/(PSDOR(JL)+RSIGORMAX)
        ZBWS=MAX(MIN(ZROEFF,0.5_JPRB),0.01_JPRB)
        ZB1=1.0_JPRB+ZBWS
        ZBM=1.0_JPRB/ZB1
        ZWK(:)=MAX(0.0_JPRB,(PWSAM1M(JL,:)-RWPWPM(JS)))*(1.0_JPRB-ZF(JL,:))+RWPWPM(JS)
        ZW=SUM(ZFRK(:)*ZWK(:)*RDAW(:))                                !Units m

        ZWMK(:)=((RWSATM(JS)-RWPWPM(JS))*(1.-ZF(JL,:))+RWPWPM(JS))
        ZWMAX=SUM(ZFRK(:)*ZWMK(:)*RDAW(:))                            !Units m

        ZCONW1=ZWMAX*ZB1
        ZLYEPS=MAX(0.0_JPRB,ZW-ZWMAX)                                 !Units m
        ZLIMRS=-1.0_JPRB*ZLYEPS
        IF (ZLYEPS.GT.0.1_JPRB*ZWMAX) THEN
           ZLIMRS=0.0_JPRB
        ENDIF
!       VIC Saturated area calculation
        ZLYSIC=MIN(1.0_JPRB,MAX(0.0_JPRB,(ZW-ZLYEPS)/ZWMAX))                    !Units -
        ZVOL=MAX(0.0_JPRB,(1.0_JPRB-ZLYSIC)**ZBM-ZRSFL/(ZINVTMST*RHOH2O*ZCONW1)) !Units -
!       Saturation excess runoff
        ZROS=ZRSFL/(ZINVTMST*RHOH2O)-MAX(ZWMAX-ZW,ZLIMRS)              !Units m
        IF (ZVOL.GT.0.0_JPRB) THEN
!       VIC runoff
          ZROS=ZROS+ZWMAX*ZVOL**ZB1                                   !Units m
        END IF
        ZROS=MAX(ZROS,0.0_JPRB)                                       !Units m
        ZROT=ZROS*RHOH2O*ZINVTMST                                     !Units kg/m2/s
      ELSE
        ZROT=0.
      ENDIF

    ELSE

!          SURFACE RUNOFF DUE TO INFILTRATION RATE LIMIT.
!          ----------------------------------------------

      ZDSURF=ZDMAX
      ZKSURF=RWCONSM(JS)
      IF (LLFREEZ) THEN
        ZFF=ZF(JL,1)
```

```
        ZDSURF=ZFF*ZDMIN+(1.-ZFF)*ZDMAX
        ZKSURF=ZFF*0.+(1.-ZFF)*RWCONSM(JS)
      ENDIF
      ZINFMAX=(ZDSURF*(RWSATM(JS)-PWSAM1M(JL,1))/(0.5_JPRB*RDAW(1))+ZKSURF)*RHOH2O

!          LARGE SCALE PRECIPITATION
      ZROL=MAX(0.0_JPRB,PTSFL(JL)+PMSN(JL)-ZINFMAX)

!          CONVECTIVE PRECIPITATION
      ZROC=MAX(0.0_JPRB,RPSFR*PTSFC(JL)-ZINFMAX)*ZPSFR
      ZROT=ZROL+ZROC
    ENDIF

!  Contribution of throughfall, melting, and runoff to the r.h.s.
    ZWSFL=PTSFL(JL)+PMSN(JL)+PTSFC(JL)-ZROT

!*             TILE CONTRIBUTIONS
!              ------------------
!  Tile by tile contribution of evaporation to the r.h.s.
!  Tile 3
    ZWSFL=ZWSFL+PFRTI(JL,3)*PEVAPTI(JL,3)-PEINTTI(JL,3)
!  Tile 4
    ZEXTK=(PFRTI(JL,4)*PEVAPTI(JL,4)-PEINTTI(JL,4))*ZROOTW(JL,1,4)/ZEXT(JL,4)
    ZSAWEXT(JL,1)=ZEXTK
    ZCONDS(JL)=ZCONDS(JL)+MAX((PFRTI(JL,4)*PEVAPTI(JL,4)-PEINTTI(JL,4)),0.0_JPRB)
    ZWSFL=ZWSFL+ZEXTK
!  Tile 6
    ZEXTK=(PFRTI(JL,6)*PEVAPTI(JL,6)-PEINTTI(JL,6))*ZROOTW(JL,1,6)/ZEXT(JL,6)
    ZSAWEXT(JL,1)=ZSAWEXT(JL,1)+ZEXTK
    ZCONDS(JL)=ZCONDS(JL)+MAX((PFRTI(JL,6)*PEVAPTI(JL,6)-PEINTTI(JL,6)),0.0_JPRB)
    ZWSFL=ZWSFL+ZEXTK
!  Tile 7
    ZEXTK=(PFRTI(JL,7)*(PEVAPTI(JL,7)-PEVAPSNW(JL))-PEINTTI(JL,7))&
     & *ZROOTW(JL,1,7)/ZEXT(JL,7)
    ZSAWEXT(JL,1)=ZSAWEXT(JL,1)+ZEXTK
    ZCONDS(JL)=ZCONDS(JL)+MAX((PFRTI(JL,7)*(PEVAPTI(JL,7)-PEVAPSNW(JL))-
PEINTTI(JL,7)),0.0_JPRB)
    ZWSFL=ZWSFL+ZEXTK
!  Tile 8
    ZEXTK=PFRTI(JL,8)*PEVAPTI(JL,8)+PEMSSN(JL)-PEINTTI(JL,8)
    ZCONDS(JL)=ZCONDS(JL)+MAX((PFRTI(JL,8)*PEVAPTI(JL,8)+PEMSSN(JL)-PEINTTI(JL,8)),0.0_JPRB)
    ZWSFL=ZWSFL+ZEXTK

!           SOIL WATER DIFFUSIVITY
    PCFW(JL,1)=ZD*PTMST*RSIMP/(0.5_JPRB*(RDAW(1)+RDAW(2)))

!           RIGHT-HAND SIDE
    PRHSW(JL,1)=PTMST*(-ZK+ZWSFL*ZHOH2O)/RDAW(1)

!          BUDGETS AND RUN-OFF PROPERLY SCALED.
    PSAWGFL(JL,1)=RHOH2O*ZK
    PROS(JL)=PTMST*ZROT                                  !Units kg/m2
    PFWEL1(JL)=PFWEL1(JL)+&
     & (PFRTI(JL,3)*PEVAPTI(JL,3)-PEINTTI(JL,3)+ZSAWEXT(JL,1)+&
     & PFRTI(JL,8)*PEVAPTI(JL,8)-PEINTTI(JL,8))
  ELSE
!          SEA POINTS.
    PCFW(JL,1)=0.0_JPRB
    PRHSW(JL,1)=0.0_JPRB
    PROS(JL)=0.0_JPRB
    PSAWGFL(JL,1)=0.0_JPRB
    ZSAWEXT(JL,1)=0.0_JPRB
  ENDIF
ENDDO

!*          2.4 COEFFICIENTS FOR OTHER LAYERS

DO JK=2,KLEVS
  DO JL=KIDIA,KFDIA
    IF (LDLAND(JL)) THEN

!           HYDRAULIC PROPERTIES.

!           VAN GENUCHTEN
      IF (JK < KLEVS) THEN
        JS=KSOTY(JL)
        ZW=MAX(MAX(PWSAM1M(JL,JK),PWSAM1M(JL,JK+1)),RWRESTM(JS))
```

```
      ELSE
        JS=KSOTY(JL)
        ZW=MAX(PWSAM1M(JL,JK),RWRESTM(JS))
      ENDIF
      ZDMAX=RDMAXM(JS)
      ZDMIN=RDMINM(JS)
      ZSE=(ZW-RWRESTM(JS))/(RWSATM(JS)-RWRESTM(JS))
      ZWFAC=RWSATM(JS)-RWRESTM(JS)
      ZLAM=RLAMBDAM(JS)
      ZMFAC=RMFACM(JS)
      ZRMFAC=1./ZMFAC
      ZWCONS=RWCONSM(JS)
      ZALPHA=RMVGALPHA(JS)
      IF (ZW.LE.(1.001*RWRESTM(JS))) THEN
      ZD=ZDMIN
        ZK=0.0_JPRB
      ELSEIF ((ZW.GT.(1.001_JPRB*RWRESTM(JS))).AND.(ZW.LE.(0.999_JPRB*RWSATM(JS)))) THEN
        ZKD=ZWCONS*ZSE**ZLAM* &
     &    (1.0_JPRB-((1.0_JPRB-(ZSE**ZRMFAC))**ZMFAC))**2.0_JPRB
        ZDD=(((1.0_JPRB-ZMFAC)*ZWCONS)/ &
     &    (ZALPHA*ZMFAC*ZWFAC))*(ZSE**(ZLAM-ZRMFAC)) &
     &    *(((1.0_JPRB-(ZSE**ZRMFAC))**ZMFAC) &
     &    +((1.0_JPRB-(ZSE**ZRMFAC))**(-ZMFAC))-2.0_JPRB)
        ZK=ZKD
        ZD=ZDD
      ELSE
        ZK=RWCONSM(JS)
        ZD=ZDMAX
      ENDIF

      ZWM=MAX(MAX(PWSAM1M(JL,JK-1),PWSAM1M(JL,JK)),RWRESTM(JS))
      ZSE=(ZWM-RWRESTM(JS))/(RWSATM(JS)-RWRESTM(JS))
      IF (ZWM.LE.RWRESTM(JS)) THEN
        ZKM=0.0_JPRB
      ELSEIF ((ZWM.GT.RWRESTM(JS)).AND.(ZWM.LT.(0.999_JPRB*RWSATM(JS)))) THEN
        ZKMD=ZWCONS*ZSE**ZLAM*(1.0_JPRB-((1.0_JPRB-(ZSE**ZRMFAC))**ZMFAC))**2.0_JPRB
        ZKM=ZKMD
      ELSE
        ZKM=RWCONSM(JS)
      ENDIF

      IF (JK == KLEVS) ZD=0.0_JPRB

      IF (LLFREEZ) THEN
        IF (JK < KLEVS) THEN
          ZFF=MIN(ZF(JL,JK),ZF(JL,JK+1))
          ZD=ZFF*ZDMIN+(1.0_JPRB-ZFF)*ZD
        ELSE
          ZFF=ZF(JL,JK)
        ENDIF
        ZFFM=MIN(ZF(JL,JK-1),ZF(JL,JK))
        ZK=ZFF*0.0_JPRB+(1.0_JPRB-ZFF)*ZK
        ZKM=ZFFM*0.0_JPRB+(1.0_JPRB-ZFFM)*ZKM
      ENDIF

!*             TILE CONTRIBUTIONS
!              ------------------
!  Tile by tile contribution of root extraction to the r.h.s.
!  Tile 4
      ZEXTK=(PFRTI(JL,4)*PEVAPTI(JL,4)-PEINTTI(JL,4))*&
       & ZROOTW(JL,JK,4)/ZEXT(JL,4)
      ZSAWEXT(JL,JK)=ZEXTK
      ZWSFL=ZEXTK
!  Tile 6
      ZEXTK=(PFRTI(JL,6)*PEVAPTI(JL,6)-PEINTTI(JL,6))*&
       & ZROOTW(JL,JK,6)/ZEXT(JL,6)
      ZSAWEXT(JL,JK)=ZSAWEXT(JL,JK)+ZEXTK
      ZWSFL=ZWSFL+ZEXTK
!  Tile 7
      ZEXTK=(PFRTI(JL,7)*(PEVAPTI(JL,7)-PEVAPSNW(JL))-PEINTTI(JL,7))*&
       & ZROOTW(JL,JK,7)/ZEXT(JL,7)
      ZSAWEXT(JL,JK)=ZSAWEXT(JL,JK)+ZEXTK
      ZWSFL=ZWSFL+ZEXTK

!           SOIL WATER DIFFUSIVITY
      IF (JK < KLEVS) THEN
        PCFW(JL,JK)=ZD*PTMST*RSIMP/(0.5_JPRB*(RDAW(JK)+RDAW(JK+1)))
```

```
      ELSE
        PCFW(JL,JK)=0.0_JPRB
      ENDIF

!           RIGHT-HAND SIDE
      PRHSW(JL,JK)=PTMST*(ZKM-ZK+ZWSFL*ZHOH2O)/RDAW(JK)

!          BUDGETS AND RUN-OFF PROPERLY SCALED.
      PSAWGFL(JL,JK)=RHOH2O*ZK
      PFWE234(JL)=PFWE234(JL)+ZSAWEXT(JL,JK)

    ELSE
!          SEA POINTS.
      PCFW(JL,JK)=0.0_JPRB
      PRHSW(JL,JK)=0.0_JPRB
      PSAWGFL(JL,JK)=0.0_JPRB
      ZSAWEXT(JL,JK)=0.0_JPRB
    ENDIF
  ENDDO
ENDDO

!*          3. DDH diagnostics
!              ---------------
! Soil water ans soil ice water
DO JK=1,KLEVS
  DO JL=KIDIA,KFDIA
    PDHWLS(JL,JK,1)=RHOH2O*RDAW(JK)*PWSAM1M(JL,JK)
    PDHWLS(JL,JK,2)=ZF(JL,JK)*PDHWLS(JL,JK,1)
  ENDDO
ENDDO
! Large-scale throughfall
DO JL=KIDIA,KFDIA
  PDHWLS(JL,1,3)=PTSFL(JL)
! Convective throughfall
  PDHWLS(JL,1,4)=PTSFC(JL)
! Melt throughfall
  PDHWLS(JL,1,5)=PMSN(JL)
ENDDO

! zero out fluxes
DO JK=2,KLEVS
  DO JL=KIDIA,KFDIA
    PDHWLS(JL,JK,3)=0.0_JPRB
    PDHWLS(JL,JK,4)=0.0_JPRB
    PDHWLS(JL,JK,5)=0.0_JPRB
    PDHWLS(JL,JK,10)=0.0_JPRB
  ENDDO
ENDDO

! Runoff top layer (negative values mean water lost by the layer)
DO JK=1,KLEVS
  DO JL=KIDIA,KFDIA
    PDHWLS(JL,JK,6)=0.0_JPRB
  ENDDO
ENDDO
DO JL=KIDIA,KFDIA
  PDHWLS(JL,1,6)=PDHWLS(JL,1,6)-ZINVTMST*PROS(JL)
ENDDO

! Root extraction (<0) without condensation on tile 4 6 7 8
DO JL=KIDIA,KFDIA
  PDHWLS(JL,1,7)=ZSAWEXT(JL,1)-ZCONDS(JL)
  DO JK=2,KLEVS
    PDHWLS(JL,JK,7)=ZSAWEXT(JL,JK)
  ENDDO
ENDDO
! Bare ground evaporation including mismatches from snow and interception layer
DO JL=KIDIA,KFDIA
  PDHWLS(JL,1,9)=PFRTI(JL,8)*PEVAPTI(JL,8)-&
   & PEINTTI(JL,8)+&
   & PEMSSN(JL)+&
   & PFRTI(JL,3)*PEVAPTI(JL,3)-&
   & PEINTTI(JL,3)
  DO JK=2,KLEVS
    PDHWLS(JL,JK,9)=0.0_JPRB
  ENDDO
ENDDO
```

```
! Condensation (>0) due to excess dew deposition on tile 3 (clipped to WLmax)
DO JL=KIDIA,KFDIA
  PDHWLS(JL,1,10)=ZCONDS(JL)
ENDDO
IF (LHOOK) CALL DR_HOOK('SRFWEXC_VG_MOD:SRFWEXC_VG',1,ZHOOK_HANDLE)

END SUBROUTINE SRFWEXC_VG
END MODULE SRFWEXC_VG_MOD
```

F VSURF module

The changes applied to this module are marked with yellow.

```
MODULE VSURF_MOD
CONTAINS
SUBROUTINE VSURF(KIDIA,KFDIA,KLON,KLEVS,KTILE,&
 & KTVL,KTVH,&
 & PFRTI, PLAIL, PLAIH,&
 & PTMLEV, PQMLEV  ,PAPHMS,&
 & PTSKM1M,PWSAM1M,PTSAM1M,KSOTY,&
 & PSRFD ,PRAQ  ,PQSAM ,&
 & PQS   ,PDQS  ,&
 & PWETB ,PCPTS ,PWETL, PWETH, PWETHS)

USE PARKIND1  ,ONLY : JPIM     ,JPRB
USE YOMHOOK   ,ONLY : LHOOK,   DR_HOOK

USE YOS_VEG   ,ONLY : RCEPSW   ,RVROOTSA ,RVRSMIN  ,RVHSTR   ,RVLAI
USE YOS_CST   ,ONLY : RCPD     ,RETV     ,RLVTT    ,RLSTT    ,RTT
USE YOS_THF   ,ONLY : R2ES     ,R3LES    ,R3IES    ,R4LES    ,R4IES &
                  &  ,R5LES    ,R5IES    ,RVTMP2
USE YOS_SOIL  ,ONLY : RWCAP    ,RWPWP    ,RQWEVAP  &
                  &  ,RWCAPM   ,RWPWPM   ,RQWEVAPM , RWRESTM &
                  &  ,RTF1     ,RTF2     ,RTF3     ,RTF4 &
                  &  ,LEVGEN
USE YOS_EXC   ,ONLY : LEOCSA

#ifdef DOC
!     ------------------------------------------------------------------

!**   *VSURF* - PREPARES SURFACE BOUNDARY CONDITION FOR T AND Q

!     DERIVED FROM VDIFF (CY34) BY
!     A.C.M. BELJAARS       E.C.M.W.F.    18-1-90
!     Modified P.VITERBO AND A.C.M. BELJAARS  E.C.M.W.F.    16-3-93
!     Modified ACM Beljaars  26-03-99  Tiling of the surface
!     P. Viterbo     24-05-2004     Change surface units
!     P. Viterbo ECMWF 12/05/2005 Externalize SURF
!                     (based on VDFSURF)
!     G. Balsamo ECMWF 22/05/2006   Evaporative fraction f(soil)
!     G. Balsamo ECMWF 03/07/2006   Add soil type
!     E. Dutra/G. Balsamo 01/05/2008   Add lake tile
!     G. Balsamo ECMWF 9/3/2010 Bare ground evaporation
!     S. Boussetta/G.Balsamo May 2009 Add lai


!     PURPOSE
!     -------

!     PREPARE SURFACE BOUNDARY CONDITION FOR Q AND T, E.G. FRACTIONAL
!     SURFACE COVER (SNOW AND VEGETATION), SATURATION SPECIFIC HUMIDITY
!     AT THE SURFACE, RELATIVE HUMIDITY OVER BARE LAND AND THE STOMATAL
!     RESISTANCE.

!     INTERFACE
!     ---------

!     *VSURF* IS CALLED BY *SURFEXCDRIVER*

!     INPUT PARAMETERS (INTEGER):

!     *KIDIA*        START POINT
!     *KFDIA*        END POINT
!     *KLON*         NUMBER OF GRID POINTS PER PACKET
!     *KLEVS*        NUMBER OF SOIL LAYERS
!     *KTILE*        TILE INDEX
!     *KTVL*         VEGETATION TYPE FOR LOW VEGETATION FRACTION
!     *KTVH*         VEGETATION TYPE FOR HIGH VEGETATION FRACTION
!     *PLAIL*        LAI OF LOW VEGETATION
!     *PLAIH*        LAI OF HIGH VEGETATION

!     *KSOTY*        SOIL TYPE (1-7)

!     INPUT PARAMETERS (REAL):

!     *PFRTI*      TILE FRACTIONS                                    (0-1)
!            1 : WATER                  5 : SNOW ON LOW-VEG+BARE-SOIL
!            2 : ICE                    6 : DRY SNOW-FREE HIGH-VEG
!            3 : WET SKIN               7 : SNOW UNDER HIGH-VEG
!            4 : DRY SNOW-FREE LOW-VEG  8 : BARE SOIL
```

```
!     *PTMLEV*      TEMPERATURE AT T-1, lowest model level
!     *PQMLEV*      SPECIFIC HUMIDITY AT T-1, lowest model level
!     *PAPHMS*      PRESSURE AT T-1, surface
!     *PTSKM1M*      SURFACE TEMPERATURE
!     *PWSAM1M*      SOIL MOISTURE ALL LAYERS                    M**3/M**3
!     *PTSAM1M*      SOIL TEMPERATURE ALL LAYERS
!     *PSRFD*        DOWNWARD SHORT WAVE RADIATION FLUX AT SURFACE
!     *PRAQ*         PRELIMINARY AERODYNAMIC RESISTANCE

!     OUTPUT PARAMETERS (REAL):

!     *PQSAM*        SPECIFIC HUMIDITY AT THE SURFACE
!     *PQS*          SATURATION Q AT SURFACE
!     *PDQS*         DERIVATIVE OF SATURATION Q-CURVE AT SURFACE T
!     *PWETB*        BARE SOIL RESISTANCE
!     *PCPTS*        DRY STATIC ENRGY AT SURFACE
!     *PWETL*        CANOPY RESISTANCE LOW VEGETATION
!     *PWETH*        CANOPY RESISTANCE HIGH VEGETATION, SNOW FREE
!     *PWETHS*       CANOPY RESISTANCE HIGH VEGETATION WITH SNOW

!     METHOD
!     ------

!     SEE DOCUMENTATION

!     ------------------------------------------------------------------
#endif

IMPLICIT NONE

INTEGER(KIND=JPIM),INTENT(IN)    :: KLON
INTEGER(KIND=JPIM),INTENT(IN)    :: KLEVS
INTEGER(KIND=JPIM),INTENT(IN)    :: KIDIA
INTEGER(KIND=JPIM),INTENT(IN)    :: KFDIA
INTEGER(KIND=JPIM),INTENT(IN)    :: KTILE
INTEGER(KIND=JPIM),INTENT(IN)    :: KTVL(:)
INTEGER(KIND=JPIM),INTENT(IN)    :: KTVH(:)
REAL(KIND=JPRB)   ,INTENT(IN)    :: PLAIL(:)
REAL(KIND=JPRB)   ,INTENT(IN)    :: PLAIH(:)
INTEGER(KIND=JPIM),INTENT(IN)    :: KSOTY(:)
REAL(KIND=JPRB)   ,INTENT(IN)    :: PTMLEV(:)
REAL(KIND=JPRB)   ,INTENT(IN)    :: PFRTI(:,:)
REAL(KIND=JPRB)   ,INTENT(IN)    :: PQMLEV(:)
REAL(KIND=JPRB)   ,INTENT(IN)    :: PAPHMS(:)
REAL(KIND=JPRB)   ,INTENT(IN)    :: PTSKM1M(:)
REAL(KIND=JPRB)   ,INTENT(IN)    :: PWSAM1M(:,:)
REAL(KIND=JPRB)   ,INTENT(IN)    :: PTSAM1M(:,:)
REAL(KIND=JPRB)   ,INTENT(IN)    :: PSRFD(:)
REAL(KIND=JPRB)   ,INTENT(IN)    :: PRAQ(:)
REAL(KIND=JPRB)   ,INTENT(INOUT) :: PQSAM(:)
REAL(KIND=JPRB)   ,INTENT(OUT)   :: PQS(:)
REAL(KIND=JPRB)   ,INTENT(OUT)   :: PDQS(:)
REAL(KIND=JPRB)   ,INTENT(INOUT) :: PWETB(:)
REAL(KIND=JPRB)   ,INTENT(OUT)   :: PCPTS(:)
REAL(KIND=JPRB)   ,INTENT(INOUT) :: PWETL(:)
REAL(KIND=JPRB)   ,INTENT(INOUT) :: PWETH(:)
REAL(KIND=JPRB)   ,INTENT(INOUT) :: PWETHS(:)

!*    LOCAL STORAGE
!     ----- -------

REAL(KIND=JPRB) ::      ZLIQH(KLON,KLEVS),ZLIQL(KLON,KLEVS),ZLIQR(KLON,KLEVS),ZLIQ(KLON,KLEVS)

INTEGER(KIND=JPIM) :: JK, JL, JS

REAL(KIND=JPRB) ::   &
 & ZCOR, ZEPSF3, ZF, ZF1H, ZF1L, ZF2H, ZF2L, ZF2B, &
 & ZF3H, ZF3L, ZHSTRH, ZHSTRL, ZLAIH, ZLAIL, &
 & ZQSAIR, ZROOT1H, ZROOT1L, ZROOT2H, ZROOT2L, &
 & ZROOT3H, ZROOT3L, ZROOT4H, ZROOT4L, ZRSMINH, &
 & ZRSMINL, ZRSMINB, ZRVA, ZRVB, ZSRFL, ZWROOTH, ZWROOTL, &
 & ZQWEVAP, ZWPWP, ZQWEVAPBARE, ZBARE, ZWPBARE,&
 & ZSALIN, FH, FL
REAL(KIND=JPRB) :: ZHOOK_HANDLE

!     ------------------------------------------------------------------
```

```
#include "fcsttre.h"

!     ------------------------------------------------------------------

!*       1.     INITIALIZE CONSTANTS
!               ---------- ----------

IF (LHOOK) CALL DR_HOOK('VSURF_MOD:VSURF',0,ZHOOK_HANDLE)

ZRVA=5000._JPRB
ZRVB=10._JPRB
ZEPSF3=0.00001_JPRB ! security value for exponential sat-deficit dependence
ZRSMINB=50._JPRB  ! bare soil minimum resistance

!       SET FH AND FL - FRACTIONS FOR ROOTZONE EXTRACTION
FH = 0.92_JPRB
FL = 0.73_JPRB

!     ------------------------------------------------------------------

!          2.    PREPARE SURFACE BOUNDARY CONDITION
!                ------- ------- -------- ---------

!*         2.1   RELATIVE HUMIDITY OVER THE BARE LAND PART

!                BARE SOIL RESISTANCE IS COMPUTED FOR KTILE=4

!*         2.2   SATURATION PARAMETERS,

IF (LEOCSA .AND. KTILE  ==  1) THEN
  ZSALIN=0.98_JPRB
ELSE
  ZSALIN=1.0_JPRB
ENDIF

DO JL=KIDIA,KFDIA
  PQS(JL)=FOEEW(PTSKM1M(JL))/PAPHMS(JL)
  ZCOR=ZSALIN/MAX(1.0E-3,1.0_JPRB-RETV  *PQS(JL))
  PQS(JL)=PQS(JL)*ZCOR
  PDQS(JL)=PQS(JL)*ZCOR*FOEDESU(PTSKM1M(JL))
ENDDO

!*         2.3   DEFINITION OF THE STOMATAL RESISTANCE AND BARE SOIL RES
!*               DOES WORK FOR TYPE 4, 6 AND 8 WHEN ROUTINE IS CALLED FOR
!*               TYPE 4

IF (KTILE  ==  4) THEN

!                Compute first liquid fraction of soil water to
!                be used later in stress functions
!          CONTRIBUTION TO APPARENT ENERGY, TAKING INTO ACCOUNT
!          FREEZING/MELTING OF SOIL WATER.

  DO JK=1,KLEVS
    DO JL=KIDIA,KFDIA
      IF(PTSAM1M(JL,JK) < RTF1.AND.PTSAM1M(JL,JK) > RTF2) THEN
        ZF=0.5_JPRB*(1.0_JPRB-SIN(RTF4*(PTSAM1M(JL,JK)-RTF3)))
      ELSEIF (PTSAM1M(JL,JK) <= RTF2) THEN
        ZF=1.0_JPRB
      ELSE
        ZF=0.0_JPRB
      ENDIF
      IF (LEVGEN) THEN
        JS=KSOTY(JL)
        ZLIQH(JL,JK)=MAX(RWPWPM(JS),MIN(FH*RWCAPM(JS),PWSAM1M(JL,JK)*(1.0_JPRB*FH-ZF)))
        ZLIQL(JL,JK)=MAX(RWPWPM(JS),MIN(FL*RWCAPM(JS),PWSAM1M(JL,JK)*(1.0_JPRB*FL-ZF)))
       ZLIQR(JL,JK)=MAX(RWRESTM(JS),MIN(RWCAPM(JS),PWSAM1M(JL,JK)*(1.0_JPRB-ZF)))
      ELSE
        ZLIQ(JL,JK)=MAX(RWPWP,MIN(RWCAP,PWSAM1M(JL,JK)*(1.0_JPRB-ZF)))
       ZLIQR(JL,JK)=MAX(0.05_JPRB,MIN(RWCAP,PWSAM1M(JL,JK)*(1.0_JPRB-ZF)))
      ENDIF
    ENDDO
  ENDDO

  DO JL=KIDIA,KFDIA
!           minimal stomatal resistance : ZRSMIN
    ZRSMINL=RVRSMIN(KTVL(JL))
```

```
      ZRSMINH=RVRSMIN(KTVH(JL))

!           leaf area index  : ZLAI
      ZLAIL=PLAIL(JL)
      ZLAIH=PLAIH(JL)

!           bare ground fraction
      ZBARE=PFRTI(JL,8)
!           soil moisture stress function : F2
      ZROOT1L=RVROOTSA(1,KTVL(JL))
      ZROOT2L=RVROOTSA(2,KTVL(JL))
      ZROOT3L=RVROOTSA(3,KTVL(JL))
      ZROOT4L=RVROOTSA(4,KTVL(JL))
      ZROOT1H=RVROOTSA(1,KTVH(JL))
      ZROOT2H=RVROOTSA(2,KTVH(JL))
      ZROOT3H=RVROOTSA(3,KTVH(JL))
      ZROOT4H=RVROOTSA(4,KTVH(JL))

      ZWROOTL=ZLIQL(JL,1)*ZROOT1L+&
       & ZLIQL(JL,2)*ZROOT2L+&
       & ZLIQL(JL,3)*ZROOT3L+&
       & ZLIQL(JL,4)*ZROOT4L
      ZWROOTH=ZLIQH(JL,1)*ZROOT1H+&
       & ZLIQH(JL,2)*ZROOT2H+&
       & ZLIQH(JL,3)*ZROOT3H+&
       & ZLIQH(JL,4)*ZROOT4H
      IF (LEVGEN) THEN
         JS=KSOTY(JL)
         ZWPWP=RWPWPM(JS)
         ZQWEVAP=RQWEVAPM(JS)
!        bare ground evaporation stress is calculated with the weighted average of
!        residual and wilting point soil moisture (since it is common soil)
         ZWPBARE=(RWPWPM(JS)*(1.0_JPRB-ZBARE)+RWRESTM(JS)*ZBARE)
         IF (JS >=1 ) THEN
            ZQWEVAPBARE=1._JPRB/(RWCAPM(JS)-ZWPBARE)
         ELSE
            ZQWEVAPBARE=0._JPRB
         ENDIF
         ZF2B=MAX(RCEPSW,MIN(1.0_JPRB,(ZLIQR(JL,1)-ZWPBARE)*ZQWEVAPBARE))
      ELSE
         ZWPWP=RWPWP
         ZQWEVAP=RQWEVAP
         ZWPBARE=(RWPWP*(1.0_JPRB-ZBARE)+0.05_JPRB*ZBARE)
         ZQWEVAPBARE=1._JPRB/(RWCAP-ZWPBARE)
!        Formula for bare ground evaporation in TESSEL
!        ZF2B=MAX(RCEPSW,MIN(1.0_JPRB,(ZLIQR(JL,1)-ZWPBARE)*ZQWEVAPBARE))
         ZF2B=MAX(RCEPSW,MIN(1.0_JPRB,(ZLIQ(JL,1)-ZWPWP)*ZQWEVAP))
      ENDIF
      ZF2L=MAX(RCEPSW,MIN(1.0_JPRB,(ZWROOTL-ZWPWP)*ZQWEVAP))
      ZF2H=MAX(RCEPSW,MIN(1.0_JPRB,(ZWROOTH-ZWPWP)*ZQWEVAP))

!           radiation stress function (proposed by Alan Betts): ZF1
      ZSRFL=PSRFD(JL)/250._JPRB
      ZF1L=1.0_JPRB/MAX(1.0_JPRB,0.81_JPRB*(1.+ZSRFL)/(ZSRFL+0.05_JPRB))
      ZF1H=ZF1L

!           atmospheric moisture deficit stress function : F3
      ZHSTRL=RVHSTR(KTVL(JL))
      ZHSTRH=RVHSTR(KTVH(JL))
      ZQSAIR=FOEEW(PTMLEV(JL))/PAPHMS(JL)
      ZCOR=1.0_JPRB/(1.0_JPRB-RETV  *ZQSAIR)
      ZQSAIR=ZQSAIR*ZCOR
      ZF3L=EXP(-ZHSTRL*(ZQSAIR-PQMLEV(JL)))
      ZF3H=EXP(-ZHSTRH*(ZQSAIR-PQMLEV(JL)))
      ZF3L=MAX(ZEPSF3,MIN(1.0_JPRB,ZF3L))
      ZF3H=MAX(ZEPSF3,MIN(1.0_JPRB,ZF3H))

      IF(ZLAIL /= 0.0_JPRB) THEN
        PWETL(JL)=ZRSMINL/(ZLAIL*ZF1L*ZF2L*ZF3L)
      ELSE
        PWETL(JL)=1.0E+6_JPRB
      ENDIF

      IF(ZLAIH /= 0.0_JPRB) THEN
        PWETH(JL)=ZRSMINH/(ZLAIH*ZF1H*ZF2H*ZF3H)
      ELSE
        PWETH(JL)=1.0E+6_JPRB
```

```
    ENDIF

    PWETHS(JL)=PWETH(JL)
    PWETB(JL)=ZRSMINB/ZF2B

  ENDDO
ENDIF

IF (KTILE == 4) THEN
  DO JL=KIDIA,KFDIA
    IF (PQMLEV(JL) > PQS(JL)) THEN
      PWETL(JL)=0.0_JPRB
    ENDIF
  ENDDO
ELSEIF (KTILE == 6) THEN
  DO JL=KIDIA,KFDIA
    IF (PQMLEV(JL) > PQS(JL)) THEN
      PWETH(JL)=0.0_JPRB
    ENDIF
  ENDDO
ELSEIF (KTILE == 7) THEN
  DO JL=KIDIA,KFDIA
    IF (PQMLEV(JL) > PQS(JL)) THEN
      PWETHS(JL)=0.0_JPRB
    ENDIF
  ENDDO
ELSEIF (KTILE == 8) THEN
  DO JL=KIDIA,KFDIA
    IF (PQMLEV(JL) > PQS(JL)) THEN
      PWETB(JL)=0.0_JPRB
    ENDIF
  ENDDO
ENDIF

!*         2.4   APPARENT SURFACE HUMIDITY

IF (KTILE  ==  1.OR. KTILE  ==  2.OR. KTILE  ==  3.OR. KTILE  ==  5 .OR. KTILE == 9 ) THEN
  DO JL=KIDIA,KFDIA
    PQSAM(JL)=PQS(JL)
  ENDDO
ELSEIF (KTILE  ==  8) THEN
  DO JL=KIDIA,KFDIA
    PQSAM(JL)=PQS(JL)+(PQMLEV(JL)-PQS(JL))*PWETB(JL)/(PWETB(JL)+PRAQ(JL))
  ENDDO
ELSEIF (KTILE  ==  4) THEN
  DO JL=KIDIA,KFDIA
    PQSAM(JL)=PQS(JL)+(PQMLEV(JL)-PQS(JL))*PWETL(JL)/(PWETL(JL)+PRAQ(JL))
  ENDDO
ELSEIF (KTILE == 6) THEN ! I.E. HIGH VEGETATION, SNOW FREE
  DO JL=KIDIA,KFDIA
    PQSAM(JL)=PQS(JL)+(PQMLEV(JL)-PQS(JL))*PWETH(JL)/(PWETH(JL)+PRAQ(JL))
  ENDDO
ELSE ! I.E. HIGH VEGETATION WITH SNOW (7)
  DO JL=KIDIA,KFDIA
    PQSAM(JL)=PQS(JL)+(PQMLEV(JL)-PQS(JL))*PWETHS(JL)/(PWETHS(JL)+PRAQ(JL))
  ENDDO
ENDIF

!*         2.5   DRY STATIC ENERGY AT THE SURFACE

DO JL=KIDIA,KFDIA
  PCPTS(JL)=PTSKM1M(JL)*RCPD*(1.0_JPRB+RVTMP2*PQSAM(JL))
ENDDO

IF (LHOOK) CALL DR_HOOK('VSURF_MOD:VSURF',1,ZHOOK_HANDLE)
END SUBROUTINE VSURF
END MODULE VSURF_MOD
```

G Model parameters

Table G.1: Moisture depth values for the study catchments (MD model)

Catchments	z_{total} (m)	z_4 (m)	z_3 (m)	z_2 (m)	z_1 (m)
A	1.061	0.061	0.720	0.210	0.070
Av	0.816	0.200	0.336	0.210	0.070
D	1.064	0.064	0.720	0.210	0.070
EA	2.103	1.103	0.720	0.210	0.070
EB	1.622	0.622	0.720	0.210	0.070
G1	0.976	0.200	0.496	0.210	0.070
G2	0.892	0.200	0.412	0.210	0.070
He	2.420	1.420	0.720	0.210	0.070
K	1.703	0.703	0.720	0.210	0.070
Mi	2.216	1.216	0.720	0.210	0.070
Mu	0.820	0.200	0.340	0.210	0.070
Na	0.842	0.200	0.362	0.210	0.070
No	3.903	2.903	0.720	0.210	0.070
P	0.638	0.200	0.158	0.210	0.070
R	1.948	0.948	0.720	0.210	0.070
W	2.532	1.532	0.720	0.210	0.070

Table G.2: Moisture Availability Factor (MAF) values for the study catchments (MA model)

Catchment	MAF low (-)	MAF high (-)
A	0.57	0.67
Av	0.58	0.66
D	0.47	0.61
EA	0.73	0.92
EB	0.67	0.90
G1	0.77	0.91
G2	0.52	0.77
He	0.81	0.94
K	0.63	0.81
Mi	0.68	0.93
Mu	0.45	0.55
Na	0.55	0.63
No	0.93	1.27
P	0.56	0.72
R	0.60	0.79
W	0.71	0.92

Table G.3: Moisture depth values for the study catchments with 33% root distribution (MD-33 model)

Catchments	$\mathbf{z_{total}}$ **(m)**	$\mathbf{z_4}$ **(m)**	$\mathbf{z_3}$ **(m)**	$\mathbf{z_2}$ **(m)**	$\mathbf{z_1}$ **(m)**
A	1.061	0.500	0.781	0.210	0.070
Av	0.816	0.500	0.536	0.210	0.070
D	1.064	0.500	0.784	0.210	0.070
EA	2.103	0.500	1.823	0.210	0.070
EB	1.622	0.500	1.342	0.210	0.070
G1	0.976	0.500	0.696	0.210	0.070
G2	0.892	0.500	0.612	0.210	0.070
He	2.420	0.500	2.140	0.210	0.070
K	1.703	0.500	1.423	0.210	0.070
Mi	2.216	0.500	1.936	0.210	0.070
Mu	0.820	0.500	0.540	0.210	0.070
Na	0.842	0.500	0.562	0.210	0.070
No	3.903	0.500	3.623	0.210	0.070
P	0.638	0.500	0.358	0.210	0.070
R	1.948	0.500	1.668	0.210	0.070
W	2.532	0.500	2.252	0.210	0.070

H Total rootzone storage capacities

Table H.1: Total rootzone storage capacities (S_R) estimated with mass balance approach and HTESSEL in the 15 study catchments. The high, average and low S_R outputs are presented (Table 4.3) for high (H) and low (L) vegetation.

Catchment	MB avg L S_R (mm)	MB avg H S_R (mm)	MB avg total S_R (mm)	MB high L S_R (mm)	MB high H S_R (mm)	MB high total S_R (mm)	MB low L S_R (mm)	MB low H S_R (mm)	MB low total S_R (mm)	HTESSEL S_R (mm)
A	134	231	208	172	282	256	108	196	175	566
Av	142	224	160	171	257	190	117	198	135	566
D	136	288	266	170	313	293	109	245	226	725
EA	346	481	389	419	529	454	273	412	317	535
EB	300	461	300	366	510	366	242	402	242	535
G	194	373	194	251	429	251	152	317	152	513
He	243	412	409	305	466	463	185	355	353	491
K	271	399	315	316	423	353	237	369	283	535
Mi	307	488	410	369	518	454	247	439	356	535
Mu	113	222	205	154	270	251	91	191	175	725
Na	113	191	165	144	231	202	90	162	138	566
No	484	726	722	563	761	759	403	670	666	535
P	125	289	125	162	329	162	93	238	93	566
R	282	492	487	336	539	534	240	444	440	725
W	403	633	633	490	678	678	315	544	544	725